

PHASE TRANSFORMATIONS IN SOLIDS

A Thesis Submitted
In Partial Fulfilment of the Requirements
for the Degree of
DOCTOR OF PHILOSOPHY

474

✓ CHM-1970-D-NAT-PHA

BY
M. NATARAJAN

POST GRADUATE OFFICE
This thesis has been approved
for the award of the Degree of
Doctor of Philosophy (Ph.D.)
in accordance with the
regulations of the Indian
Institute of Technology Kanpur
Dated: 25/9/70 *h*

to the

DEPARTMENT OF CHEMISTRY
INDIAN INSTITUTE OF TECHNOLOGY KANPUR

1970

thesis
544.363
N191 p

THE SECRET OF SUCCESS LIES IN THE
CONSTANCY OF PURPOSE.

S. T.

STATEMENT

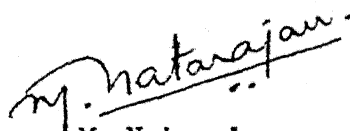
I hereby declare that the matter presented in this THESIS is the result of the investigations carried out by me in the Department of Chemistry, Indian Institute of Technology, Kanpur, India, under the supervision of Professor C.N.R. Rao.

In keeping with the general practice in the reporting of scientific observations, due acknowledgement has been made wherever the work described is based on the findings of other investigators.

Statement Verified


C.N.R. Rao

Thesis Supervisor


M. Natarajan
Candidate

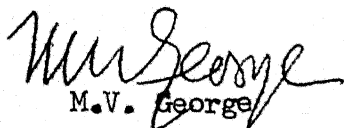
DEPARTMENT OF CHEMISTRY
INDIAN INSTITUTE OF TECHNOLOGY, KANPUR, INDIA

CERTIFICATE

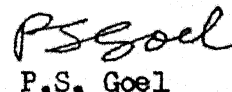
This is to certify that Mr. M. Natarajan has satisfactorily completed all the course requirements for the Ph.D. degree programme in Chemistry. The courses include:

Chm 500 Mathematics for Chemists I
Chm 501 Advanced Organic Chemistry
Chm 521 Chemical Binding
Chm 523 Chemical Thermodynamics
Chm 524 Modern Physical Methods in Chemistry
Chm 541 Advanced Inorganic Chemistry
Chm 600 Mathematics for Chemists II
Met.E 683 Properties of Materials
Met.E 684 Experimental Methods in Metallurgy
Chm 800 General Seminar
Chm 841 Graduate Seminar
Chm 900 Graduate Research

Mr. M. Natarajan was admitted to the candidacy of the Ph.D. degree in February, 1967, after he successfully completed the written and oral qualifying examinations.


M.V. George

Head, Department of Chemistry


P.S. Goel

Convener, Post-graduate
Studies Committee
Department of Chemistry

ACKNOWLEDGEMENT

I would like to express my deep sense of gratitude to Professor C.N.R. Rao for his inspring guidance throughout the investigations. He combines in himself an excellent and zealous research worker as well as an enthusiastic teacher. It has always been a pleasure for me to work with one like Professor C.N.R. Rao. His contribution to my scientific knowledge has been very valuable and highly useful. In short, what I am today is his 'gift' to me. He has been very kind and tolerant during my stay in his laboratory. The only way I can repay my debt to him is by working hard and achieving high standards in my scientific carreer both as a teacher and as a research worker.

I am extremely grateful to my senior colleagues Drs. A.S.N. Murthy, G.V. Chandrashekhar, K.R. Bhaskar, K.C. Patil, K.J. Rao, S.N. Bhat and G.V. Subba Rao for their cooperation and encouragement throughout my research investigations. I am also thankful to my friends Dr. B. Prakash, Mr. S. Ramdas, Mr. G. Rama Rao and Mr. T.S. Sarma for helping me with various measurements.

I am grateful to Professors M.V. George, P.T. Narasimhan, A. Chakravorty, J.C. Ahluwalia, D. Devaprabhakara, S. Ranganathan and D. Balasubramanian of the Chemistry Department, for their kind encouragement. Thanks are due to Dr. A.R. Das of the Metallurgical Engineering Department for helpful discussions.

I am thankful to Professors V. Subbarao and C.V. Seshadri of Chemical Engineering Department for their encouragement.

I am particularly thankful to Dr. P.K. Kelkar and Dr. M.S. Muthana who evinced keen interest in my research work and encouraged me enthusiastically.

I am grateful to Mr. R.D. Tripathi for excellent typing of the manuscript of the thesis. It is my pleasant duty to acknowledge my gratefulness to Mr. S.J. Dubey, O.P. Saksena and Mr. B.B. Srivastava of the Graphic Arts Section. I am thankful to Mr. B.N. Shukla and Mr. R.S. Singh as well as Mr. T.G. Rao and Mr. R.K. Jha of the Chemistry Department for their services.

I would like to avail of this opportunity to express my gratitude to my teachers, Mr. K.R. Subramanian, B.Sc., B.T., Professors E.S. Neelakantan, C.A. Padmanabhan, K. Nagaraja Rao K. Kalyanasundaram, P.N. Rangan and Mr. C. Thirunavukkarasu. I am grateful to Professors Sp. Shammuganathan, S. Krishnamoorthy, T. Ramalingam and D. Sri Rama Rao (Pachaiyappa's College, Madras) who have contributed much to my aptitude for research.

I wish to place on record my thanks to Dr. R. Venkatarama M.B., B.S., (Kumbakonam), Mr. T.V. Rajagopal ('Thathaji') and my uncle Mr. S. Rajagopalan (S.R.V.S., Ltd., Kumbakonam) who have helped me a lot throughout my higher education.

I am ever grateful to my beloved parents who have suffered quite a lot to educate me upto this level and thus bestowed upon me

the boon of knowledge. I am quite aware of the sacrifices they had to make for my college education and I can assure them that I will act responsibly and diligently to fulfill their high expectations. I wish to express my great admiration to my brother Mr. M. Somasundaram who supported my education, sacrificing his own. It is my duty to take note of his magnanimity and to reward him at the appropriate time.

I conclude by thanking the authorities of the Institute for kindly providing me a research scholarship during 1966-67 and also permitting me to avail of the various facilities including the Central Library, the Computer etc., for my research investigations. I am particularly grateful to the U.S. National Bureau of Standards for financial support since 1967.

This Thesis is Dedicated to the

LOVING MEMORY OF MY BELOVED

S. THRIPURASUNDARI, M. Sc.

PREFACE

A brief review on phase transformations in solids has been presented in Chapter I. In addition to discussing the thermodynamics and kinetics of phase transformations, various types of transformations encountered in inorganic solids have been described in this chapter.

Cesium chloride undergoes a first order thermal transition from the CsCl (Pm $\bar{3}$ m) structure to the NaCl (Fm $\bar{3}$ m) structure at $\sim 480^\circ\text{C}$. Addition of KCl, RbCl and other alkali halides to CsCl markedly affects the characteristics of this Pm $\bar{3}$ m-Fm $\bar{3}$ m transition. While KCl or RbCl stabilizes the Fm $\bar{3}$ m phase at a fixed composition, CsBr increases the transformation temperature. We have examined the Pm $\bar{3}$ m-Fm $\bar{3}$ m transitions of the solid solutions of CsCl with KCl and CsBr in detail employing differential thermal analysis and variable temperature x-ray diffraction (Chapter II). We have then attempted to explain the widely different behaviours with the KCl and CsBr solid solutions by employing the Born treatment of ionic solids. In order to examine the influence of Schottky defects on the Pm $\bar{3}$ m-Fm $\bar{3}$ m transition, we have studied the transformations of the solid solutions of CsCl with SrCl $_2$.

In Chapter III, defect energies in CsCl and its solid solutions with KCl, RbCl and CsBr have been estimated from ionic conductivity measurements. It was our interest to obtain Schottky formation energies in the Pm $\bar{3}$ m and Fm $\bar{3}$ m phases of CsCl and to examine the variation of the migration energy in the two structures of CsCl with the incorporation of K $^+$, Rb $^+$ and Br $^-$ ions. In addition, we have also

estimated the binding energy of the complex, $\text{Sr}_{\text{Cs}}^{+2} \text{V}_{\text{Cs}}^{-}$, with and without the Debye-Hückel approximations.

Phase transitions of silver halides, particularly those of silver iodide, form the subject matter of Chapter IV. The major interest in this study were: (i) to establish the presence of the B3 polytype (cubic, sphalerite type) of AgI and its possible transformation to the B4 form (hexagonal, wurtzite type); (ii) to study the transitions of B3 and B4 forms to the B23 (high temperature cubic) form, and (iii) to investigate the applicability of the Born model of ionic solids to the pressure transitions of AgCl and AgBr as well as the thermal and pressure transitions of AgI.

The effect of particle size on the thermal hysteresis and enthalpy changes in reversible crystal structure transformations have been reported in Chapter V. Turnbull's theory of heterogeneous nucleation has been employed to understand particle size effects; a thermodynamic treatment of thermal hysteresis has also been attempted. Interfacial energies of CsCl, NH_4Cl , NH_4Br , AgI, K_2SO_4 and quartz have been estimated by different methods.

In Chapter VI, crystallization of amorphous oxides has been examined by differential thermal analysis. The more interesting study in this chapter refers to thermal and particle size effects in magnesium oxide. This problem has been investigated by careful measurements of the particle size, surface areas and heats of solution of MgO samples prepared at various temperatures in the range,

350° - 1200°C. The purpose of this study was to understand the nature of the "pseudocrystallization" and the associated thermal anomaly in finely divided oxides such as MgO prepared by low-temperature decomposition of hydroxides etc.

In Chapter VII, some aspects of the semiconductor-semimetal transitions in VO_2 , NbO_2 and their solid solutions have been investigated. DTA, x-ray diffraction and conductivity measurements have been employed to investigate these interesting transformations. It may be mentioned here that semiconductor-semimetal transitions form an important new area in the transport properties of oxides and related materials. Crystal distortion plays an important role in determining the nature (and magnitude) of such electrical transitions. The systems presently studied include $\text{VO}_2\text{-TiO}_2$, $\text{VO}_2\text{-NbO}_2$, $\text{VO}_2\text{-MoO}_2$ and $\text{NbO}_2\text{-VO}_2$ solid solutions.

Preliminary results on the phase transitions of some mixed halides such as CsPbX_3 ($\text{X} = \text{Cl, Br or I}$) and RbCdCl_3 have been presented in Chapter VIII. The reported crystal structures (and space groups) of these halides tempted us to look for possible ferroelectricity in these compounds. New phase transitions in other related mixed halides (CsCuCl_3 , RbCdBr_3 and RbCdI_3) have also been examined.

It can be seen that the research work carried out by the author as part of the Ph.D. training programme was meant to familiarise him with a wide variety of phase transitions exhibited by inorganic

solids. While this has been a good education to the author, he hopes that the material will be of some value to the scientific literature as well.

The author has taken care to give due credit for the work of other workers. There are approximately 200 references to the literature in the thesis. However, the author would like to be excused for any omissions which might have occurred by oversight or error in judgement.

CONTENTS

	Page
STATEMENT	i
CERTIFICATE	ii
ACKNOWLEDGEMENT	iii
PREFACE	vi
CONTENTS	x
CHAPTER I Phase Transformations in Solids: - A Brief Account	1
CHAPTER II Fm3m-Fm3m Transformations of Alkali Halides	34
CHAPTER III Ionic Conductivity in CsCl and its Solid Solutions with KCl, RbCl and CsBr	50
CHAPTER IV Phase Transitions of Silver Halides	61
CHAPTER V Particle Size Effects and Thermal Hysteresis in Crystal Structure Transformations	88
CHAPTER VI Crystallization and Pseudocrystallization in Oxides	110
CHAPTER VII Phase Transitions in the Solid Solutions of VO_2 with TiO_2 , NbO_2 and MoO_2	127
CHAPTER VIII Phase Transformations in Some Halide Systems	148
SUMMARY	161
VITA E	

CHAPTER I

PHASE TRANSFORMATIONS IN SOLIDS

CHAPTER I

PHASE TRANSFORMATIONS IN SOLIDS

-A Brief Account

I.1 INTRODUCTION

Polymorphism is a common phenomenon in solids and the change of one polymorph to another constitutes an important aspect of phase transformations in solids. Phase transformations in many solids are accompanied by interesting changes in electrical, magnetic, dielectric and thermal properties in addition to changes in the crystal structure of the material. The subject of phase transformations in solids has been reviewed by Ubbelohde¹, Rao and Rao² and Smoluchowski³. A brief account of various types of phase transformations will be presented in this chapter.

I.2 Thermodynamics of Phase Transformations in Solids

Classical thermodynamics gives a simple treatment of the equilibrium between two phases. The equilibrium properties of each phase are defined by the Gibbs free energy function, G , the pressure,

P, and the temperature, T. The G-P-T surfaces of two phases are considered to be independent of each other and in a phase transformation the surfaces intersect at the transition point. If the transformation takes place from a low-temperature to a high-temperature form, there will be an increase in entropy and an associated volume change. The two thermodynamic relations which describe the differences between the slopes of the tangents at the intersection are :

$$(\partial G / \partial T)_P = -S \quad (1)$$

$$(\partial G / \partial P)_T = V \quad (2)$$

These two relations are related by the Clausius-Clapeyron equation.

The classical thermodynamic approach in describing phase transformations is inadequate since a variety of systems are known to exhibit transformations occurring over a wide range of temperatures. These systems show anomalous changes in specific heats and specific volumes and show evidence of premonitory phenomena. The transition temperature, T_t , in these transformations is taken to be that in which the heat capacity or the coefficient of expansion shows a maximum variation. This class of transformations has often been referred to as gradual, smeared or diffuse transformations.

The earliest attempt to treat the thermodynamics of the gradual transitions was by Ehrenfest who considered the case where the free energies as well as their differential coefficients of two forms or structures are equal, but there is a discontinuity in their

second differential coefficients. In such cases, the intersections of the G-P-T surfaces will not be sharp, but the surfaces may come into contact with each other at the transition point. According to Ehrenfest, when the G-P-T surfaces touch each other with the same slope but different curvatures at a temperature, there will be discontinuity in the second or higher derivatives of free energies:

$$(\partial^2 G / \partial T^2) = - C_p / T \quad (3)$$

$$(\partial^2 G / \partial T \partial P) = (\partial V / \partial T) \quad (4)$$

$$(\partial^2 G / \partial P^2) = (\partial V / \partial P) \quad (5)$$

The free energy-temperature curves of three typical cases are shown in Fig. I.1. The curves in Fig. I.1(a) represent transformations predicted by classical thermodynamics where the G - curves intersect sharply at a finite temperature. The diffuse transitions, on the other hand, can be represented by curves in Fig. I.1(b). Justi and Von Laue have pointed out that in gradual transitions, the third differential coefficients of G change and not the second at T_t , so that the free energy curves of forms I and II can cross each other. This argument is not entirely satisfactory since it is difficult to conceive of two forms of a substance separated by the anomaly as two phases existing on both sides of the transition point.

From the discussion above, it becomes apparent that one can distinguish, in principle, two types of transformations based on

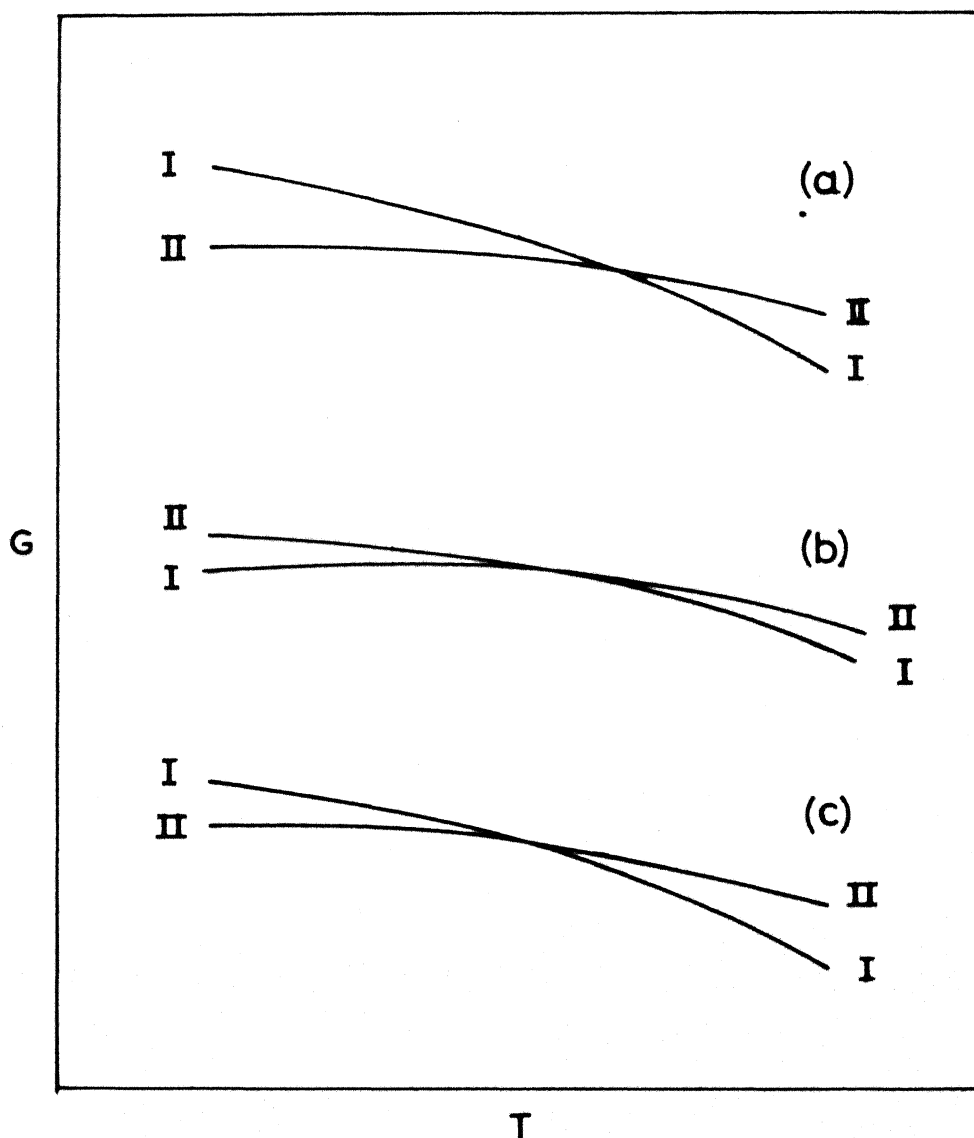


Fig.I.1 Free-energy-temperature relations in phase transformations: (a) first-order , (b) and (c) higher order.

thermodynamics. The discontinuous or the first-order transitions which follow the predictions of classical thermodynamics and the continuous (or the diffuse or the so-called second - or higher-order) transformations.

In the first-order or discontinuous transformations, the difference in the free energies of the two phases is given by:

$$\begin{aligned} 0 &= \Delta G = G_2 - G_1 = \Delta H - T\Delta S = \Delta E - T\Delta S + P\Delta V \quad (6) \\ &= \Delta E + P\Delta V - T(S_2 - S_1) \end{aligned}$$

where ΔE is the difference in internal energies of two phase; if $P\Delta V$ in a transformation is small, one can compare the stabilities of the two phases in terms of their Helmholtz free energies:

$$0 = \Delta A = \Delta E - T\Delta S = (E_2 - E_1) - T(S_2 - S_1) \quad (7)$$

According to this equation, the transformation results from the compensation of the lattice energy difference by the entropy difference at the transition temperature. The thermodynamic relations in first-order transitions are graphically represented in Fig. I.2. It can be seen that at T_t , the free energy curves intersect each other and $\Delta A = 0$. These transformations involve step-wise increase in energy with increase in temperature and show discontinuity in energy and all other properties at T_t .

Many instances are known where phase transformations are induced by application of pressure. Whenever there is a decrease in volume during a transformation, pressure would favour such a

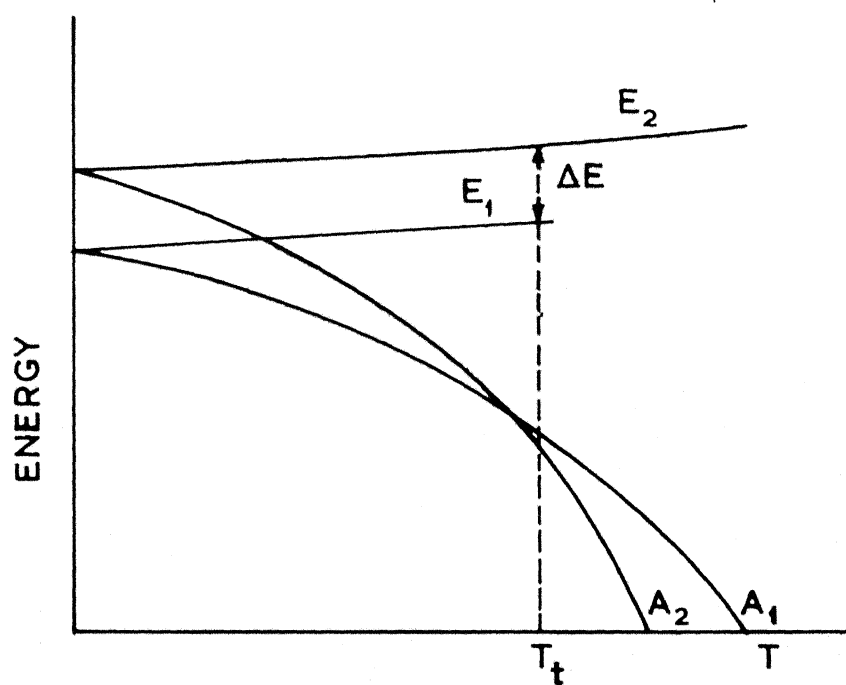


Fig.I.2 Variation of the internal energies and free energies with temperature in first order transformations.

transformation and the thermodynamic variables are simply correlated by the Clausius-Clayperon equation. Since the phase produced by the application of pressure will have a lower volume, the decrease in volume is compensated by an increase in the E or in the coordination number. The increase in entropy may be seen as a decrease in disorder.

In higher-order or continuous transformations, the energy increases gradually with temperature until T_t where the rate of increase of energy falls sharply. As a result of this, discontinuity is found in specific heats or specific volumes. Since lambda-shaped specific heat curves are generally obtained in these transformations, these are also called lambda-transformations (Fig. I.3). Second or higher-order transformations occur over a temperature interval and are generally associated with increase in disorder with rising temperature. If a solid has perfect order at absolute zero of temperature, a rise in temperature disturbs the order of the structure and with progressive increase in temperature, the structure gets more and more disordered until the transformation temperature T_t is reached. One can introduce an order parameter ξ which is equal to unity at absolute zero and becomes zero at T_t (Fig. I.3). The free energy function for such a system may be written as:

$$A(T, \xi) = E(\xi) - TS(\xi) \quad (8)$$

Although for the sake of simplicity, we may classify transformations as first-order and second-order types, in reality it is

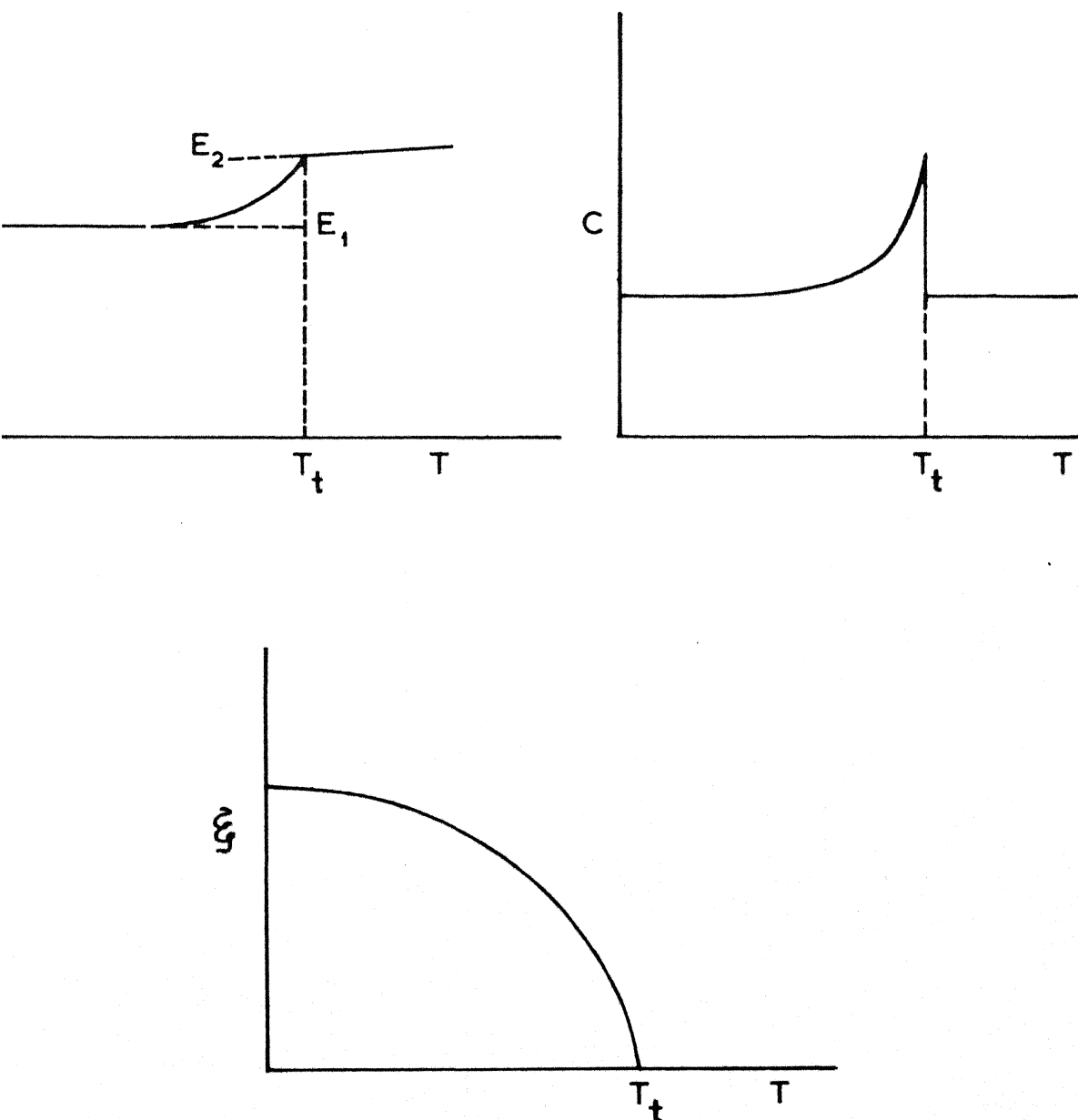


Fig. I.3. Variation of internal energy, E , specific heat, C , and the order parameter, ξ , in second (or higher) order transformations.

difficult to find out exactly whether a transformation belongs to either of these two types. By definition, first order transformation should occur sharply at one temperature and two phases of the same substance should not coexist at temperatures other than T_t . If a single crystal of a substance is taken through a transition point, the crystal should break up into a random assembly of one or more crystals of the other phase at T_t . If the temperature is then decreased below T_t , the first phase should reform randomly from the second phase and there should be no persistence of the crystal axis of the first phase.

There are a number of transformations which have been classified as first order: tin (grey-white, $\sim 19^\circ\text{C}$); cesium chloride (CsCl-NaCl , $\sim 480^\circ\text{C}$); NH_4Cl (CsCl-NaCl , $\sim 184^\circ\text{C}$); sulphur (rhombic-monoclinic, $\sim 96^\circ\text{C}$). While the transformations classified as first order are structurally discontinuous and may involve drastic variations in energy, there are indications of higher order effects (as well as of premonitory phenomena and hysteresis) in many of these transformations. Many transformation have been found to proceed through the formation of hybrid crystals where the two structures coexist within a general pattern of orientation.

There are many phase transformations which strictly belong to neither first order nor second order. For example, the ferroelectric transformation of KH_2PO_4 should theoretically be first order but conforms more closely to the second order. The transformations of BaTiO_3 and related materials show lambda-like changes in properties

as well as small changes in latent heat. There is super-position of second-order behaviour on first-order transformations in the transformations of alkali sulphates. Many transformations are actually mixed transformations and can not be placed in either category. Even the order-disorder change in second-order transformations may be seen as an abrupt change towards the termination.

Many reversible transformations show hysteresis effects either in terms of the formation of metastable structures in one of the directions or in terms of differences in the transformation temperatures in the two directions⁴. Observation of thermal hysteresis clearly shows that the equilibrium is not complete at all the stages of the transformation as required by thermodynamics. Hysteresis is a necessary consequence of the coexistence mechanism of continuous transformations. An examination of the available data on reversible transformations shows that the thermal hysteresis is related to the volume changes in the transformations; thermal hysteresis is generally small when the volume change in the transformation is small (e.g., α - β inversion in quartz).

Occurrence of metastable intermediate phases has been noted in some transformations. The metastable phases in such instances are probably related crystallographically to either of the two phases. The occurrence of a metastable phase in KNO_3 is shown in Fig. I.4. Bi_2O_3 transforms from the monoclinic phase to the cubic phase at 730°C and on cooling the cubic phase it reverts back to the monoclinic phase through a metastable tetragonal phase (Fig. I.4).

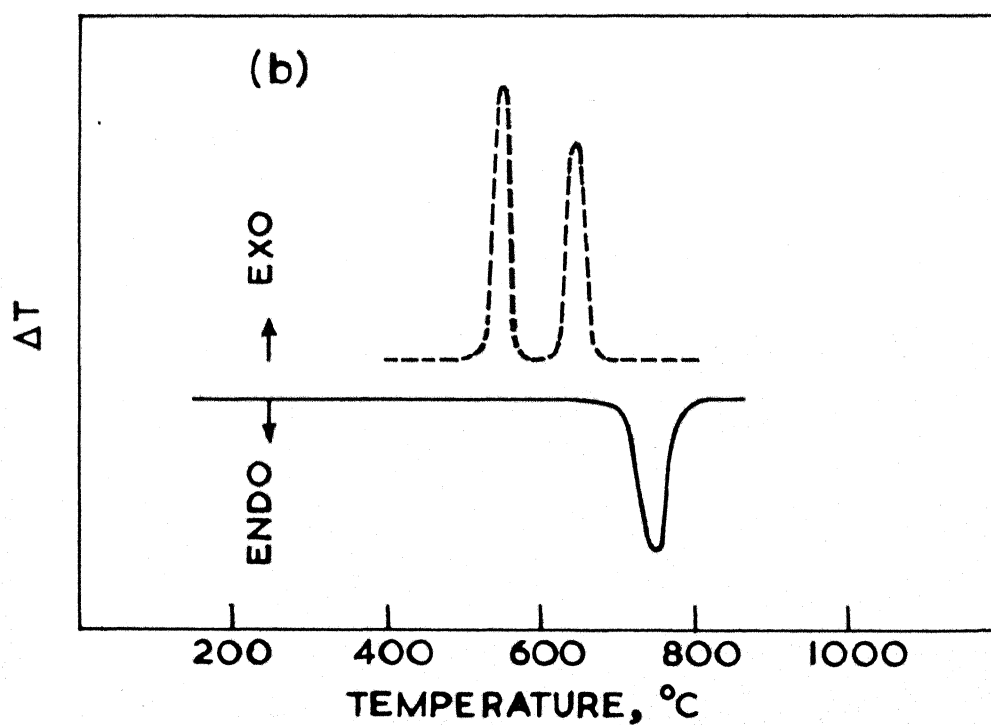
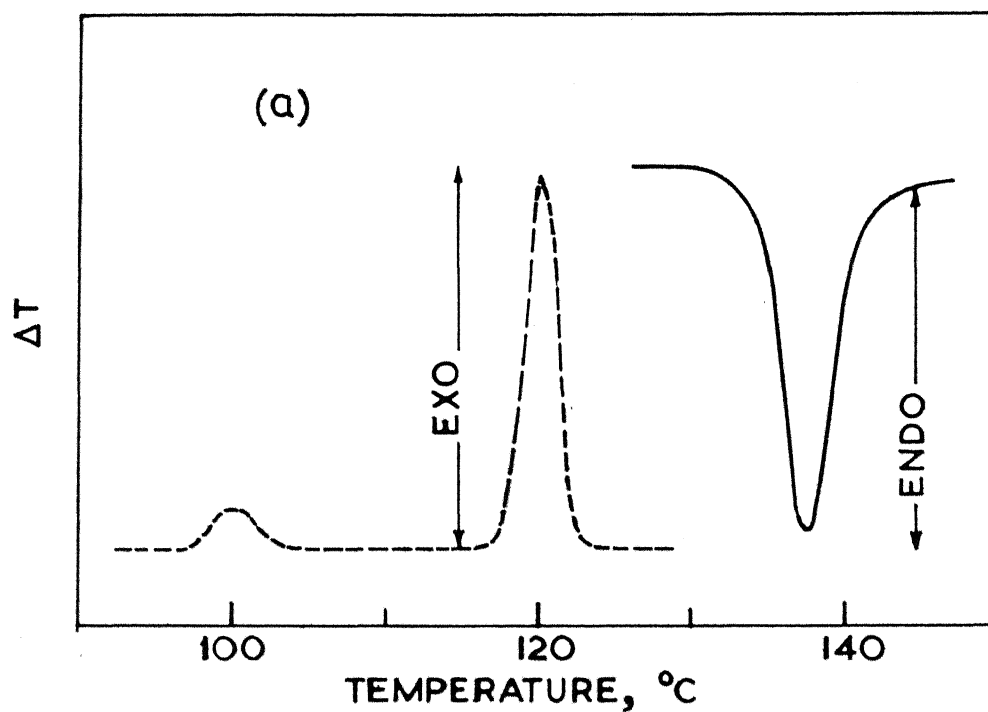


Fig.I.4. Occurrence of metastable phases as shown by DTA curves: (a) KNO_3 transformation⁴ (broken line is the cooling curve); (b) Bi_2O_3 transformation.⁵

Irreversible crystal structure transformations are found in many systems where one of the polymorphs is metastable in a particular temperature (or pressure) range. In such transformations, a polymorph transforms to the other form on heating above a particular temperature and remains in the new transformed structure even after cooling. It is not possible to assign any critical transformation temperature in an irreversible transformation and the transformation will be a function of time as well as temperature. Typical examples of the irreversible transformations are the following: anatase - rutile (cf TiO_2); aragonite-calcite (of CaCO_3); cubic-hexagonal or cubic-monoclinic (of rare-earth sesquioxides).

Simple thermodynamic considerations indicate that one polymorph of a solid can be more stable under a specified set of conditions than the others. It is however, difficult to strictly define the thermodynamic stability of a polymorph since a variety of physical factors as well as compositional differences drastically affect the stability of polymorphs markedly. Thus, if there is any difference in the stoichiometry between two polymorphs, one can not really classify them as belonging to the same polymorphic group. An interesting example of a transformation where physical factors affect the stability of a polymorph is provided by ZrO_2^6 . ZrO_2 undergoes a reversible monoclinic-tetragonal transformation at 1175°C (1035°C on cooling). The tetragonal ZrO_2 can be made stable at ordinary temperatures if the particle size is small; the stabilization is apparently due to the excess surface energy of the small particle size samples.

If different samples of a solid contain different quantities of impurities, the regions of thermodynamic stability will vary. Thus, calcium carbonate with a small amount of strontium will tend to make the aragonite phase more stable than the calcite phase⁷. Presence of small quantities of sulphate ions or other impurities in TiO_2 (anatase) enhances the temperature of transformation to rutile considerably⁸. It is therefore difficult to define the thermodynamic stability unless the detailed history of the sample including its exact chemical composition is known.

I.3 Structural Changes in Transformations

Buerger⁹ has classified various types of thermal transformations based on structural changes involving the primary or higher coordination. Transformations where there are changes in the primary coordination involve a more drastic change in energy and structure rather than those where there are changes in the higher coordination. Accordingly, one can classify thermal transformations of the first order into two categories: first coordination transformations and higher-coordination transformations.

Changes in primary coordination can take place by a reconstructive transformation, where the first-coordination bonds are broken and reformed. Such transformations will involve higher energies of activation and will be sluggish. Further, there may be no symmetry relation between the two phases. Reconstructive transformations give rise to large changes in cell dimensions,

symmetry, internal energy, specific heat etc. Typical of these transformations is the aragonite-calcite transformation of CaCO_3 (400°C) where the coordination number changes from 6 to 9. Changes in primary coordination may take place through a dilational mechanism as suspected in the thermal transformation of cesium chloride (480°C) or ammonium chloride (184°C). Dilational transformations are likely to be rapid compared to reconstructive transformations.

Many of the transformations involving changes in higher coordination may also proceed through the breaking of the primary bonds and for this reason, the energy changes and other features of the reconstructive transformations involving higher coordination may resemble those of the reconstructive first coordination transformations. Typical examples of these are the sphalerite-wurtzite (ZnS), cristobalite-tridymite-quartz (SiO_2) transformations. Transformations between polytypes may also fall under this category. The transformation of TiO_2 (anatase or brookite to rutile) involves changes in secondary coordination, but show the characteristics of first coordination transformations.

In some transformations, changes in higher coordination can be effected by a distortion of the primary bond. Such transformations may be called distortional or displacive transformations. These transformations may involve considerably smaller changes in energy and are usually fast. In the displacive transformations, the high-temperature form is usually more open and has higher specific

volume, specific heat and symmetry. Examples of displacive transformations include the high-low transformations of quartz (575°C), tridymite (160° and 105°C). Anatase (TiO_2) shows a displacive transformation prior to its transformation to rutile.

I.4 Kinetics of Transformations

The rate of a phase transformation is determined by the energy barrier opposing the process and an energy of activation will be required to surmount the energy barrier to enable the reaction to proceed. The basic equation relating rate constants with temperature in a thermal transformation is the classical Arrhenius equation:

$$k = A \exp (-E_a/RT) \quad (9)$$

where E_a is the energy of activation, k is the rate constant and A is a constant for the transformation.

The magnitude of E_a of a transformation depends on the mechanism of the transformation and the changes in coordination involved. Any transformation which involves changes in primary coordination (directly or indirectly) will need a much larger E_a than those involving changes only in higher coordination.

Phase transformations are generally initiated by the formation of a number of small particles or nuclei of the new phase which then grow until the transformation is complete. The presence of the phase boundary or surface between two phases increases the

free energy and provides the energy barrier in the kinetics of nucleation. Nucleation involves the assembly of suitable kinds of atoms or units by diffusion or some other mechanism, change of the structure into the intermediate structure(s), followed by the formation of the nuclei of the new phase. An activation energy may be associated with each of these steps, but the experimental energy of activation will refer to the rate-determining step.

Nucleation may be homogeneous or heterogeneous. Heterogeneous nucleation takes place preferentially at grain boundaries, foreign impurities or dislocations. Homogeneous nucleation can occur in the absence of such defects; once a nucleus of the new phase is formed, however, it produces an imperfection in the host structure. The number of nuclei formed per unit volume is given by,

$$n = N \exp(-\Delta G_n/RT) \quad (10)$$

where ΔG_n is the free energy of formation of a nucleus. Also,

$$\Delta G_n = \Delta G_c + \Delta G_s + \Delta G_E \quad (11)$$

where the subscripts c, s and E refer to the free energy change due to the chemical change, the surface free energy and the elastic strain energy respectively. ΔG_s and ΔG_E are both positive, while ΔG_c is negative; ΔG_c is proportional to the volume of the nuclei and ΔG_s to the surface area of the nuclei. Ignoring ΔG_E , we can therefore define the free energy change, ΔG_n , for

the formation of one nucleus as,

$$\Delta G_n' = (4/3)\pi r^3 \Delta G_c' + 4\pi r^2 \Delta G_s' \quad (12)$$

where r is the radius of the nucleus and $\Delta G_c'$ and $\Delta G_s'$ stand for the free energy change per unit volume and surface free energy per unit area, respectively. The critical size of nuclei is found by setting the derivative of equation (12), with respect to r equal to zero.

$$r^* = -2\Delta G_s' / \Delta G_c' \quad (13)$$

In Fig. I.5, the dependence of the free energy change on the radius of the nucleus is shown schematically. Imperfections in solids generally decrease $\Delta G_n'$ and favour the nucleation process. In such heterogeneous nucleation processes, the interfacial energy between the new phase and the imperfection would be an important factor.

The over-all activation energy and the transformation rate depend not only on the kinetics of nucleation, but also the propagation (or growth) processes. The propagation process may involve material transfer across the phase boundary into the new phase and the transfer into the interior of the new phase by diffusion. Each of these steps is associated with an activation energy. In experimental studies, the kinetics of phase transformations are usually discussed in terms of the rates of nucleation and the propagation steps. Most of the activation energy of a transformation is generally utilized in the nucleation process.

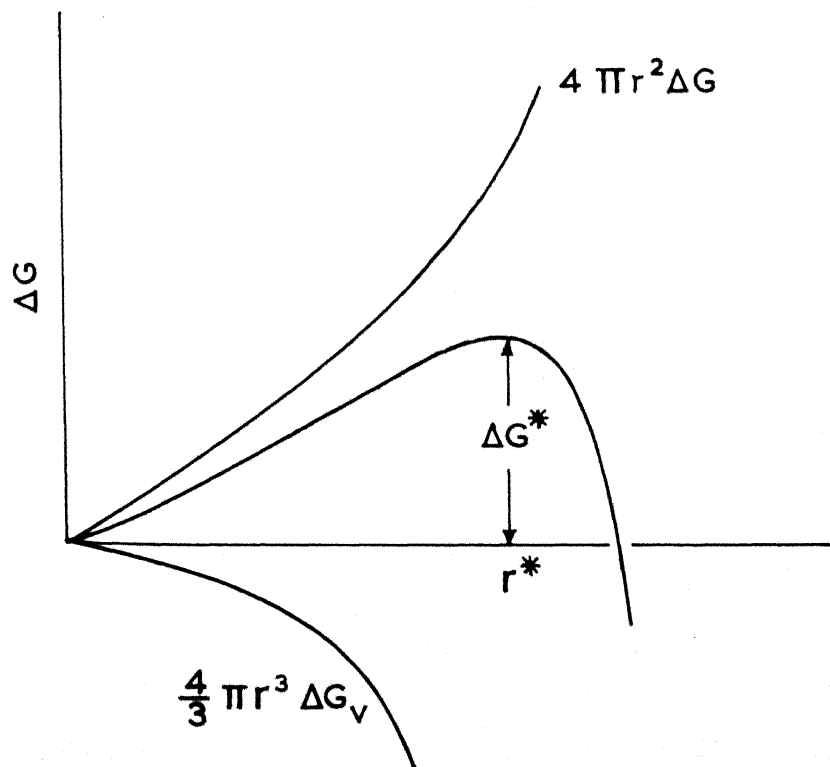


Fig. 1.5 Dependence of the free energy change upon the radius of the nucleus.

In recent years, the kinetics of various phase transformations have been reported in the literature. Thus, the kinetics of the transformation of tin¹⁰ (white - grey) are found to comply with Avrami's equation¹¹:

$$(1 - f) = \exp(-At^k) \quad (14)$$

where f is the fraction transformed, t is the time and $k = 3$. The results seem to be in agreement with the three-dimensional growth of the nuclei formed during the beginning of the transformation. For the grey-white transformation of tin the value of k varied between 1.5 and 2. The results show that the rate of nucleation and not the rate of propagation, determines the value of k . For a value of $k = 1$, the above equation (14) becomes the first order rate equation. For $k > 1$ the reaction is autocatalytic, spontaneously giving rise to nuclei after initial induction.

Several other forms of Avrami's equation^{8,12} have been employed to interpret kinetics of phase transformations, but we shall not discuss them presently. Many workers have reported that the first-order rate-law is obeyed in some crystal structure transformations. Typical of these are the transformations of brookite (TiO_2) and anatase (TiO_2) to rutile. The first-order law has also been found in the transformations of germanium dioxide¹³. Transformations of defect cubic oxides of the rare earths to the hexagonal or monoclinic forms are also found to obey the first order law^{14,15}.

I.5 Order-Disorder Transitions

Many substitutional solid solutions show ordered structure at low temperatures, if they are properly annealed. The ordered structure transforms into the disordered structure over a wide temperature range (typical of second-order transformations) and the change becomes very rapid near the transition temperature. The transformation temperature is often referred to as the curie point of order. The degree of order in the arrangement of atoms in the lattice site is measured by a long-range order parameter, s , and a local order parameter, σ . Both s and σ decrease (from a value of 1) with increase in temperature. The rate of decrease is large at T_t typical of cooperative phenomena. Good statistical theories for the variation of order and associated physical properties with temperature have been developed.¹⁶

I.6 Martensite Transformations

One of the best documented phase transformations in solids is the Martensite transformation, commonly encountered in metal systems¹⁷. Unlike the nucleation and growth transformations, the Martensite transformations proceed by coordinated movements of a large number of atoms within a relatively short time. These transformations are essentially diffusionless since the atomic displacements are very small. It is not possible to stop or slow down a martensite transformation by thermal quenching because of the high rates associated with the transformation (even at very low

temperatures). Martensite products have little in common with regard to the structure and there appears to be no simple way to predict the structure of the martensite product on the basis of the structure of the parent.

Martensite may denote the product phase resulting from the reaction or the mechanism of a specific type of phase transformation. Martensite transformations are mainly found in metal systems and originally referred to the transformation of austenite (FCC, Fe-C) to martensite (BCT). There are also some compounds which are known to show martensite transformations. NaCN which exists in the NaCl structure above 15°C ¹⁸ (and in the orthorhombic structure below this temperature) shows the presence of an ordered rhombohedral structure when heated above 150°C ; the rhombohedral structure persists even on cooling.

I.7 Ferroelectric Transformations

Ferroelectrics form a subgroup under the pyroelectrics and are characterized by the reversibility of their permanent polarization by an applied electric field¹⁹. Such a reversal gives rise to non-linear dielectric behaviour and to a hysteresis loop. In ferroelectric materials the temperature at which the free energies of the polar state and non-polar state (or the less-polar state), approach each other, is called the Curie temperature. At the Curie temperature, where $\Delta F = 0$, a phase transformation is observed as evidenced by the spontaneous polarization. In some ferroelectrics,

the temperature dependence above the Curie point follows the Curie-Weiss Law,

$$\epsilon = \epsilon_0 + (C/T - T_c) \quad (15)$$

where T_c is the Curie-Weiss temperature and C is the Curie constant. The dielectric constant becomes very large near T_c (Fig. I.6) and may be related to the susceptibility by the equation:

$$\epsilon/4\pi \approx k \quad (16)$$

Phase transformations from a ferroelectric phase I to another ferroelectric phase II, from a ferroelectric phase to a paraelectric phase or from a ferroelectric phase to an antiferroelectric phase have been observed in a variety of substances.

Accompanying these transformations one finds anomalies in heat capacity, breaks in thermal expansion curves and variations in optical properties (including vibrational spectra) in addition to changes in crystal structure and dielectric properties (Fig. I.6).

I.8 Magnetic Transitions

Many of the magnetic solids show interesting transitions at the Curie or the Néel temperature²⁰. For example, the high-temperature paramagnetic phases of ferrites (MFe_2O_4 or $MFeO_3$ where M is a metal ion) transform to the low-temperature ferromagnetic phases below the T_c . Similarly, many magnetic solids (e.g., MnO , FeO , NiO) transform to the antiferromagnetic state at the T_c . These

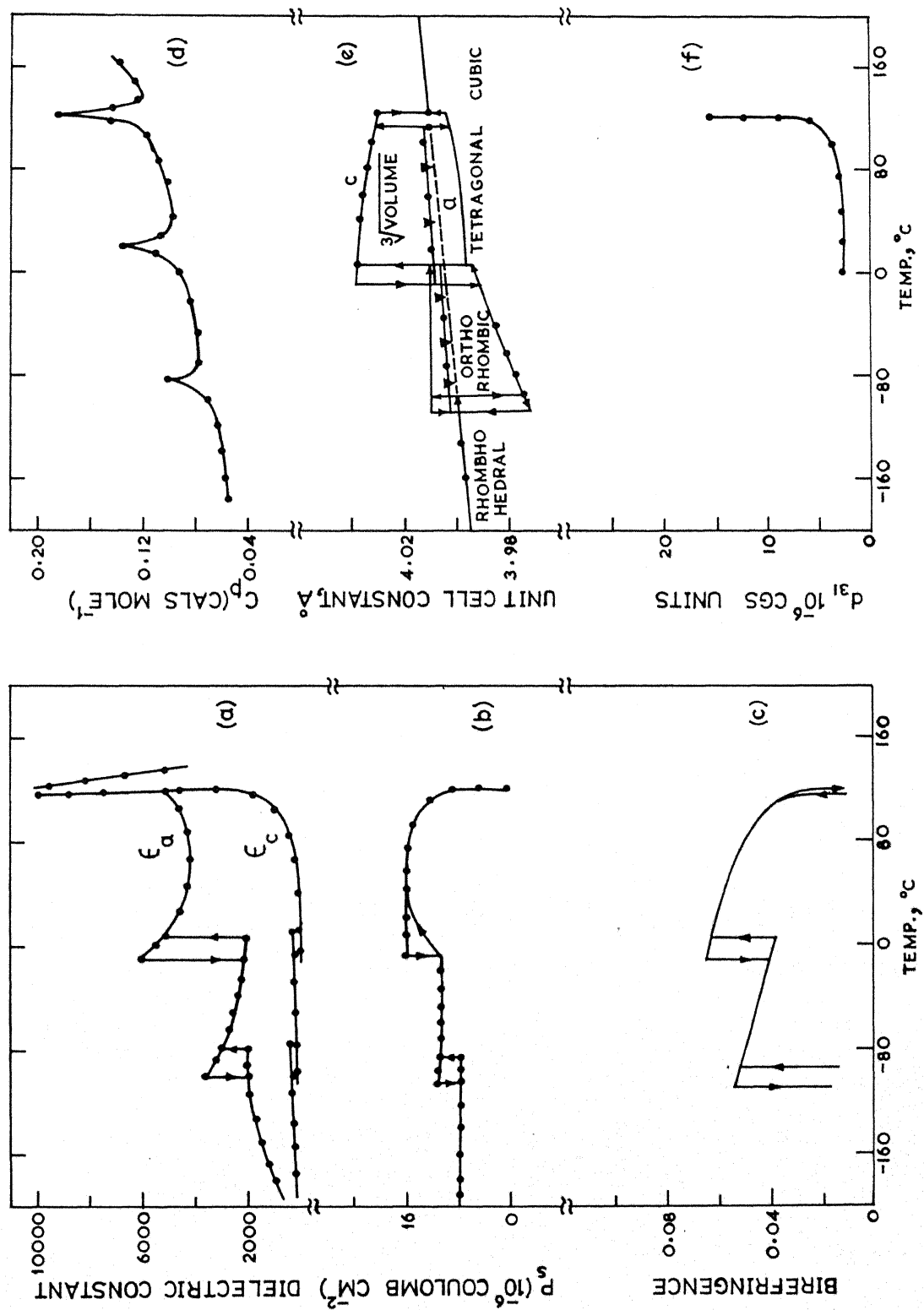


Fig. 1.6 Transformation in BaTiO_3 accompanied by changes in (a) dielectric constant (b) spontaneous polarization (c) birefringence (d) heat capacity (e) lattice dimensions and (f) piezoelectric coefficient d_{31} . (ref. 19).

transformations involve the cooperative transformation of magnetic dipoles and show the features of the order \rightleftharpoons disorder transformations. At the transition temperature marked anomalies are noticed in the specific heat, thermal expansion coefficient, electrical resistivity and magnetic susceptibility. Some of the transitions exhibit thermal hysteresis similar to first order transitions.

Besides paramagnetic \rightleftharpoons ferromagnetic and paramagnetic \rightleftharpoons antiferromagnetic transitions, magnetic solids may also undergo paramagnetic \rightleftharpoons ferrimagnetic, antiferromagnetic \rightleftharpoons ferrimagnetic or antiferromagnetic \rightleftharpoons ferromagnetic transitions.

I.9 Semiconductor-Metal Transitions

Solids have been classified as metals, semiconductors or insulators on the basis of their electrical resistivities. Many of the common substances such as NiO, MnO, Fe₂O₃, TiO₂, Pr₆O₁₁, and MnS₂ are either insulators or semiconductors. There are many inorganic compounds which are metals, typical of these being TiO, NbO, ReO₃ and CrO₂.

Some solid state materials are semiconducting upto a specific temperature at which the conductivity rises sharply by several orders of magnitude. Such semiconductor \rightleftharpoons semimetal transitions have been observed in VO₂, V₂O₃, Ti₂O₃ and a few other substances. The semiconductor \rightleftharpoons semimetal transitions are generally accompanied by marked changes in lattice dimensions, magnetic susceptibility and heat capacity of the solid²¹ (see Figs. 1.7 and 1.8).

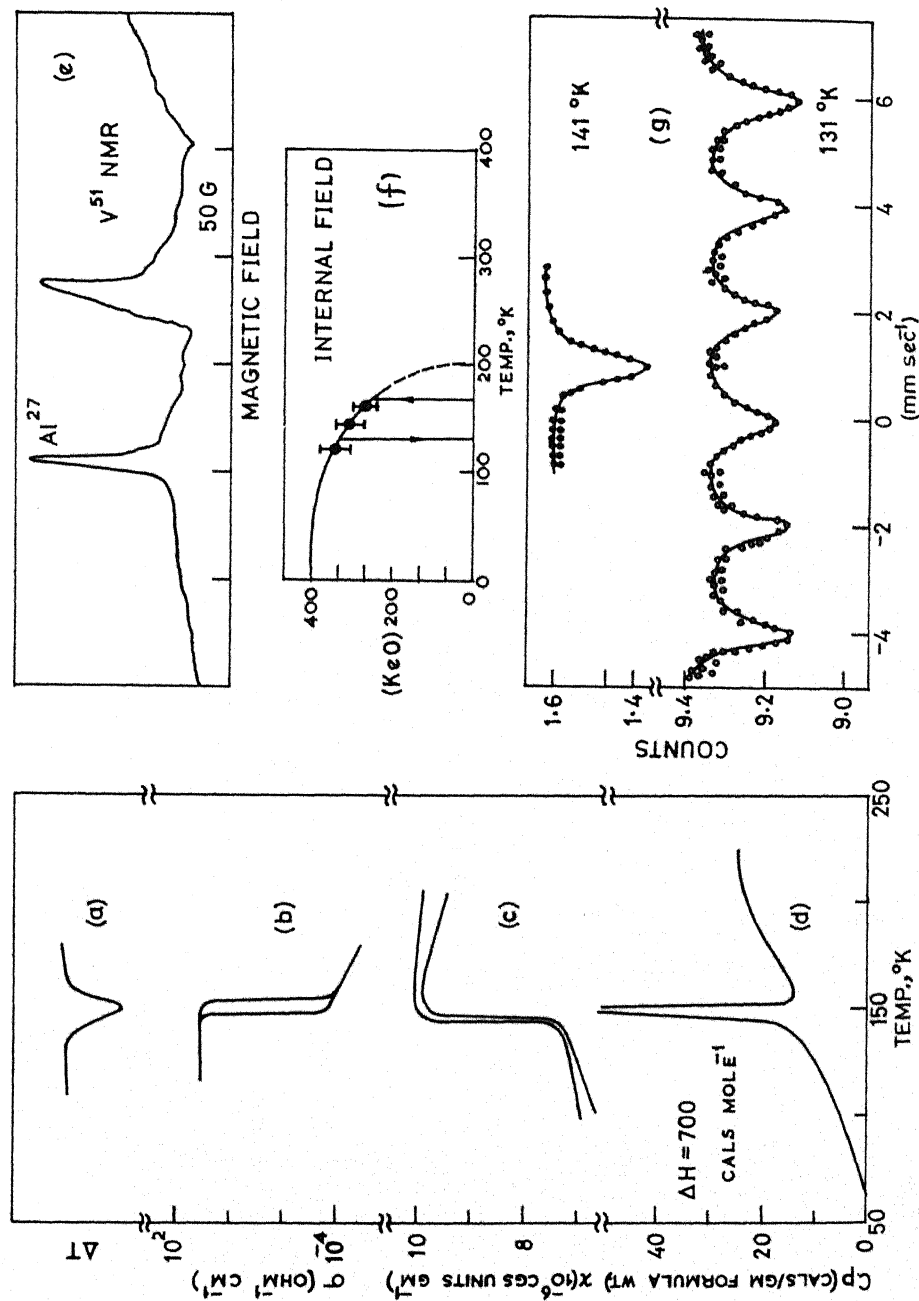


Fig. 1.7 Semiconductor-metal transition observed in V_2O_3 by (a) DTA anomaly²³(a); measurements of (b) electrical conductivity²⁴; (c) magnetic susceptibility²⁵ and (d) heat capacity as a function of temperature²⁹; (e) NMR spectrum of ^{51}V in V_2O_3 above T_t . The signal disappears below T_t ; (f) variation of internal field of ^{57}Fe doped V_2O_3 ²⁸ (g) Mössbauer spectra of ^{57}Fe doped V_2O_3 ²⁸.

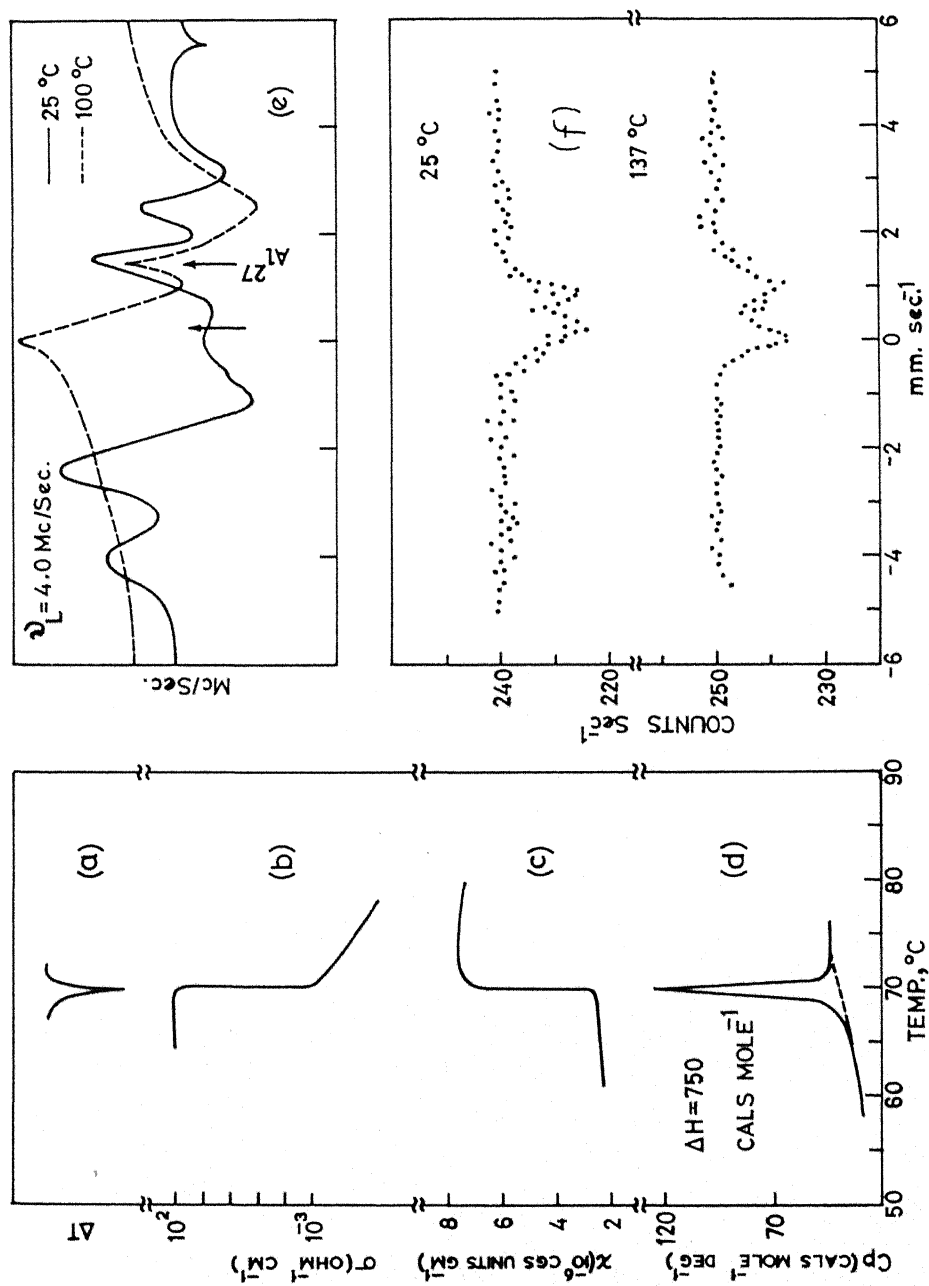


Fig. 1.8 Semicondutor-metal transition observed in VO_2 by

(a) DTA anomaly³³; measurements of (b) electrical conductivity³³ (c) magnetic susceptibility³⁰ and (c) heat capacity as a function of temperature; (e) NMR spectra of ^{51}V in VO_2 below and above T_t . (f) Mössbauer spectra of ^{57}Fe doped VO_2 below and above T_t .

The metallic conductivity above the transition temperature probably results from the formation of a conduction band through direct cation-cation (or cation-oxygen-cation) bonding since the radii of ions like Ti^{+3} or V^{+3} are quite large. In order to account for the origin of the energy gap in the low temperature phase several models have been proposed. Morin²² suggested that the transition is associated with a change from a paramagnetic to an antiferromagnetic state. Mott proposes that the substances are metallic or non-metallic depending on the degree of overlap between the 3d wave functions; the non-metallic state according to him should be in a ferromagnetic or antiferromagnetic spin arrangement. Goodenough²⁰, on the other-hand, suggests that the origin of the energy gap in the low-temperature phase is not magnetic ordering but a change in chemical bonding (due to the pairing of neighbouring cations). Adler and Brooks²³ have proposed that the transition originates from crystalline distortion and is not related to magnetic ordering. We shall now briefly examine the features of some of the semiconductor-semimetal transitions.

V_2O_3 has the corundum structure (rhombohedral symmetry) at room temperature and transforms to a monoclinic symmetry around 150°K with a volume change of 3.5% and thermal hysteresis of about 18°. The electrical resistivity changes from 10^4 to 10^{-3} ohm cm at the transition temperature T_t^{24} . The magnetic susceptibility also shows an anomaly at T_t^{25} . Recent neutron diffraction studies have shown evidence of magnetic ordering in the low temperature phase²⁶, NMR (V^{51})²⁷ and Mossbauer studies²⁸ also establish antiferromagnetic

ordering in this phase (see Fig. I.7 for changes in various properties at T_t). A specific heat anomaly is seen to accompany the transformation²⁹. If the antiferromagnetism of the low-temperature phase is ignored the Goodenough model appears to be satisfactory in explaining the gross features of the transition.

VO_2 transforms from monoclinic phase (MoO_2 type) to tetragonal phase (rutile type) at 340°K . There is also an appreciable thermal hysteresis ($\sim 15^\circ$). Magnetic susceptibility measurements³⁰ as well as NMR (V^{51})³¹ and Mossbauer studies³² show no evidence of magnetic ordering in VO_2 . The electrical resistivity shows a sharp transition at 340°K ³³ (with a change by a factor of 10^5). All the experimental observations (see Fig. I.8 for changes in various properties at T_t), seem to fit the model of Goodenough. As one would expect, the magnitude of the change in susceptibility accompanying the magnetic transition of VO_2 decreases in solid solutions of $\text{VO}_2\text{-TiO}_2$ as the percentage of TiO_2 is increased³⁴.

Unlike V_2O_3 and VO_2 , Ti_2O_3 (corundum structure) shows an electrical transition over a wide range of temperatures ($390\text{--}470^\circ\text{K}$) which is not accompanied by a change in crystal symmetry. The lattice dimensions, however, show abrupt changes in the same temperature range. The volume change in the transition is about 7%. Recent neutron diffraction studies show no evidence of antiferromagnetic ordering in Ti_2O_3 . The magnetic susceptibility shows a small change around the transition temperature. The transition is also evidenced by a specific heat anomaly. All the experimental

observations on the Ti_2O_3 transition can be explained in terms of the distortions of the unit cell and the accompanying changes in the band gap. Interestingly, it is found that a solid solution of 10% V_2O_3 in Ti_2O_3 does not show the electrical transition; instead it is metallic throughout the temperature range. The lattice parameters of this solid solution are nearly the same as the corresponding values for pure Ti_2O_3 after it undergoes the transition.

I.10 High Pressure Transformations

Considerable progress has been made in recent years in attaining high pressures³⁵ and these new developments have made it possible to examine the P-V-T relations as well as various phenomena in solids under high pressures. High pressures may be produced by static methods or by the shock method. Crystal structure changes under high pressures have been studied in a variety of systems by employing optical, x-ray diffraction and electrical measurements. The high pressure phases are always more dense and are generally associated with higher coordination numbers. In addition to phase changes, other interesting changes in physical properties are often noticed under the influence of high pressures. Thus, many insulators are transformed into metals at high pressures; graphite is converted to diamond at high pressures and temperatures.

Pressure transformations of different kinds have also been studied in alloys (two component system). The types of transformations studied include the diffusionless martensite transformations and the order-disorder transformations.

The reconstructive transformation of graphite to diamond has been recently shown to take place under high pressures; the transformation is accompanied by a change in the coordination of carbon from 3 to 4. It has been shown that diamond on application of pressure transforms to a metallic state. It is interesting to note that while yellow phosphorus does not give any new modification under pressures upto $20,000 \text{ kg. cm}^{-2}$, the red phosphorous exhibits a reversible transformation even at about 4000 kg. cm^{-2} and at 600°C .

The halides of potassium and rubidium have been shown to transform from the rock salt structure to the CsCl structure under pressure. The fluorides do not exhibit any change in structure under these conditions. The pressure transformation data of alkali halides have been successfully employed in the calculation of lattice energies and repulsive parameters in ionic halides (see section I.11). Calcium carbonate undergoes a transformation from calcite to aragonite on application of pressure; the transformation is reconstructive and is accompanied by a change in the primary coordination. The transformation of aragonite to calcite takes place on heating. The same change is also effected by grinding. TiO_2 and AgI are wellknown examples where grinding produces the more stable form at the temperature of grinding. The transformation takes place under the influence of shearing-stresses superimposed on quasi-static pressures as verified in the transformations of SiO_2 (quartz - coesite), and CaCO_3 (calcite-aragonite). Trans-

formations which do not normally take place below 300°C can be made to occur between 0° and 100°C by the application of displacive shearing stresses; rates of reactions are also considerably enhanced.

In the transformation of quartz to coesite at high pressures only changes in the secondary coordination take place, coesite having higher secondary coordination. The transformation temperature of high-low quartz is decreased by application of pressure. The coordination number increases with increasing pressures as evidenced in the case of aluminium silicates.

High pressure pulses of a short duration can be accomplished by the 'shock method'. Shock produced phase transition studies have been investigated and compared with studies of transition under static pressures. Under shock-induced pressures, no transition is possible unless the phase change can occur within a microsecond, and instead, the system may remain in a metastable state. Application of a one-dimensional shock to a sodium chloride single crystal in different orientations indicated that the decrease in the interatomic distances is in part compensated by the redistribution of atoms. The static and shock data do not differ much. Potassium chloride transformed within the shock time and on removing the shock, the crystal assumed the original structure; the transformation is reversible well within one μ sec. since the pressure release is very fast. Red phosphorus was known to transform to the black variety at ~ 45 kbars at room temperature

in the presence of shear. But with shock technique, the transformation takes place around 30 kbars. Diamond becomes metallic at about 600 kbars. The transformation of iodine to metallic iodine takes place at about 240 kbars.

I.11 Born Treatment of the Phase Transformations in Alkali Halides

The Born expression³⁶ for the potential energy of an ionic solid as modified by Huggins and Mayer³⁷ is given by:

$$U = (\mathcal{L}e^2/r) + (C/r^6 + D/r^8) - B(r) + \phi_0 \quad (17)$$

where U is the lattice energy of the ionic solid per pair of ions, r , the equilibrium interionic distance, ϕ_0 , the zero point energy, C and D are the van der Waals terms for dipole-dipole and dipole quadrupole interactions respectively. Different forms of the repulsive energy $B(r)$ have been employed in the literature. The most general form of the repulsive term is given by the four parameter expression:

$$B(r) = M_1 b_1 \exp(-r/\rho_1) + M_2 b_2 \exp(-ar/\rho_2) \quad (18)$$

in which M_1 and M_2 are the numbers of nearest and next to nearest neighbours, b_1 , b_2 , ρ_1 and ρ_2 are repulsive parameters and a is the ratio of the distance between next-to-nearest and nearest neighbours. Other forms of equation (18) have been employed by (i) setting $\rho_1 = \rho_2$ (three parameters) (ii) by setting $b_1 = b_2$ and $\rho_1 = \rho_2$ (two parameters) or (iii) by ignoring the second term

due to the non-nearest neighbour interactions. Equation (17) with a two parameter repulsive term has not been very successful in explaining the relative stabilities of the $Fm\bar{3}m$ and $Pm\bar{3}m$ structures of the alkali halides^{36,38-42}.

In an attempt to explain the greater stability of the $Pm\bar{3}m$ structure of CsCl, May³⁸ assumed a higher van der Waals term with a three parameter repulsive term given by:

$$U = (\alpha e^2/r) + K(C/r^6 + D/r^8) - B(r) + \phi_0 \quad (19)$$

where $K = 3.6$ and $B(r)$ is given by equation (18) with $\rho_2 = \rho_1$. Tosi and Fumi³⁹ have objected to the use of higher values of $K > 1$ and have instead employed structure-dependent repulsive parameters to explain the pressure transitions of alkali halides of $Fm\bar{3}m$ structures. The use of three or four-parameter repulsive term in the phase transition studies necessitates employing $K > 1$ in most alkali halides; otherwise b_2 comes out to be negative.

Rao and coworkers⁴²⁻⁴⁴ have examined the pressure transitions of several alkali halides as well as the thermal transformation of CsCl and its solid solutions with RbCl, KCl and CsBr, in some detail, by employing the four parameter repulsive term. They have obtained satisfactory solutions by employing $K > 1$ (equation 19). They find, however, that at a critical value of $K (=K^*)$, b_2 changes sign from negative to positive (i.e., $b_2 = 0$). Rao and coworkers⁴²⁻⁴⁴ could therefore employ $K = K^*$ and the associated repulsive terms as well to obtain

satisfactory solutions. The need for increased van der Waals term has been established by Rao and coworkers^{43,45} by employing the new van der Waals coefficients of Hajj⁴⁶ and Lynch^{46a}, to obtain solutions for phase transitions of alkali halides.

I.12 Experimental Techniques for the Study of Phase Transformations

A variety of techniques have been employed for the study of phase transformations in addition to x-ray diffraction which is an essential part of the study of any crystal structure transformation. Once a phase transition is identified in a solid by anyone of the usual techniques, one has to investigate the same, by other methods depending on the particular properties of interest. We recall the various methods listed in sections I.7 and I.9 in the study of Ferroelectric as well as semiconductor-to-metal transitions. The transformation of KNO_2 provides another interesting example where a variety of methods (Fig. I.9) of particular importance have been employed to study the transformation⁴⁷. The reversible transition of KNO_2 was established by differential thermal analysis (DTA); x-ray diffraction was utilized to prove that the change was from monoclinic to cubic structure. Based on their crystal structures and also analogy with NaNO_2 ⁴⁸, it was suspected that the transformation may be associated with a change from a ferroelectric to a paraelectric state. Accordingly, the dielectric hysteresis loop disappeared around 40°C (Curie temperature); the dielectric anomaly was also

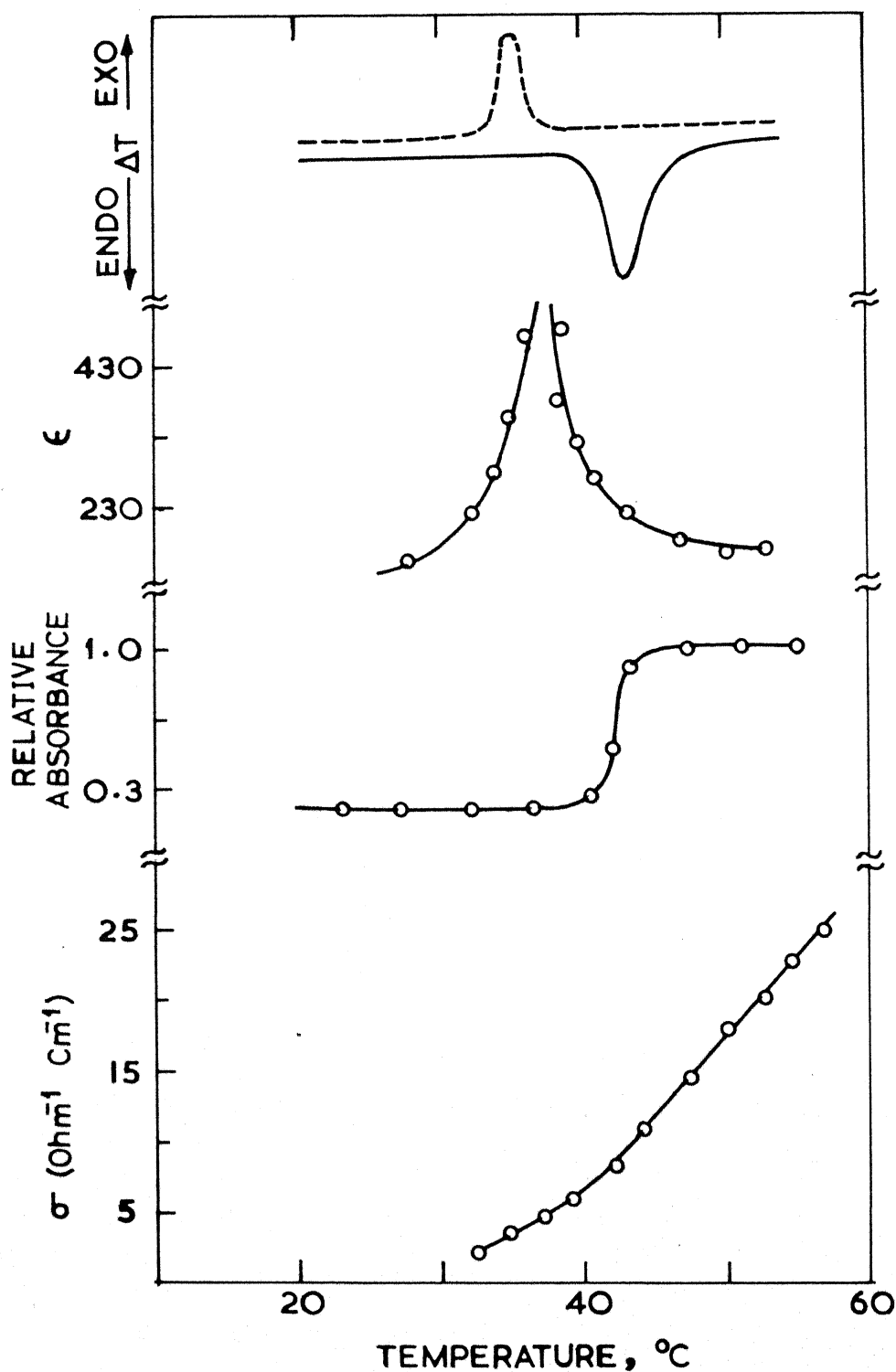


Fig.I.9. Investigation of the ferroelectric transition in KNO_2 ⁴⁷ by (a) DTA anomaly ; (b) dielectric constant (c) absorption spectra (IR) and (d) electrical conductivity measurements as a function of temperature.

observed at this temperature. A plot of electrical conductivity against temperature indicated a break at $\sim 40^\circ\text{C}$. A study of the temperature-dependent infrared spectrum of KNO_2 showed that the absorbance of the NO_2 deformation frequency (830 cm^{-1}) showed a marked increase in intensity at the Curie temperature⁴⁷; this is similar to the behaviour observed in the ferroelectric-paraelectric transformation of KNO_3 ⁴⁹. Literature is replete with many such examples where several techniques have been employed to examine the phase transformation in solids.

X-ray diffraction methods are by far the most important tools for the study of crystal structure transformations. Identification of structures of various phases by x-ray diffraction is very essential irrespective of what other techniques one employs to identify or examine the changes in the system accompanying the transformation. Single crystal work with Laue and Weissenberg photographs are particularly useful for a detailed knowledge of the mechanism of the phase transformation. Thus, Ubbelohde and co-workers^{49a} have examined the co-existence of phases or formation of hybrid crystals during transformations. Change in the intensities of the x-ray lines also furnish valuable information. Single crystal studies enable one to find out the persistence or otherwise of the crystal axis throughout the transformation. Neutron diffraction has been employed effectively as a tool to examine the positions of light atoms as well as to study magnetic structures. For example, the antiferromagnetism of the semiconducting phase of V_2O_3 or the absence of antiferro-

magnetism in Ti_2O_3 could be established conclusively by neutron diffraction studies.

The microscope has proved a very valuable tool for studying phase transformations, particularly with respect to movement of boundaries, growth of nuclei and changes in grain size. Many pressure transitions are directly identified by optical methods.

Both electronic and infrared spectroscopy are useful tools provided a characteristic absorption band of the substance shows variations during a transformation. Thus, the phase transitions of KNO_3 , NaNO_3 ^{49,50} and KNO_2 ⁴⁷ have been examined by infrared spectroscopy⁵¹.

Wide line NMR has been useful in the study of transformations containing the suitable nuclei. Gutowski and coworkers^{52,53} examined the phase transformations in NaCN and NaHS employing NMR spectroscopy. ESR spectroscopy has been employed to study phase transformations by doping a crystal undergoing the transition with a paramagnetic ion.

Electrical measurements such as (a. c. or d. c.) conductivity and dielectric constant are important techniques for the study of phase transformations. The transitions are indicated by a break in the conductivity versus temperature curves. For instance, the transformations of CsCl ⁵⁴ (CsCl structure \rightleftharpoons NaCl structure) and rare earth sesquioxides⁵⁵ (cubic \rightleftharpoons hexagonal)

have been examined by measuring the electrical conductivity as a function of temperature. Electrical conductivity measurements are particularly useful in the study of order-disorder transformations of alloys and semiconductor-metal transitions. Needless to point out the importance of dielectric constant measurements in the study of transformations associated with ferroelectricity. Many other transformations (e.g. kinetics of anatase-rutile transformation) have also been examined by dielectric measurements.

Magnetic transitions (paramagnetic \rightleftharpoons ferromagnetic) or paramagnetic-antiferromagnetic) are generally studied by employing magnetic susceptibility measurements. Changes of magnetic anisotropy as a function of temperature has also been used to study polymorphic changes. Mossbauer spectroscopy containing (or doped with) the appropriate nuclei provides valuable information on such transitions if the spectra are recorded at different temperatures.

Measurements of heat capacities as a function of temperature are valuable in the study of phase transformations (particularly in the case of second or higher order transitions). Differential thermal analysis is another powerful tool in the study of phase transformations. This technique has been employed to study the enthalpy change, activation energy and thermal hysteresis in transformations^{4,56}.

In principle, any technique that can measure a property of the substance which undergoes marked change during the transformation can be employed for the study of phase transformations. Dilatometric

measurements, change in Young's modulus, thermal expansion of solids are some of the important classical methods employed for the study of phase transformations.

REFERENCES

1. A.R. Ubbelohde, *Quart. Rev.*, 11, 246 (1957).
2. C.N.R. Rao and K.J. Rao, in 'Progress in Solid State Chemistry', ed. by H. Reiss, Vol. 4 (Pergamon Press, Oxford, 1967).
3. "Phase Transformations in Solids" ed. by R. Smoluchowski, John Wiley & Sons, Inc., New York (1957).
4. K.J. Rao and C.N.R. Rao, *J. Materials Sci.*, 1, 238 (1966).
5. C.N.R. Rao, G.V. Subba Rao and S. Ramdas, *J. Phys. Chem.*, 73, 672 (1969).
6. R.C. Garvey, *J. Phys. Chem.*, 69, 1991 (1965).
7. G.V. Subba Rao, M. Natarajan and C.N.R. Rao, *J. Am. Ceramic Soc.*, 51, 179 (1968).
8. S.R. Yoganarasimhan and C.N.R. Rao, *Trans. Faraday Soc.*, 58, 1579 (1962).
9. M.J. Buerger, in "Phase Transformations in Solids" ed. by R. Smoluchowski, John Wiley, New York, 1957.
10. W.G. Buergers and L.J. Gruen, *Discussions of the Faraday Soc.*, 23, 183 (1957).
11. M. Avrami, *J. Chem. Phys.*, 81, 988 (1951).
12. J.H. de Boer, *Discussions of the Faraday Soc.*, 23, 171 (1957).
13. Y. Kotera and M. Yonemura, *Trans. Faraday Soc.*, 59, 147 (1963).
14. Unpublished results of C.N.R. Rao and coworkers from this laboratory.
15. S. Stecura, U.S. Bur. Mines Report. 6616 (1965).
16. F.C. Nix and W. Shockley, *Rev. Modern Phys.*, 10, 1 (1938).
17. J.W. Christian, "The Theory of Transformations in Metals and Alloys Pergamon Press, Oxford (1965).
18. L.A. Seigel, *J. Chem. Phys.*, 17, 1146 (1949).
19. F. Jona and G. Shirane, "Ferroelectric Crystals", (Pergamon Press, New York, 1962).

20. J.B. Goodenough, "Magnetism and the Chemical Bond", (Interscience Publ, Inc. and John Wiley Inc., New York, 1963).
21. "International Conference on the Metal-Non-Metal Transitions", San Francisco, California, USA, March, 1968, Publ. in Rev. Modern Physics, 40(4), 677-844 (1968).
22. F.J. Morin, Phys. Rev. Letters, 3, 34 (1959).
23. D. Adler and H. Brooks, Phys. Rev., 155, 826 (1967).
- 23a. K. Kosuge, J. Phys. Chem. Solids, 28, 1618 (1967).
24. J. Feinleib and W. Paul, Phys. Rev., 155, 841 (1967).
25. P.H. Carr and E. Foner, J. Appl. Phys., 31, 345S, (1960).
26. H. Kendrick, A. Arrott and S.A. Werner, J. Appl. Phys., 39, 535 (1968).
27. E.D. Jones, Phys. Rev., 137, A 978 (1965).
28. T. Shinjo and K. Kosuge, J. Phys. Soc., (Japan), 21, 2622 (1966).
29. C.T. Anderson, J. Am. Chem. Soc., 564 (1936).
30. T. Kawakubo and T. Nakagawa, J. Phys. Soc., Japan, 19, 517 (1964).
31. J. Umeda, H. Kusumoto, K. Narita and E. Yamada, J. Chem. Phys., 42, 1458 (1965).
32. C.N.R. Rao and coworkers (to be published)
33. M. Natarajan, G.V. Subba Rao and C.N.R. Rao (to be published).
34. S.M. Ariya and G. Grossmann, Soviet Physics, Solid State, 2, 1166 (1960).
35. 'Solids Under Pressure', ed. by W. Paul and D.M. Warchauner, McGraw-Hill, New York (1963).
- 36a. M. Born and K. Huang, "Dynamical Theory of Crystal Lattices", Oxford University Press (1954).
- 36b. M. Born and J.E. Mayer, Z. Phys., 75, 1 (1932).
37. M.L. Huggins and J.E. Mayer, J. Chem. Phys., 1, 637 (1933).
38. A. May, Phys. Rev., 52, 339 (1937); 54, 629 (1938).

39. M.P. Tosi and F.J. Fumi, J. Phys. Chem. Solids, 23, 359 (1962).
40. R.B. Jacobs, Phys. Rev., 54, 468 (1938).
41. F. Hund, Z. Phys., 34, 833 (1925).
42. K.J. Rao, G.V. Subba Rao and C.N.R. Rao, Trans. Faraday Soc., 63, 1013 (1967).
43. M. Natarajan, K.J. Rao and C.N.R. Rao, Trans. Faraday Soc., 65, 0000, (1969) (in print).
44. K.J. Rao and C.N.R. Rao, Proc. Phys. Soc., (London) 91, 754 (1967).
45. K.J. Rao, G.V. Subba Rao and C.N.R. Rao, J. Phys. C (Proc. Phys. Soc.), Ser. 2, 1, 1134 (1968).
46. F. Hajj, J. Chem. Phys., 44, 4618 (1966).
- 46a. D.W. Lynch, J. Phys. Chem. Solids., 28, 1941 (1967).
47. K.J. Rao and C.N.R. Rao, Brit. J. Appl. Phys., 17, 1653 (1966).
48. S. Tanisaki, J. Phys. Soc. Japan, 18, 1181 (1963).
49. R.K. Khanna, J. Lingscheid and J.C. Decius, Spectrochim. Acta, 20, 1109 (1964).
- 49a. A.R. Ubbelohde in "Reactivity in Solids", ed. by J.H. De Boer, Elsevier Publishing Co., Amsterdam (1961).
50. R.M. Hexter, Spectrochim. Acta, 10, 281 (1958).
51. C.N.R. Rao, "Chemical Applications of Infrared Spectroscopy" (Academic Press, New York, 1963).
52. C.K. Coogan and H.S. Gutowski, J. Chem. Phys., 40, 3419 (1964).
53. C.K. Coogan, G.G. Belford and H.S. Gutowski, J. Chem. Phys., 39, 3061 (1963).
54. I.M. Hoodless and J.M. Morrison, J. Phys. Chem., 66, 557 (1962).
55. P.N. Mehrotra, G.V. Chandrashekar, E.C. Subba Rao and C.N.R. Rao, Trans. Faraday Soc., 62, 3582 (1966).
56. M. Natarajan, A.R. Das and C.N.R. Rao, Trans. Faraday Soc., 65, 3081 (1969).

CHAPTER II

Pm3m-Fm3m TRANSFORMATIONS OF ALKALI HALIDES

CHAPTER II

Pm3m - Fm3m TRANSFORMATIONS OF ALKALI HALIDES*

Solid solutions of CsCl
with KCl, CsBr and SrCl₂

II.1 INTRODUCTION

Cesium chloride transforms from the CsCl structure (Pm3m) to the NaCl structure (Fm3m) around 480°C¹. The transformation is thermodynamically first order and is associated with considerable thermal hysteresis. The Pm3m - Fm3m transformations of CsCl and other alkali halides have been examined in this laboratory in some detail by employing the Born treatment of ionic solids^{2,3}. The Born-Mayer expression with four repulsive parameters seems to explain the relative stabilities of the Pm3m and Fm3m structures fairly satisfactorily. Further, this treatment also accounts for the stabilization of solid solutions of CsCl with RbCl in the Fm3m structure; earlier studies² indicate that the behaviour of CsCl-KCl solid solutions appears to be similar to that of CsCl-RbCl solid solutions. On the otherhand, in the

* A paper based on this work has been published in Transactions of Faraday Society, 65, 0000 (1969).

transformation of CsCl-CsBr solid solutions, the transformation temperature seems to increase with the percentage of CsBr^{4,5}.

We have presently studied the transformation of the CsCl-KCl and CsCl-CsBr solid solutions with a view to find out the limitations and applicability of the Born treatment in explaining the entirely different behaviours shown by these two systems of solid solutions. Such a study would be of value since theoretical approaches to explain the relative stabilities of structures of ionic solids have hitherto not been very successful. We feel that it is important to be able to explain the relative stabilities of at least the two simplest structure types in ionic solids, viz., the NaCl and CsCl structures. Another aspect of interest in the present study was to find out whether the first order characteristics of Pm $\bar{3}$ m-Fm $\bar{3}$ m transitions are retained in the solid solutions. For this purpose we have examined the crystallography of the Pm $\bar{3}$ m and Fm $\bar{3}$ m phases of the solid solutions as a function of temperature; on the basis of these data, coefficients of expansion, α , of the two structures have also been estimated.

Menary, Ubbelohde and Woodward¹, reported that a large increase in vacancies occurs during the transformation of CsCl. It is also known that the formation energy of a Schottky pair in CsCl is considerably lower in the Pm $\bar{3}$ m phase compared to the Fm $\bar{3}$ m phase^{6,7} (see also Chapter III). We have now examined the Pm $\bar{3}$ m-Fm $\bar{3}$ m transformations of two CsCl-SrCl₂ solid solutions to find out whether the vacancies produced by the incorporation of Sr⁺² favour the transformation.

II.2 RESULTS AND DISCUSSION

(a) CsCl-KCl solid solutions

The results on the transformation of various CsCl-KCl solid solutions are summarized in Table II.1, and typical differential thermograms are shown in Fig. II.1. The lattice dimensions (at 25°C) of the Pm3m and Fm3m forms of the solid solutions are also given in Table II.1. The a_0 values of both the forms decrease with the increase in percentage of KCl. The calculated value of the change in molar volume accompanying the transformation, ΔV , increases slightly with the percentage of KCl (Fig. II.2) suggesting thereby that the transformation remains first order (thermodynamically) even in the solid solutions.

The volume coefficient of expansion of the Pm3m and Fm3m phases of pure CsCl are found to be 1.25×10^{-4} and $1.50 \times 10^{-4} \text{ deg}^{-1}$ respectively, in the transition region. The η^{Fm3m} values for the solid solutions determined experimentally are given in Table II.1 along with the calculated values of η^{Pm3m} . The ratio $\eta^{\text{Pm3m}}/\eta^{\text{Fm3m}}$, is about 0.30 for pure CsCl, a value which satisfactorily accounts for the melting behaviour of CsCl⁸. The $\eta^{\text{Pm3m}}/\eta^{\text{Fm3m}}$ ratio for CsCl - KCl solid solutions increases in the range 0.80 to 2.60 with the % of KCl. The melting points of these solid solutions are known to decrease slightly with % KCl.

The results from DTA and x-ray studies (Table II.1) indicate that the Pm3m-Fm3m transformations of CsCl-KCl solid solutions is reversible only upto about 3% KCl. With further increase in the

TABLE II.1

Pm3m-Fm3m Transitions of CsCl - KCl Solid Solutions

% KCl (mole)	T _t , °C forward (DTA peak)	T _t , °C reverse (DTA peak)	ΔH _{tr} cals mole ⁻¹	E _a Kcal mole ⁻¹	a _o , Pm3m 25°C	a _o , Fm3m 570°C	a _o , Fm3m 25°C (extrapolated)	ΔV(25°C) (c)	η _{Pm3m} deg ⁻¹	η _{Fm3m} deg ⁻¹ (e)
0	479	444	580	180	4.1210	7.0980	6.9050	7.34	1.25x10 ⁻⁴	1.5x10 ⁻⁴
2.5	470	-	520	114	4.1125	7.0750	6.8960	7.48	2.24x10 ⁻⁴ (d)	2.8x10 ⁻⁴
5.0	470	-	465	100	4.1000	7.0630	6.8820	7.49	2.16x10 ⁻⁴ (d)	2.7x10 ⁻⁴
10.0	470	-	420	-	4.0760	7.0250	6.8580	7.61	1.20x10 ⁻⁴	1.2x10 ⁻⁴
20.0	470	-	258	-	4.0400	7.0100	6.8100	7.83	2.60x10 ⁻⁴	1.0x10 ⁻⁴
25.0	no transition	-	-	-	-	-	-	-	-	-

(a) The a_o (Pm3m) of pure KCl found by linear extrapolation was 3.65 Å (3.76 Å is the value calculated by assuming a_o (Pm3m)/a_o (Fm3m) = 0.598).

(b) The a_o (Fm3m) of pure KCl found by linear extrapolation was 6.30 Å (NBS value = 6.295 Å).

(c) Change in molar volume.

(d) The η_{Pm3m} values in these solid solutions were calculated assuming a_o (Pm3m)/a_o (Fm3m) ≈ 0.598; the η_{Pm3m} / η_{Fm3m} values are in the range 0.8 - 2.6, the value increasing with % KCl in the solid solution. The η_{Pm3m} / η_{Fm3m} for pure CsCl and the solid solutions with 10% and 20% KCl are obtained from experimental a_o values.

(e) Calculated from a_o values in the temperature range, 500-570°C.

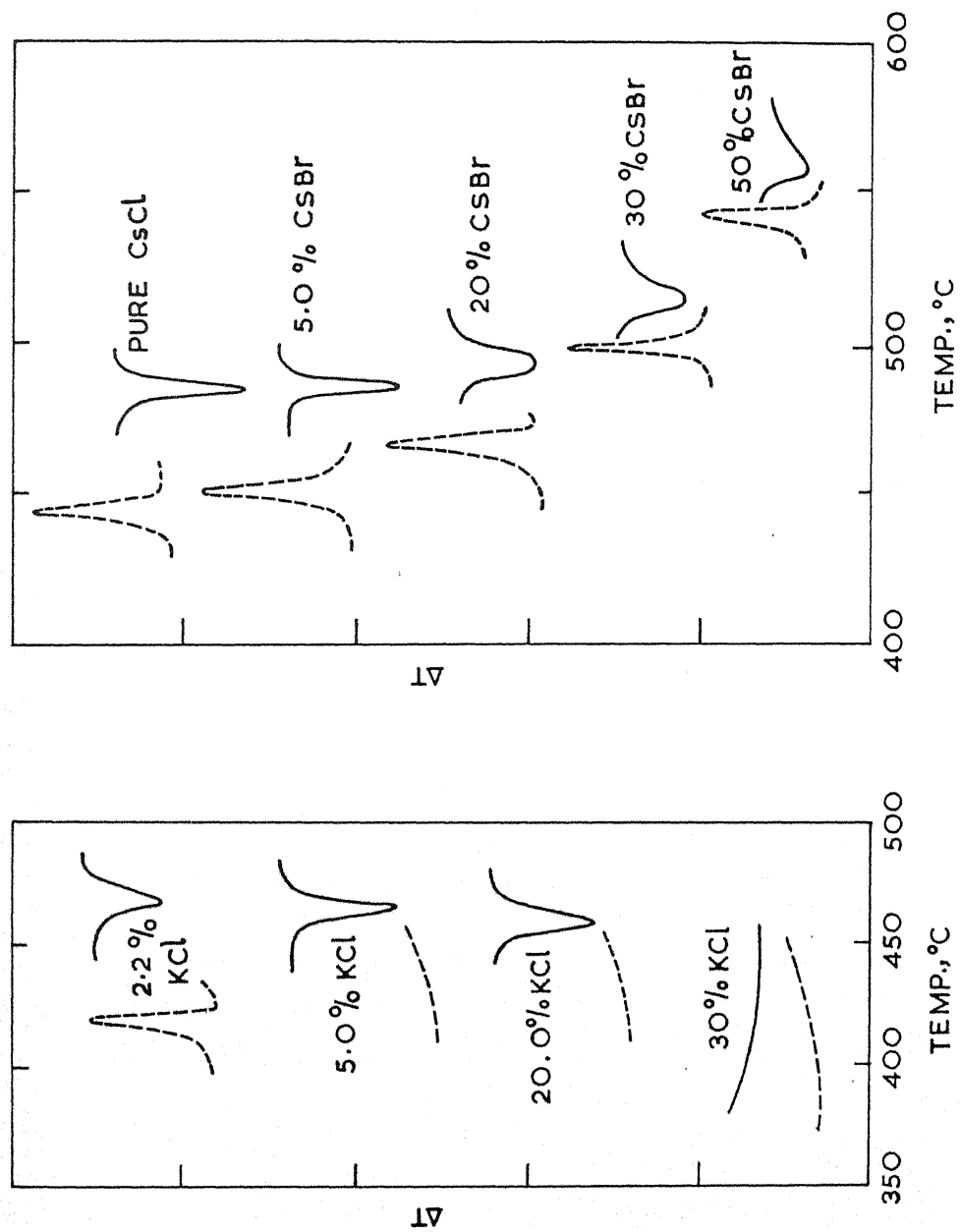


Fig. II.1. DTA curves of CsCl- KCl and CsCl -CsBr solid solutions.

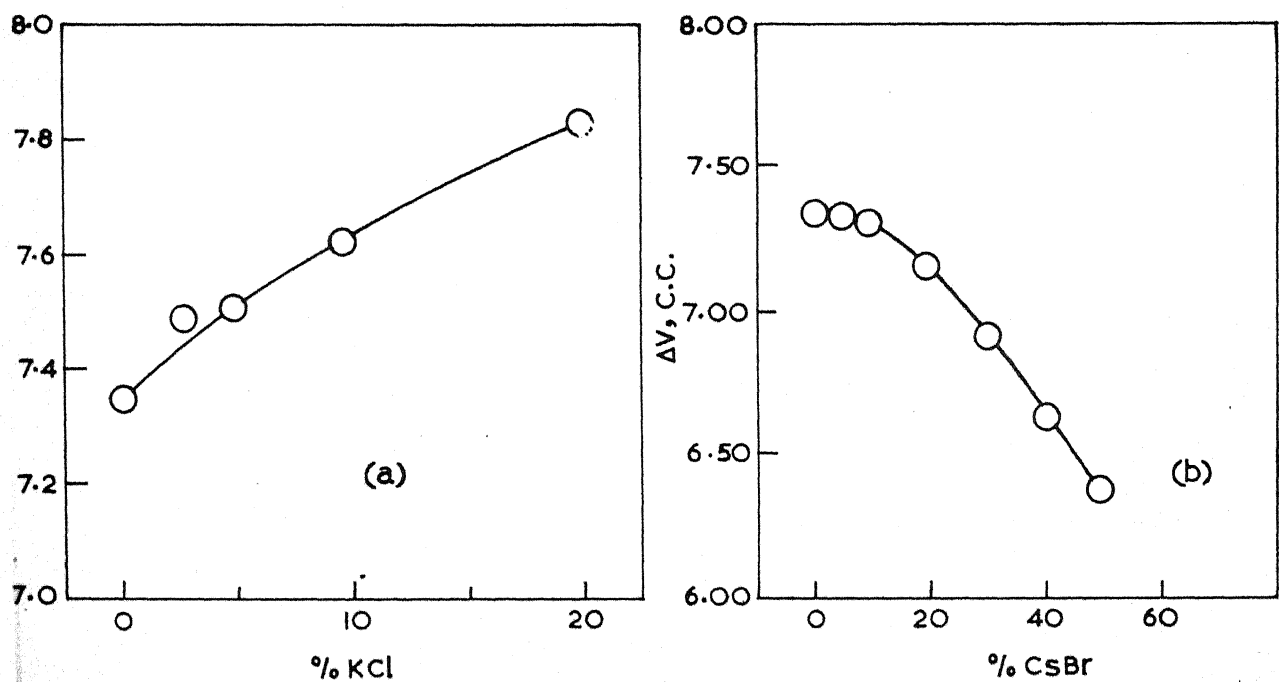


Fig. II.2. Change in molar volume, ΔV , of the Pm3m-Fm3m transformation with % of KCl(a) and CsBr (b) in the solid solutions.

proportion of KCl, the transformation becomes irreversible and at $\sim 25\%$ KCl the $Fm\bar{3}m$ phase of CsCl gets stabilized. At or above 25% KCl, the solid solutions showed no indication of transformation*. The fraction of the transformation decreases continuously with the percentage of KCl in the solid solutions upto $\sim 25\%$ KCl. While it is easy to visualise how high percentages of KCl or RbCl stabilize the $Fm\bar{3}m$ of the solid solutions by causing an appreciable decrease in the interionic distance, it is rather difficult to understand the reversibility of the $Pm\bar{3}m$ - $Fm\bar{3}m$ transformation ceases above 25% (or 5% RbCl). The energy of activation also decreases with increasing KCl indicating that the transformation is favoured by these additions.

The behaviour of the CsCl-KCl solid solutions may be understood in terms of the modified Born treatment^{2,3} just as in the case of the CsCl-RbCl system². The lattice energy difference between $Pm\bar{3}m$ and $Fm\bar{3}m$ structures of a solid solution is given by,

$$\Delta U^{s.s} = U_{Pm\bar{3}m}^{s.s} - U_{Fm\bar{3}m}^{s.s}$$

where $U_{Pm\bar{3}m}^{s.s}$ and $U_{Fm\bar{3}m}^{s.s}$ are given by the weighted sum of the energies of CsCl and KCl of the appropriate structures² as per equation (2):

$$\Delta U^{s.s} = \left\{ U_{CsCl}^{Pm\bar{3}m} (1-f) + U_{KCl}^{Pm\bar{3}m} (f) \right\} - \left\{ U_{CsCl}^{Fm\bar{3}m} (1-f) + U_{KCl}^{Fm\bar{3}m} (f) \right\}$$

* We have just noticed a publication of Weijma and Arends^{8a} who found that the ΔH is zero at about 10% KCl in CsCl by x-ray studies on single crystals of pure CsCl and solid solutions of RbCl and CsBr. We have repeated our studies again and confirm our results; there appears to be some error in the work of Weijma and Arends^{8a}.

In equation (2), \underline{f} is the mole fraction of KCl. The lattice energy, U , has the general form,

$$U = N_o \left[\frac{\mathcal{A}e^2}{r_o} + K \left(\frac{C}{r_o^6} + \frac{D}{r_o^8} \right) - B(r_o) + \phi_o \right] \quad (3)$$

where the repulsive term, $B(r_o) = M_1 b_1 \exp(-r_o/\rho_1) + M_2 b_2 \exp(-ar_o/\rho_2)$. In equation (3), N_o is the Avogadro number, r_o , the equilibrium interionic distance at 25°C in the solid solutions (obtained from the x-ray data in Table II.1), \mathcal{A} , the Madelung constant of the particular structure, K , the van der Waals term multiplicand of the modified Born model^{2,3}, and C and D are the van der Waals constants. In the repulsive term $B(r_o)$, M_1 and M_2 are the numbers of nearest and next-to-nearest neighbours, while b_1 , b_2 , ρ_1 and ρ_2 are the four repulsive parameters; a is the ratio of the distance between the second nearest neighbours to that between the first nearest neighbours. All the relevant structural constants and van der Waals coefficients employed in the Born calculations are shown in Table II.2. Calculations employing equations (2) and (3) provide $\Delta U^{s.s}$ at 25°C; the experimental ΔH_{tr} values (Table II.1) are at the transformation temperatures. Thus $\Delta U^{s.s}$ (25°C) would become zero at a slightly higher value of \underline{f} . Since no transformation was noticed at $\underline{f} = 0.25$, it may be taken that $\Delta U^{s.s}$ (25°C) approaches zero at this composition.

By choosing various values of K along with the associated values of the repulsive parameters for CsCl and KCl^{2,3}, $\Delta U^{s.s}$ was calculated as a function of \underline{f} . It was found that $\Delta U^{s.s}$ becomes zero at different values of \underline{f} depending on the value of K and the

TABLE II.2

van der Waals Coefficients and Other Structural Constants
Employed in the Born Treatment of CsCl Solid Solutions

van der Waals Coefficients

	$\frac{c_{++}}{(10^{-60} \text{ ergs})}$	$\frac{c_{+-}}{(10^{-60} \text{ ergs})}$	$\frac{c_{--}}{(10^{-60} \text{ ergs})}$	$\frac{d_{++}}{(10^{-76} \text{ ergs})^a}$	$\frac{d_{+-}}{(10^{-76} \text{ ergs})^a}$	$\frac{d_{--}}{(10^{-76} \text{ ergs})^a}$
CsCl	152 ^a 512 ^b	129 ^a 164 ^b	129 ^a 98.6 ^b	178	250	260
KCl	24.8 ^a 70.0 ^b 19.2 ^c 23.0 ^d	48.0 ^a 48.6 ^b 75.6 ^c 62.4 ^d	124.5 ^a 60.5 ^b 336.0 ^c 183.0 ^d	24	73	250
CsBr	152 ^a 512 ^b	163 ^a 257 ^b	214 ^a 242 ^b	178	340	490

Structural Constants^e

	α	M_1	M_2	S'_6	S''_6	S'_8	S''_8
CsCl (Pm3m) structure	1.76267	8	8	8.7088	3.5445	8.2077	2.1476
NaCl (Fm3m) structure	1.74756	6	12	6.5952	1.8067	6.1457	0.8002

(a) Values from Mayer^{9a}

(b) Values from Hajj⁹

(c) Values (without field correction) from Lynch¹⁰

(d) Values (with field correction) from Lynch¹⁰

(e) Structural constants are taken from Jones and Ingham^{10a}. van der Waals constants C and D are given by :

$$C = S'_6 c_{+-} + S''_6 (c_{++} + c_{--}/2);$$

$$D = S'_8 d_{+-} + S''_8 (d_{++} + d_{--}/2).$$

associated parameters (Fig. II.3). From the experimental results (Table II.1) it can be seen that $\Delta U^{s.s}$ becomes zero at $f \approx 0.25$. This behaviour is best described when K is between 2.80 and 3.00 (Fig. II.3). The values of the repulsive parameters when K is 3.00 are listed below:

Repulsive parameters when $K = 3$

	b_1 (erg mole ⁻¹)	b_2 (ergs mole ⁻¹)	ρ_1 (cm)	ρ_2 (cm)
CsCl	6447×10^{-12}	795×10^{-12}	0.367×10^{-8}	0.424×10^{-8}
KCl	3879×10^{-12}	35.6×10^{-12}	0.345×10^{-8}	0.487×10^{-8}

These results indicate that the Born-Mayer expression with four repulsive parameters accounts for the relative stabilities of the solid solutions of CsCl with KCl or RbCl. It may be noted that the values of K which is satisfactory for the phase transformation of solid solutions is considerably higher than that required to explain the phase transformation of the pure alkali halides^{2,3}.

Recently several workers^{9,10} have proposed revised van der Waals coefficients in alkali halides which seem to eliminate the need for employing high van der Waals term multiplicand ($K > 1$) in explaining phase transitions in alkali halides¹¹. It was considered worthwhile to examine the use of the new van der Waals coefficients in the study of the Pn $\bar{3}$ m-Fm $\bar{3}$ m transformations of the CsCl-KCl solid solutions. By employing the van der Waals coefficients of Hajj⁹ for CsCl, it was found that $\Delta U^{s.s}$ becomes zero at $f = 0.40$; it may be pointed out

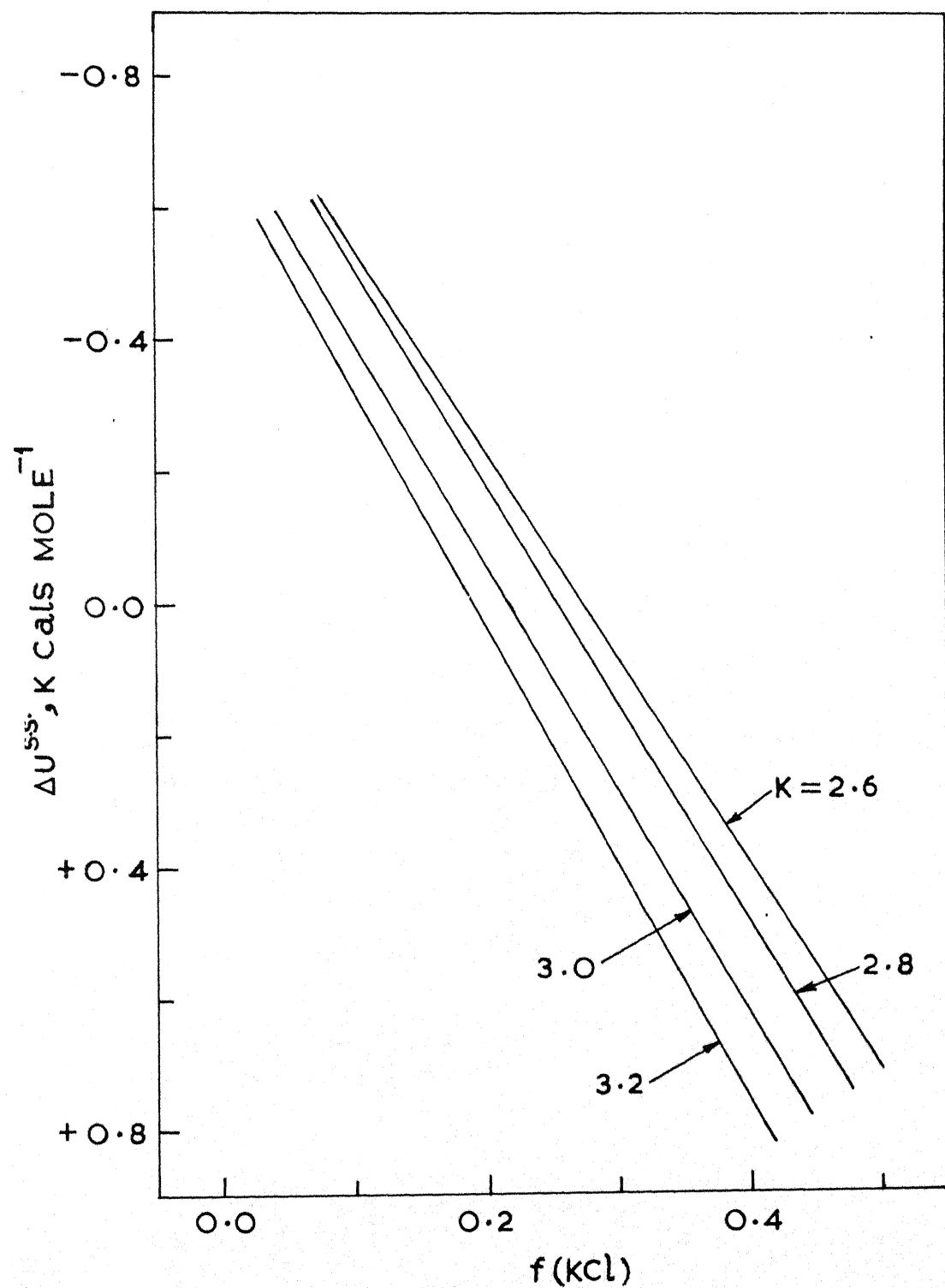


Fig. II.3. Variation of $\Delta U^{S.S.}$ of CsCl-KCl solid solutions calculated employing various values of K for CsCl and KCl (the graphs correspond to $K_{CsCl} = K_{KCl}$ = the value indicated).

that K in equation (3) was unity when employing Hajj's values⁹ (Table II.2). If we employ the van der Waals parameters of Lynch¹⁰ (without field correction) for KCl (Table II.2) along with Hajj's values for CsCl $\Delta U^{S.S}$ becomes zero at $f \approx 0.25$ and we can essentially eliminate the use of $K > 1$. These results point out the need for an upward revision of van der Waals term in the Born-Mayer description of alkali halides.

(b) CsCl-CsBr solid solutions

The results from DTA and x-ray analysis are shown in Table II.3. Typical differential thermograms are given in Fig. II.1. It can be seen that the transformation temperature increases markedly with the percentage of CsBr, the trend continuing upto the melting point of the solid solution ($\sim 60\%$ CsBr). Weijma and Arends^{8a} predict the transformation temperature for CsBr to be $\sim 880^\circ\text{C}$ from thermodynamic considerations. The transformation temperatures reported here essentially agree with those of earlier workers^{4,5}. The ΔH of the transformation seems to vary little in these solid solutions. The $\frac{\rho^{\text{Pm3m}}}{\rho^{\text{Fm3m}}}$ ratio in the solid solution with 10% CsBr is ~ 0.5 , a value much less than in pure CsCl.

Since CsBr has the same Pm3m structure as CsCl, it does not stabilize the Fm3m structure of the solid solutions; accordingly, there is an increase in the a_0 values of the Pm3m and Fm3m structures with increasing percentage of CsBr. On the otherhand, in the solid solution of CsCl with KCl (or RbCl), the a_0 values of both the

TABLE II.3

Pm3m-Fm3m Transitions of CsCl - CsBr Solid Solutions

% CsBr (mole)	T _t , °C forward (DTA peak)	T _t , °C reverse (DTA peak)	ΔH_{tr} cals mole ⁻¹	a _o (Fm3m) 25°C	a _o (Fm3m) 860°C	a _o (Fm3m) 25°C (a)	$\Delta V(25^\circ\text{C})$ cc mole ⁻¹
0	479	444	580	4.1210	7.0010	6.9050	7.34
5	480	450	600	4.1300	7.0130	6.9150	7.33
10	485	455	825	4.1350 (b)	7.0320 (b)	6.9250	7.31
20	495	462	950	4.1550	7.0600	6.9400	7.15
30	505	480	1025	4.1710	7.1000	6.9550	6.91
40	530	503	1100	4.1900	7.1300	6.9675	6.63
50	555	535	1050	4.2080	7.1515	6.9825	6.37
60	510 (c)	-	-	-	-	-	-

(a) Calculated on the basis that $a_o(\text{Fm3m})/a_o(\text{Fm3m}) \approx 0.598$ (b) The $a_o(\text{Pm3m})$ and $a_o(\text{Fm3m})$ values for this composition were determined at several temperatures; the $a_o(\text{Fm3m})$ and $a_o(\text{Pm3m})$ are found to be 1.17×10^{-4} deg⁻¹ and 0.68×10^{-4} deg⁻¹ respectively. The $a_o(\text{Pm3m})/a_o(\text{Fm3m})$ is thus seen to be 0.53

(c) Very close to the melting point (614°C).

structures decrease with the increase in percentage of KCl (or RbCl). The change in the molar volume, ΔV , accompanying the $Pm\bar{3}m$ - $Fm\bar{3}m$ transformation (Table II.3) decreases with increasing percentage of CsBr (Fig. II.2), and at 50% CsBr, the decrease in ΔV is about 14%; ΔV was expected to decrease with % CsBr on the basis of ionic size considerations². This may mean that the transformation has a component of second or higher order in CsCl - CsBr solid solutions. The DTA peaks at high percentages of CsBr also become shallow (less sharp) compared to pure CsCl. The magnitude of thermal hysteresis, ΔT , decreases slightly with increasing percentage of CsBr, thus indirectly substantiating that the transformation has components of higher order; ΔT would be expected to decrease with % CsBr since it has been recently shown that ΔT is proportional to the ΔV of the transformation¹². Samples containing 30% CsBr (or higher) showed evidence for the coexistence of the $Pm\bar{3}m$ and $Fm\bar{3}m$ phases in the transformation region (500-550°C) (Fig. II.4). The coexistence of phases and the formation of hybrid crystals have been noticed by Ubbelohde¹³ in continuous or higher order transformations.

In order to employ the Born treatment to explain the transformations of CsCl - CsBr solid solutions we were unable to obtain the repulsive parameters of CsBr as in the case of CsCl and other alkali halides^{2,3}, since CsBr itself does not undergo any phase transformation. Recently, however, the revised van der Waals coefficients of CsBr have been proposed by Hajj⁹. Since the van der Waals coefficients of Hajj could satisfactorily describe the transformation

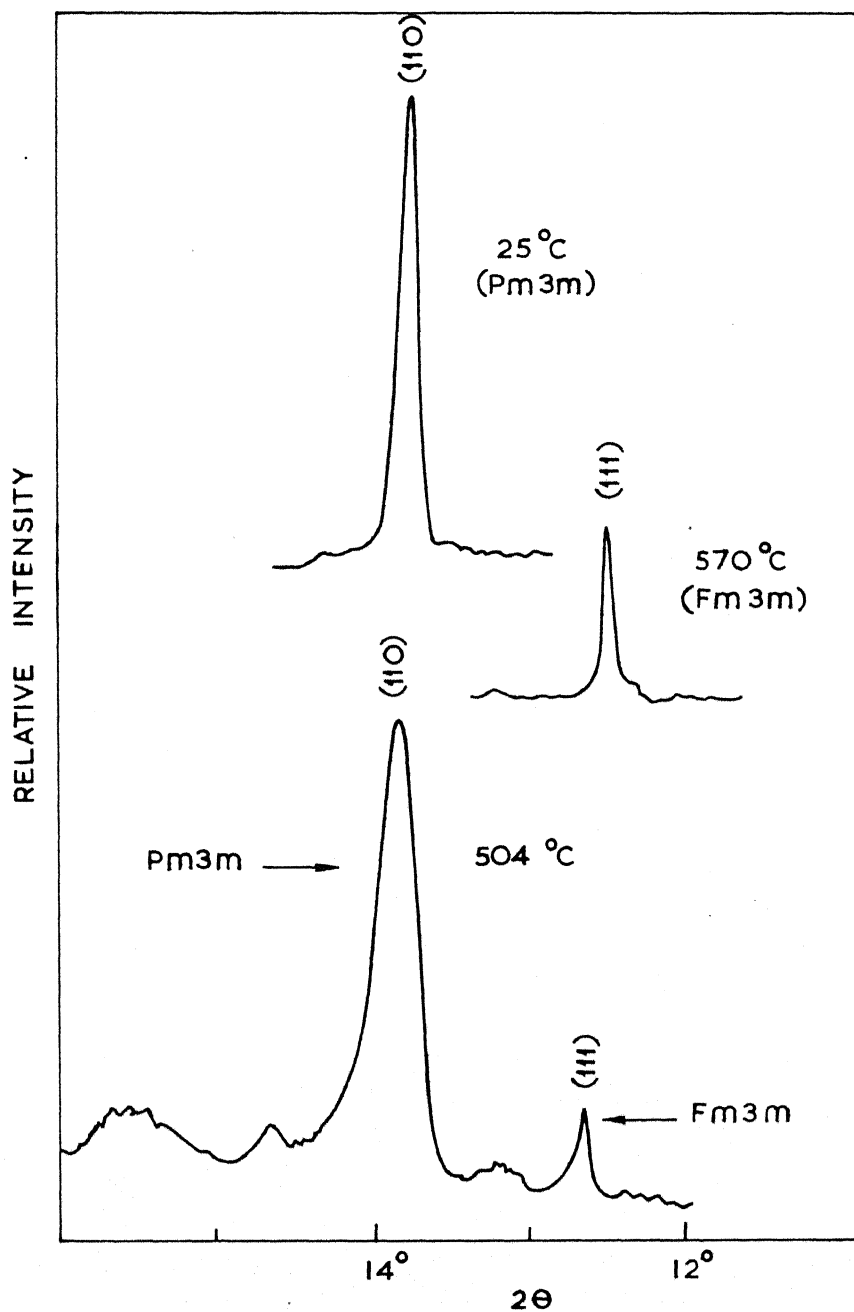


Fig.II.4. X-ray patterns of 30% CsBr, showing the coexistence of Pm3m and Fm3m phases around 505°C.

of CsCl¹¹, we felt that his van der Waals coefficients for CsBr may also be satisfactory. The various structural constants and van der Waals coefficients employed for the calculations are shown in Table II.2. The following method was employed to evaluate the repulsive parameters of CsBr: (i) the hardness parameters ρ_1 and ρ_2 are related by $\rho_2 = a \rho_1$ as proposed by Rao and Rao³ (ii) By making use of equation (4) for the lattice energy of CsBr, we can calculate $(8b_1 + 6b_2)_{\text{CsBr}}$. (iii) ρ_1 can be obtained by dividing equation (6) by (5) followed by multiplication by r_0 .

$$U^{\text{Pm3m}} = N_0 \left[\frac{1}{2} e^2 / r_0 + C / r_0^6 + D / r_0^8 - (8b_1 + 6b_2) \exp(-r_0 / \rho_1) + \phi_0 \right] \quad (4)$$

$$N_0 \left[\frac{1}{2} e^2 / r_0 + 6C / r_0^6 + 8D / r_0^8 - (r_0 / \rho_1) (8b_1 + 6b_2) \exp(-r_0 / \rho_1) \right] \\ = (3T / \beta) (\Delta V / \partial T)_P \quad (5)$$

$$N_0 \left[2 \frac{1}{2} e^2 / r_0 + 42C / r_0^6 + 72D / r_0^8 - (r_0^2 / \rho_1^2) (8b_1 + 6b_2) \exp(-r_0 / \rho_1) \right] \\ = (9V / \beta) \left[1 + (T / \beta) (\partial \beta / \partial T)_P + (T / \beta^2 V) (\partial \beta / \partial P)_T (\partial V / \partial T)_P \right. \\ \left. + (2T / 3V) (\partial V / \partial T)_P \right] \quad (6)$$

The value of $(8b_1 + 6b_2)$ thus calculated is 76867×10^{-12} ergs mole⁻¹. The $\Delta U^{\text{s.s}}$ of solid solutions of CsCl and CsBr were evaluated (equation 1) for different values of b_2 (in the range 0 to 900×10^{-12} erg mole⁻¹). The r_0 values of the Pm3m and Fm3m

structures were taken from the data in Table II.3. The results of the calculations are shown diagrammatically in Fig. II.5; the value of b_1 and b_2 are 9257×10^{-12} and 468×10^{-12} ergs mole⁻¹ respectively when $(6b_2/8b_1 + 6b_2)_{\text{CsCl}} \approx (6b_2/8b_1 + 6b_2)_{\text{CsBr}}$. It can be seen that the $U^{S.S}$ remains nearly constant or varies slightly with the percentage of CsBr when b_2 is between 400 and 500×10^{-12} erg mole⁻¹. Thus curves 3 and 4 of Fig. II.5 nearly represent the experimental situation.

The ΔU values of pure CsCl calculated from equation (2) (when f_{KCl} or $f_{\text{CsBr}} = 0$) differ slightly since the criterion employed in these calculations was that the ΔH_{tr} at T_t of CsCl be equal to the experimental value. The ΔU of CsCl at laboratory temperature would, however, be higher than ΔU at T_t . In spite of these minor differences it is heartening that the Born model of ionic solids is as successful in describing the relative stabilities of structures of alkali halides in widely different situations as manifested presently by the CsCl-KCl and CsCl-CsBr systems.

(c) CsCl-SrCl₂ solid solutions

Although some doubt has been expressed with regard to the importance of vacancies in the mechanism of Pm3m-Fm3m transformation in CsCl^{1,14}, recent experimental and theoretical studies on Schottky defects in CsCl seem to indicate that vacancies could also facilitate the Pm3m-Fm3m transformation in CsCl, to some extent. The formation energy of Schottky defects in Pm3m structure is half

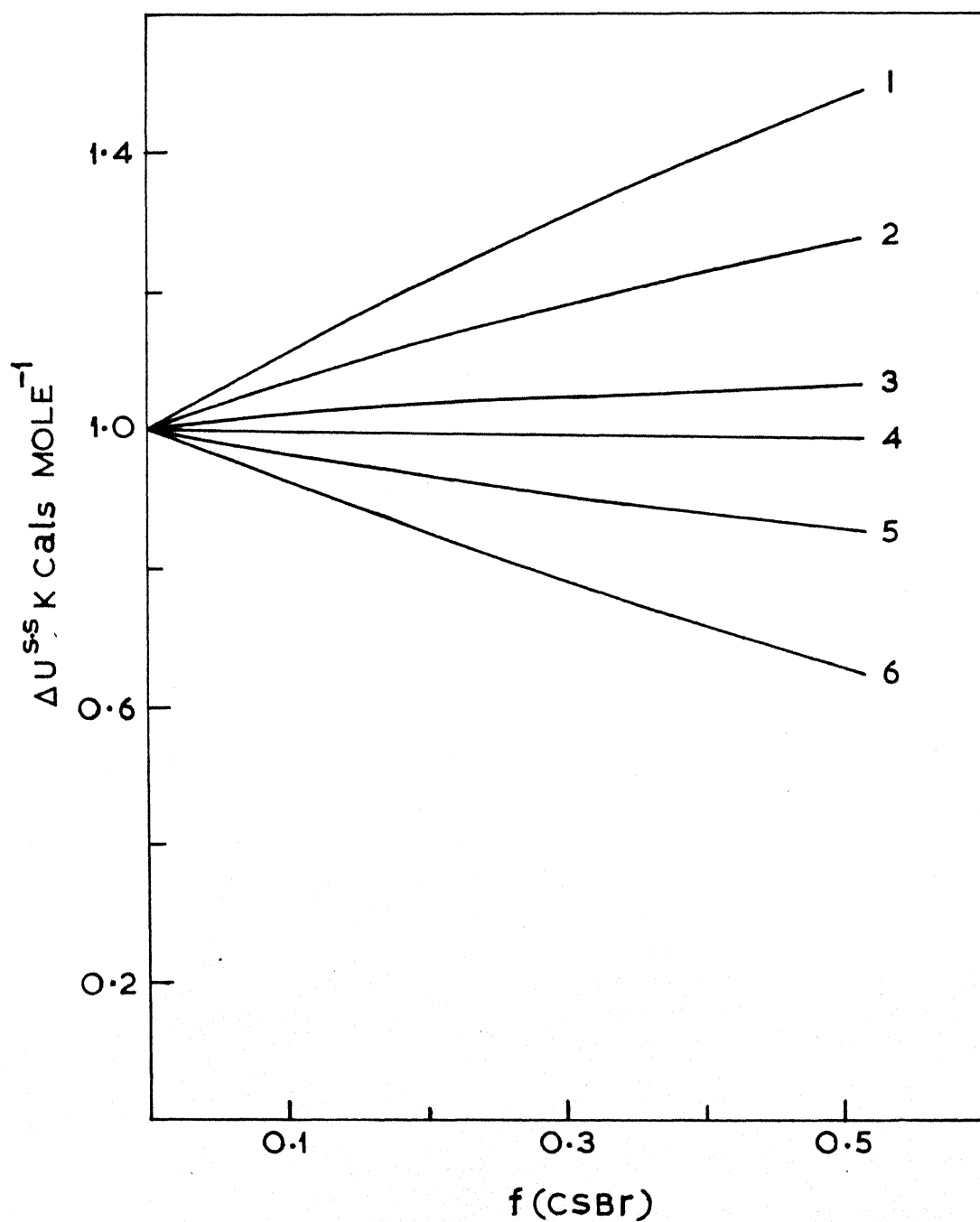


Fig.II.5. Variation of $\Delta U^{s.s.}$ of CsCl-CsBr solid solutions of different b_2 values (in 10^{-12} erg mole⁻¹): 1, 0; 2, 200; 3, 500; 4, 468; 5, 600; 6, 800.

47

of that in Fm3m structure. We have carried out some experimental studies on the formation energy of Schottky pairs in CsCl and the results are discussed in Chapter III of this thesis. The concentration of Schottky defects should therefore decrease after the Pm3m-Fm3m transformation. DTA studies on CsCl with different amounts of Sr^{+2} show that the transformation temperature decreases only slightly due to the vacancy concentration.

<u>Mole % Sr^{+2} in CsCl</u>	<u>T_t (forward)</u>	<u>T_t (reverse)</u>
0	480°C	444°C
2.5	475°C	444°C
5	474°C	444°C

The results seem to indicate that Pm3m-Fm3m transformation may essentially proceed by a dilatational mechanism¹⁵. The vacancies play a minor role, if any, in the mechanism of the transformation, in the nucleation step.

II.3 EXPERIMENTAL

All the compounds were better than 99.99% purity or of spectroscopic grade (J & M or Alfa). The preparation of solid solutions as well ^{as} the procedure for recording the differential thermal analysis (DTA) curves are described in earlier publications from this laboratory^{2,12}. The detailed procedures to obtain enthalpies of transformation, ΔH_{tr} (from DTA peak areas) and activation energies, E_a , are also described earlier^{2,12}.

The x-ray patterns were recorded (with $\text{CuK}\alpha$ - radiation) at different temperatures on a General Electric diffractometer (XRD-6) fitted with a high temperature camera, and a temperature programmer. The a_0 values of the $\text{Pm}\bar{3}\text{m}$ and $\text{Fm}\bar{3}\text{m}$ phases of the $\text{CsCl} - \text{KCl}$ solid solutions were determined at different temperatures, while the a_0 values of the $\text{CsCl} - \text{CsBr}$ solid solutions were determined at 25°C and 560°C respectively.

All the calculations employing the Born treatment were carried out on the IBM 1620 and IBM 7044 computers in this Institute.

Acknowledgement

The author's thanks are due to Dr. K.J. Rao for assistance with some of the computations.

REFERENCES

1. J.W. Menary, A.R. Ubbelohde and I. Woodward, Proc. Roy. Soc., A, 208, 158 (1951).
2. K.J. Rao, G.V. Subba Rao and C.N.R. Rao, Trans. Faraday Soc., 63, 1013 (1967).
3. K.J. Rao and C.N.R. Rao, Proc. Physic. Soc., (London), 91, 754 (1967).
4. M.J. Wood, C. Sweeney and M.T. Derbes, J. Am. Chem. Soc., 81, 6148 (1959).
5. L.J. Wood, W. Secunda and C.H. McBride, J. Am. Chem. Soc., 80, 307 (1958).
6. K.J. Rao and C.N.R. Rao, phys. stat. solidi, 28, 158 (1968).
7. Z. Morlin and J. Tremmel, Acta Phys. Hungary, 21, 129 (1966).
8. K.J. Rao and C.N.R. Rao, Chem. Phys. Letters., 1, 499 (1967).
- 8a. H. Weijma and J. Arends, phys. stat. solidi, 35, 205 (1969).
9. F. Hajj, J. Chem. Phys., 44, 4618 (1966).
- 9a. J.E. Mayer, J. Chem. Phys., 1, 327 (1933).
10. D.W. Lynch, J. Phys. Chem. Solids, 28, 1941 (1967).
- 10a. J.L. Jones and A.E. Ingham, Proc. Royal Soc., A 107, 636 (1925).
11. K.J. Rao, G.V. Subba Rao and C.N.R. Rao, Proc. Phys. Soc., (London), 1, 134 (1968).
12. K.J. Rao and C.N.R. Rao, J. Materials Sci., 1, 238 (1966).
13. A.R. Ubbelohde in "Reactivity in Solids", ed. by J.H. de Boer, Elsevier Publishing Co., Amsterdam (1961).
14. I.M. Hoodless and J.A. Morisson, J. Phys. Chem., 66, 557 (1962).
15. M.J. Buerger, in "Phase Transformation in Solids", ed. by R. Smoluchowski, John Wiley & Sons., Inc., New York, 1951.

CHAPTER III

IONIC CONDUCTIVITY IN CsCl AND ITS SOLID
SOLUTIONS WITH KCl , RbCl AND CsBr

CHAPTER III

IONIC CONDUCTIVITY IN CsCl AND ITS SOLID SOLUTIONS WITH KCl, RbCl AND CsBr

Defect Energies, Migration Energies and Phase Transitions

III.1 INTRODUCTION

Conductivity measurements on ionic solids provide valuable information regarding the activation energies for migration and energies of formation of defects^{1,2}. From the conductivity data on crystals doped with appropriate impurities (e.g., Sr^{+2} in NaCl) one can calculate the enthalpy of association between the impurity ion and the vacancy^{3,4}. Most of the theoretical and experimental studies on defects in ionic solids are on alkali halides of NaCl (Fm $\bar{3}$ m) structure^{1,2} and information on the defect energies in alkali halides of CsCl (Pm $\bar{3}$ m) structure is limited. Literature data⁵⁻⁸ indicate that the Schottky formation energy, E^S , in the Pm $\bar{3}$ m phase of CsCl is considerably lower than that generally found in alkali halides of Fm $\bar{3}$ m structure. We considered it interesting to experimentally evaluate the Schottky formation energies in the Pm $\bar{3}$ m and Fm $\bar{3}$ m phases

of CsCl by conductivity measurements on Sr^{+2} -doped CsCl samples; this study would also provide the interaction energy³ between $\text{Sr}_{\text{Cs}}^{+2}$ and the cation vacancy, (V_{Cs}^-). Schottky formation energies in the Pm3m and Fm3m phases of CsCl are of value to understand the mechanism of the Pm3m-Fm3m transformation^{9,10} (see Chapter II).

The migration energy, E^m , in alkali halides varies anywhere between 0.3 and 1 eV^{1,2}. We have now carried out conductivity measurements on solid solutions of CsCl with varying amounts of K^+ , Rb^+ and Br^- ions to examine the effect of these additives on E^m ; we would expect some effect due to the differences in ionic sizes. E^s values would also be different since Rb^+ and K^+ ions stabilize the Fm3m phase of CsCl at a fixed composition, while Br^- enhances the Pm3m-Fm3m transformation temperature of CsCl (see Chapter II). In this context we find that the recent study of Nijboer and Arends¹¹ on solid solutions of CsCl with K^+ , Rb^+ and Br^- is not conclusive and calls for a reinvestigation of the problem; these workers have measured conductivities over narrow ranges of composition ($\sim 10\%$ of the additive ions) and have not reported data at low temperatures (extrinsic region) which provide direct information on E^m . We considered it worthwhile carrying out the measurements over a wider composition range including the solid solutions where the Fm3m structure gets stabilized.

III.2 RESULTS AND DISCUSSION

(a) Schottky formation energy in CsCl

Plots of $\log \sigma$ vs $1/T$ of pure CsCl and CsCl doped with different amounts of Sr^{+2} are shown in Fig. III.1. The conductivity data in the extrinsic region (at lower temperatures) give the cation migration energy, E_c^m , to be 0.6 eV (Table III.1) in the Pm3m phase. This compares well with the literature values^{8,11,12} for E_c^m in CsCl. The conductivity data in Fig. III.1 clearly show the evidence for the Pm3m-Fm3m transformation in CsCl. The transformation temperature does not vary significantly with the incorporation of Sr^{+2} (see Chapter II). The slope of the $\log \sigma$ vs $1/T$ plot (Fig. III.1) in the intrinsic region (prior to the Pm3m-Fm3m transition) gives $(E_a^m + E^s/2)$ where E_a^m corresponds to the anion migration energy which is known to be considerably lower^{7,13} (~ 0.3 eV) than the cation migration energy, E_c^m . The E^s in the Pm3m phase of CsCl thus calculated is 1.4 eV. The experimental^{7,8,11} and theoretical^{6,14,15} values reported in the literature (Table III.2) vary between 1.2 and 1.9 eV, a majority of the data favouring a lower E^s value for the Pm3m phase.

At the temperature where CsCl transforms to the Fm3m structure, there is a marked decrease in conductivity (Fig. III.1). This decrease is likely to be due to an increase in the volume accompanying the transition; further, the Schottky formation energy, E^s , is also likely to be larger in the Fm3m phase^{5,6}. The slope of the $\log \sigma$ vs $1/T$ plot (Fig. III.1) beyond the transformation temperature is

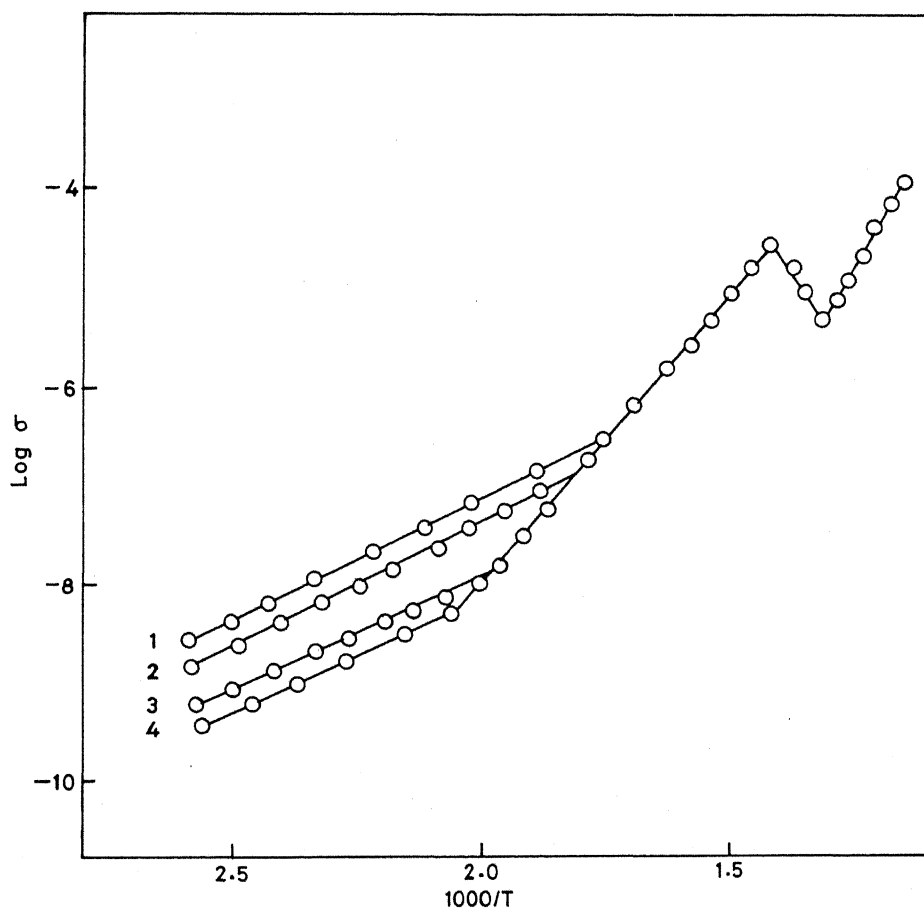


Fig.III.1. $\text{Log } \sigma$ vs $1/T$ plots of pure and Sr^{+2} doped CsCl polycrystalline samples; (1) 5×10^{-2} mole Sr^{+2} (2) 5×10^{-3} mole Sr^{+2} (3) 5×10^{-4} mole Sr^{+2} (4) pure (99.99%) CsCl.

TABLE III.1Defect Energies (in eV) in CsCl (doped with Sr^{+2})

<u>Mole % Sr^{+2}</u>	<u>$T_t, ^\circ\text{C}$</u>	<u>E_c^m</u>	<u>$E^s(a)$</u>	<u>$E(\text{Fm}\bar{3}m)(b)$</u>
0	480	0.6	1.4	2.0 ± 0.1
5×10^{-3}	480	0.6	1.4	2.1 ± 0.1
5×10^{-2}	480	0.6	1.4	2.2 ± 0.1
2.5	475	0.6	1.4	2.0 ± 0.1

(a) These values are obtained by assuming the anion migration energy to be ~ 0.3 eV.

(b) These are the slopes of the $\log \sigma^-$ vs $1/T$ plots for the $\text{Fm}\bar{3}m$ phase.

TABLE III.2

Literature Data on the Defect Energies (eV) in Cesium Chloride

<u>Pm3m structure</u>		<u>Fm3m structure</u>	
<u>Experimental</u>	<u>Theoretical</u>	<u>Experimental</u>	<u>Theoretical</u>
$\frac{E_m}{c}$			
0.60 ¹²			
0.60 [*]	-	-	-
0.64 ⁸			
0.73 ^(a)			
$\frac{E_m}{a}$			
0.30 ²	-	-	0.7 ⁷
0.34 ⁸			1.3 ^(a)
$\frac{E_s}{c}$			
1.10 ¹²	1.65 ¹⁴		1.96 ⁶
1.40 [*]	1.80	2.0 [*]	2.05 ⁷
	2.60 ^(a)		3.50 ^(a)

* Present study.

(a) J. Arends, phys. stat. solidi., 24, K219 (1967).

~ 2.0 eV (Table III.1). Even if we assume the migration energy, E^m , to be about 1 eV, the E^s will turn out to be 2.0 eV, a value which is close to the E^s in alkali halides of Fm3m structure such as NaCl and KCl^{1,2,5}.

(b) Enthalpy of association of $\text{Sr}_{\text{Cs}}^{+2}$ and V_{Cs}^-

Sr^{+2} ions in CsCl can form complexes with the cation vacancies. The equilibrium constant for the association at any temperature leading to the ground state configuration of the complex, $[\text{Sr}_{\text{Cs}}^{+2} \text{V}_{\text{Cs}}^-]$, can be calculated following the procedure of Etzel and Maurer³. By evaluating equilibrium constants at several temperatures, we obtain the enthalpy of association of the complex. The association enthalpy evaluated in the case of CsCl doped with Sr^{+2} is 0.40 ± 0.02 eV in the Fm3m phase. On applying Debye-Hückel corrections to account for long range interactions, following the procedure of Lidiard⁴, we find the enthalpy of association to be $\sim 0.48 \pm 0.04$ eV in the Fm3m phase. We have estimated the association enthalpy in the Fm3m phase of CsCl to be $\sim 0.35 \pm 0.02$ eV (in the range 500-550°C), a value which is less than that found in the Fm3m phase of CsCl.

(c) Solid Solutions of CsCl with KCl, RbCl and CsBr

The cation migration energies in solid solutions of CsCl with KCl and RbCl were estimated from the conductivity data in the extrinsic region (Figs. III.2 and 3). The migration energies in the Fm3m phase of the solid solutions varies between 0.60 and 0.65 eV (Table III.3). The solid solution with 30% KCl is stabilized in the

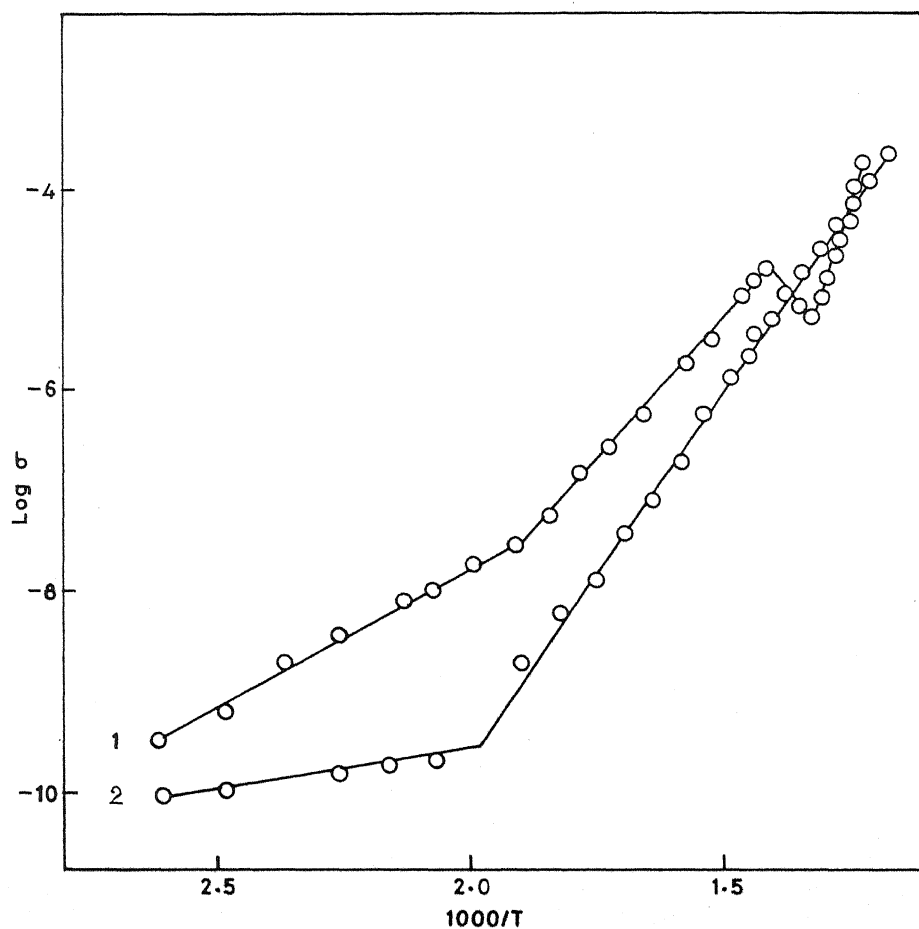


Fig. III.2. $\text{Log } \sigma$ vs $1/T$ plots of solid solutions of CsCl with (1) 2.5% KCl and (2) 30% KCl.

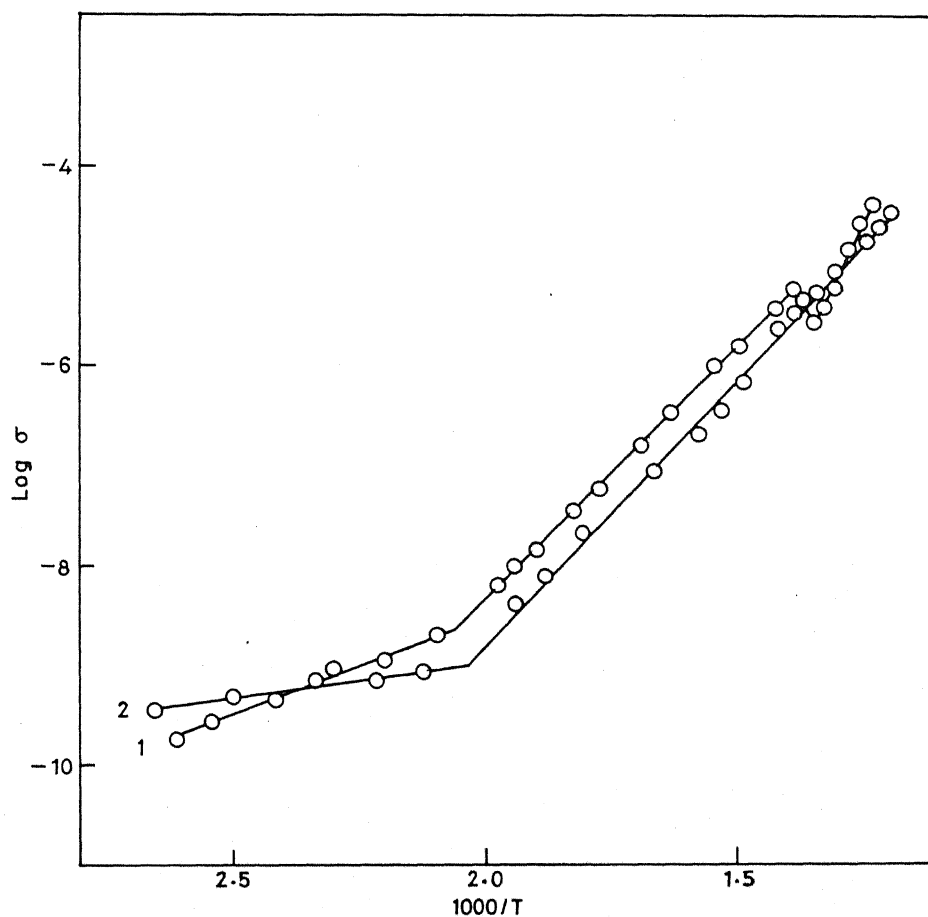


Fig.III.3. $\text{Log } \sigma$ vs $1/T$ plots of solid solutions of CsCl with (1) 2.5 % RbCl and (2) 35%RbCl.

TABLE III.3

Defect energies (in eV) in Solid Solutions
of CsCl with KCl, RbCl and CsBr

<u>Mole % KCl</u>	<u>Structure</u>	<u>T_t, °C</u>	<u>E_c^m</u>	<u>E^s(a)</u>
0	Pm3m	480	0.65	1.4
2.5 ^(b)	Pm3m	470	0.65	1.4
7.5 ^(c)	Pm3m	471	0.65	1.4
10.0 ^(c)	Pm3m	470	0.63	1.4
20.0 ^(c)	Pm3m	472	0.60	1.4
30.0 ^(d)	Fm3m	-	0.40	2.0
<u>Mole % RbCl</u>				
2.5 ^(b)	Pm3m	470	0.55	1.4
7.5 ^(c)	Pm3m	467	0.55	1.4
20.0 ^(c)	Pm3m	470	0.45	1.4
35.0 ^(d)	Fm3m	-	0.40	1.8
<u>Mole % CsBr</u>				
10 ^(b)	Pm3m	490	0.62	2.0
30 ^(b)	Pm3m	510	0.60	2.0

(a) E^s values are calculated by assuming the anion migration energy to be ~ 0.3 eV.

(b) Pm3m-Fm3m transformation is reversible.

(c) Pm3m-Fm3m transformations are irreversible.

(d) No Pm3m-Fm3m transformation. The stable room temperature phase is Fm3m.

Fm $\bar{3}$ m structure even at the laboratory temperature (see Chapter II); the conductivity data in the extrinsic region of this solid solution gives a value of E_C^m of 0.40 eV. The values of E_C^m show a decreasing trend with the incorporation of K^+ as one would expect on the basis of ionic size considerations. The more interesting aspect of these studies is that the value of E^S remains constant at 1.4 eV in the CsCl-KCl solid solutions upto 20% KCl where the structure is Pm $\bar{3}$ m. In the 30% KCl solid solution where the structure is Fm $\bar{3}$ m, the E^S value is \sim 2.0 eV, close to the value of E^S in pure KCl^{1,2} as well as in the Fm $\bar{3}$ m phase of CsCl.

The migration energies of RbCl solid solutions are slightly lower than the KCl solid solutions, contrary to expectations. The E_C^m values decrease with % RbCl similar to the behaviour of KCl solid solutions. The E^S in the solid solutions of Pm $\bar{3}$ m structure (upto 20% RbCl) is 1.4 eV just as in pure CsCl. The E^S in the 35% RbCl solid solution which occurs in the Fm $\bar{3}$ m structure is, however, very much larger. These studies clearly show that the Schottky formation energies are very sensitive to structure.

From the conductivity data on the solid solutions of CsCl with KCl and RbCl, we can calculate the preexponential factors*, A. We find that A decreases with % K^+ or Rb^+ in the solid solutions. K^+ has a greater effect than Rb^+ on the magnitude of A. These effects are undoubtedly related to the changes in the frequency spectrum of the lattice vibrations.

* Note that $\sigma = A \exp (-E/kT)$.

The conductivity data on KCl and RbCl solid solutions show the $\text{Pm}\bar{3}\text{m}$ - $\text{Fm}\bar{3}\text{m}$ transformations clearly and the data are in agreement with the findings from differential thermal analysis and x-ray diffraction studies¹⁰ (see Chapter II). The present results, however, differ from the observations of Weijma and Arends¹⁶ who report the stabilization of the $\text{Fm}\bar{3}\text{m}$ phase of CsCl at a much lower percentage of KCl ($\sim 10\%$ KCl). The conductivity data of the solid solutions with KCl and RbCl (Figs. III.2 and 3) after the phase transition show slopes of about 2.0 eV. We are unable to obtain Schottky energy in the $\text{Fm}\bar{3}\text{m}$ phases of these solid solutions due to lack of adequate data on E^{m} . We feel that the lower limit of E^{S} value in the $\text{Fm}\bar{3}\text{m}$ phases of these solid solutions is ~ 2.0 eV.

The solid solutions of CsCl with CsBr (Fig. III.4) are of $\text{Pm}\bar{3}\text{m}$ structure throughout the composition (see Chapter II). The E^{m}_{C} essentially remains constant while E^{S} increases with the incorporation of Br^- (Table III.3). The E^{S} in 30% CsBr is ~ 2.0 eV; the E^{S} in pure CsBr has been reported to be ~ 2.0 eV¹⁷. Unlike in KCl and RbCl solid solutions, the preexponential factor, A , in the CsBr solid solutions increases with % Br^- .

III.3 EXPERIMENTAL

CsCl, KCl, RbCl and CsBr were of spectroscopic grade. The solid solutions were prepared from aqueous solutions containing appropriate amounts of CsCl and the respective alkali halide.

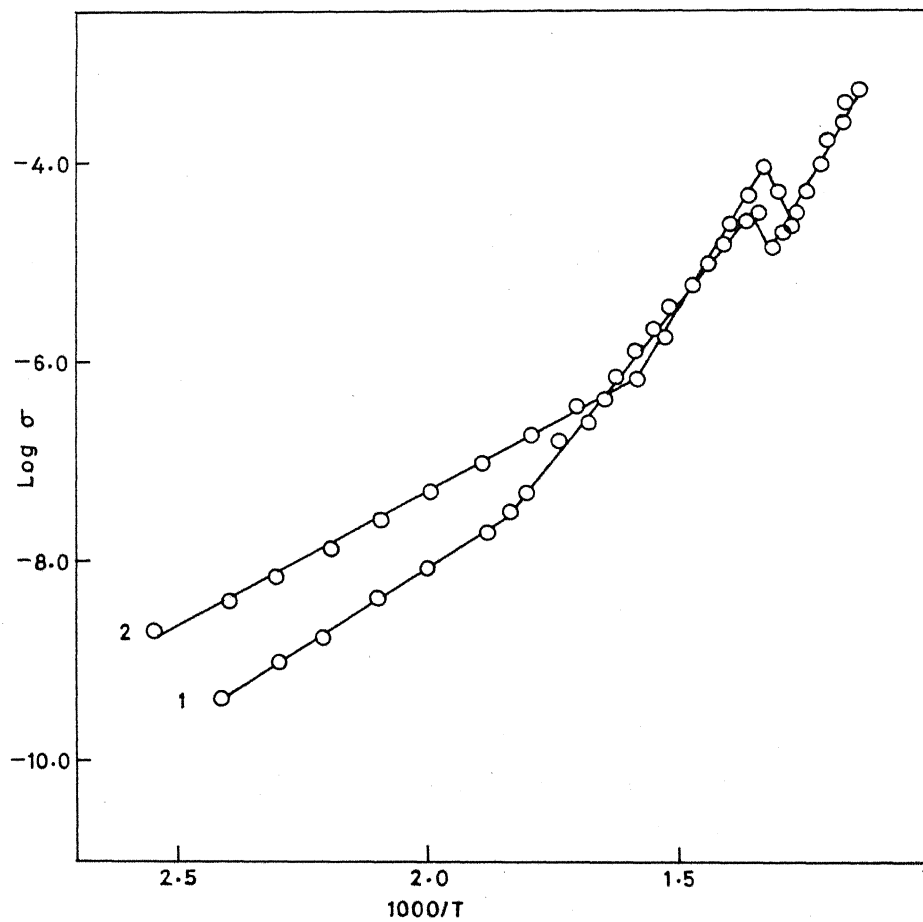


Fig.III.4. $\text{Log } \sigma$ vs $1/T$ plots of solid solutions of CsCl with (1) 10% CsBr and (2) 30% CsBr.

Conductivity measurements were made on a General Radio impedance bridge (1608-A) employing stabilized voltage. The temperature was measured by employing Leeds & Northrup millivolt potentiometer to an accuracy of $\pm 1^\circ$. The samples were made into pellets of 1.30 cm dia. and ~ 0.2 cm thick and held between two platinum discs (of 1.3 cm dia.), supported by a spring load in the conductivity cell described elsewhere¹⁸.

Acknowledgement

The author is thankful to Dr. B. Prakash for help in some conductivity measurements.

REFERENCES

1. A.B. Lidiard, Handbuch der Physik., 20, 246 (1957).
2. L.W. Barr and A.B. Lidiard in Physical Chemistry—An Advanced Treatise, Vol. 10, Academic Press, New York, 1969.
3. H. Etzel and R. Maurer, J. Chem. Phys., 18, 1003 (1950).
4. A.B. Lidiard, Phys. Rev., 94, 29 (1954).
5. K.J. Rao and C.N.R. Rao, phys. stat. solidi., 28, 157 (1968).
6. S. Ramdas and C.N.R. Rao, unpublished results.
7. H. Nijboer and J. Arends, Solid State Communications, 5, 163 (1967).
8. P.J. Harvey and I.M. Hoodless, Phil. Mag., 16, 543 (1967).
- 9a. J.W. Menary, A.R. Ubbelohde and I. Woodward, Proc. Royal. Soc., A 208, 158 (1951).
- b. I.M. Hoodless and J.A. Morrison, J. Phys. Chem., 66, 557 (1962).
10. K.J. Rao, G.V. Subba Rao and C.N.R. Rao, Trans. Faraday Soc., 63, 1013 (1967).
11. H. Nijboer and J. Arends, phys. stat. solidi., 26, 537 (1968).
12. Z. Morlin, Acta Physica Acad. Scient Hungaricae, 21(2), 137 (1966).
13. J.F. Laurent and J. Benard, J. Phys. Chem. Solids, 3, 7 (1957).
14. I.M. Boswarva, Phil. Mag., 16, 827 (1967).
15. I.M. Boswarva and A.B. Lidiard, Phil. Mag., 16, 803 (1967).
16. H. Weijma and J. Arends, phys. stat. solidi., 35, 205 (1969).
17. D.W. Lynch, Phys. Rev., 118, 468 (1960).
18. G.V. Subba Rao, Ph.D. Thesis, Indian Institute of Technology, Kampur (1969).

CHAPTER IV

PHASE TRANSITIONS OF SILVER HALIDES

CHAPTER IV

PHASE TRANSITIONS OF SILVER HALIDES

IV.1 INTRODUCTION

Silver iodide is known to exhibit as many as six polymorphic forms^{1,2}; of these the most important are the B3 (cubic ZnS or sphalerite form) and B4 (hexagonal ZnS or wurtzite type) forms which are stable at ordinary temperatures and pressure. Many workers suggest that B4 is the stable phase while B3 is a metastable one. The B3 and B4 phases (of space groups $F\bar{4}3m$ and $P6_3mc$ respectively) are polytypes and their structures have been discussed at some length by Schneer and others^{3,4}. The structures differ only in the stacking of the layers of iodine and silver atoms⁴. The existence of the B3 polytype has been questioned by Majumdar and Roy⁵. Burley⁴, however, reports that B3 transforms to B4 at measurable rates in the temperature range 120–140°C. Schneer and Whiting⁶ have suggested that the B3 \rightarrow B4 transformation is athermal.

AgI (B3 or/and B4) transforms to the cubic B23 structure at $\sim 146^\circ\text{C}$ ^{5,6}. The B23 structure consists of a space centred lattice

of iodine atoms in which the silver atoms are randomly distributed^{7,8}; the random structure may be considered as an average between the two structures of space groups $Im\bar{3}m$ and $I4m2$ ($c/a = 1$)⁸. We have presently prepared pure AgI in the B3 and B4 forms and examined their transitions to the B23 structure. The phase transitions of AgI are of significance because of its structural analogy with ZnS, SiC, CdS and other related compounds. We were particularly interested in the following aspects of AgI: (i) x-ray diffraction data and crystallography of pure B3 and B4 phases, (ii) evidence for the B3 \rightarrow B4 transition, if any, and (iii) transitions of B3 and B4 phases to the B23 phase. Further, we were also interested to find out the applicability of the Born model of ionic solids to the study of phase transitions of AgI, AgBr and AgCl. We may note here that AgI undergoes several pressure transitions including one to the NaCl structure^{1,2} (B1 form, $Fm\bar{3}m$). AgCl and AgBr which normally exist in the B1 structure undergo pressure transitions to the CsCl structure (B2 form, $Pm\bar{3}m$)⁹. In this laboratory, we have had fair success in explaining the $Pm\bar{3}m$ - $Fm\bar{3}m$ transformations of alkali halides by employing the Born treatment¹⁰⁻¹².

AgI is known to form solid solutions with AgBr, the structure of the solid solution depending on the composition and temperature¹³⁻¹⁷. There is considerable disagreement among the various reports¹³⁻¹⁷ on the solid solutions. Thus, Stasiw and Teltow¹⁵ observe that upto 50% AgBr can be replaced by AgI in the B1 structure, while Knaggs and coworkers¹⁷ report that upto 80%

of AgI enters into B1 structure. Cugnac and coworkers¹⁶ find that the a parameter of the B4 form of AgI decreases upto 5% of AgBr, above which composition the B1 structure of AgI becomes stable. We considered it interesting to examine the structures of the solid solutions of AgI and AgBr as well as their phase transitions. Besides obtaining these data related to AgI-AgBr phase diagram, we wanted to see whether the Born treatment of ionic solids could explain the stabilization of specific phases of the solid solutions.

IV.2 RESULTS AND DISCUSSION

(a) Crystal structure and phase transitions of AgI

X-ray diffraction data on the pure B3 and B4 phases as well as of the precipitate of AgI clearly show that the precipitate consists of mixture of B3 and B4 phases (Table IV.1). It can be seen from Fig. IV.1 that the most intense reflections of the B3 and B4 phase are found at about the same angles; it is, however, not difficult to distinguish the B4 form from the B3 form. The relative intensities of the B3 and B4 forms presently found (Table IV.1) agree well with those reported in the NBS monographs¹⁸. We do not agree with Berry¹⁹ who suggests that the NBS x-ray intensities¹⁸ of the B4 reflections may be erroneous because of admixture with the B3 form.

The colour of the B4 phase is bright yellow while that of B3 is orange-red due to the differences in exciton band positions¹⁹.

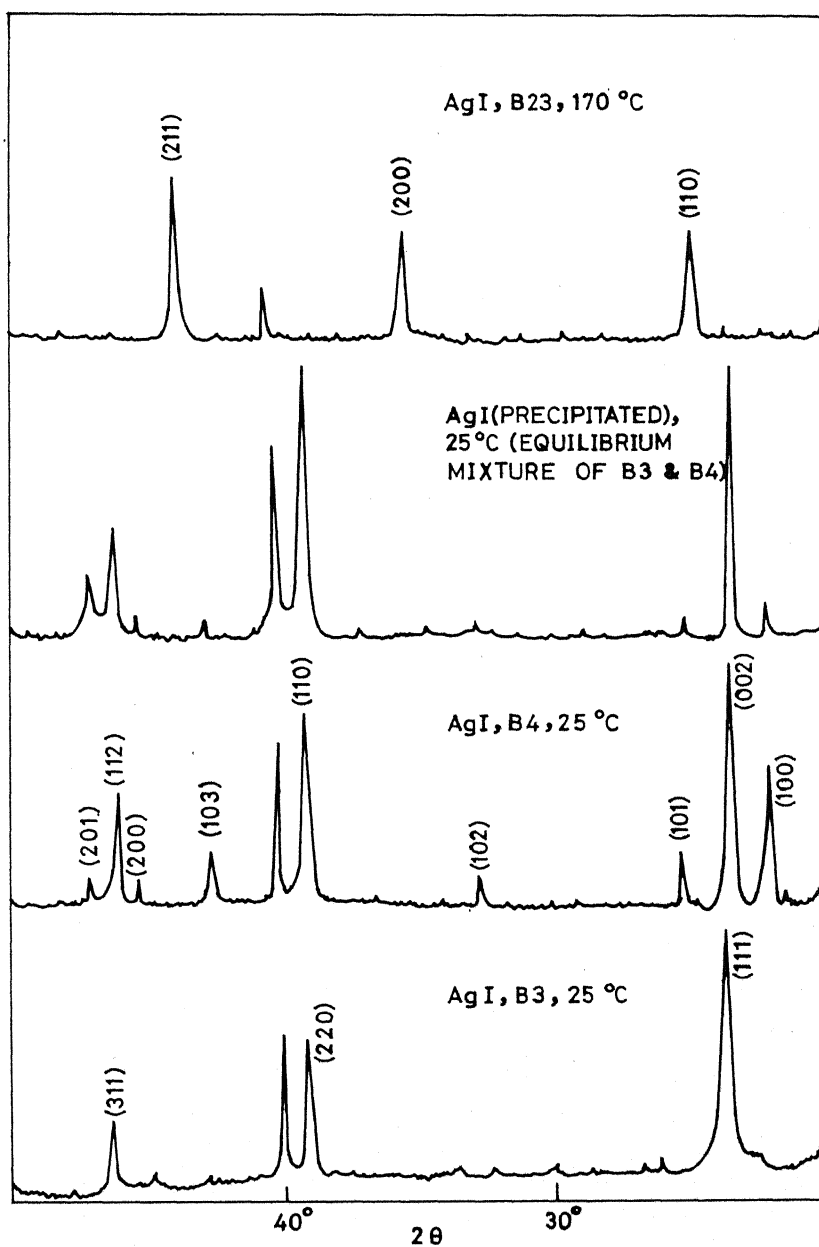


Fig. IV.1 X-ray powder diffraction patterns of pure B3, pure B4 and precipitated AgI at 25°C. The pattern of the high temperature B23 phase at 170°C is also shown.

TABLE IV.1

X-ray Diffraction Data of B3 and B4 forms
as well as Precipitated Silver Iodide

<u>B4 - AgI^(a)</u>			<u>B3 - AgI^(b)</u>			<u>B3 + B4 mixture from precipitation</u>	
2 θ	I _{rel.}	(hkl)	2 θ	I _{rel.}	(hkl)	2 θ	I _{rel.}
22.32	48	100				22.32	10
23.70	100	002	23.70	100	111	23.70	100
25.36	20	101				25.36	5
32.78	12	102				32.80	5
39.20	88	110	39.12	58	220	39.22	100
42.64	25	103				42.65	10
45.54	10	200				45.54	4
46.28	58	112	46.30	28	311	46.30	69
47.24	16	201				47.20	12
51.99	7	202					
			56.80	9	400	56.80	8
			62.30	10	331		
						62.40	12
62.98	5	211					

(a) $a = 4.591 \text{ \AA}$, $c = 7.498 \text{ \AA}$ (Literature values¹⁸,
 $a = 4.592 \text{ \AA}$, $c = 7.510 \text{ \AA}$)

(b) $a = 6.495 \text{ \AA}$ (Literature value¹⁸, $a = 6.495 \text{ \AA}$).

The far infrared spectra of the two phases show little difference in the positions of the bands; both show bands at ~ 112 and ~ 94 cm^{-1} , in agreement with the earlier report of Bottger and Geddes²⁰.

The differential thermal analysis (DTA) curves (Fig. IV.2) of the B3 and B4 forms (as well of the precipitate of AgI containing both the phases) show reversible transformations at 140 to 146°C. The structure of the high temperature phase was ascertained to be B23 by x-ray analysis (Fig. IV.1). It can be seen from Fig. IV.2 that there is no marked difference in the DTA curves of B3 and B4 phases. Specifically, there is no indication of the B3 \rightarrow B4 transition in the DTA curve of the B3 form of AgI; this was the case at all rates of heating (2° - 16° min^{-1}). We also failed to notice any evidence for the B4 phase in the high temperature x-ray patterns of B3 in the 120-145°C range. The enthalpies of transitions of B3 and B4 forms calculated from the DTA peak areas²¹ were found to be 1500 and 1600 calories per mole respectively, suggesting that the B3 \rightarrow B4 transition (if it occurs at all) is associated with a very small enthalpy change (~ 100 cal mole^{-1}); apparently the B4 phase of AgI is thermodynamically more stable than the B3 phase. The activation energies of the transitions of B3 and B4 forms (to B23) calculated from the DTA curves (Fig. IV.2) are 117 ± 10 and 124 ± 10 kcal mole^{-1} respectively; these two E_a values are quite comparable. The E_a value reported by Burley⁴ for the B3 \rightarrow B4 transformation is, on the otherhand, 10.3 ± 0.8 Kcal mole^{-1} . We find it difficult to understand Burley's results⁴, since our studies

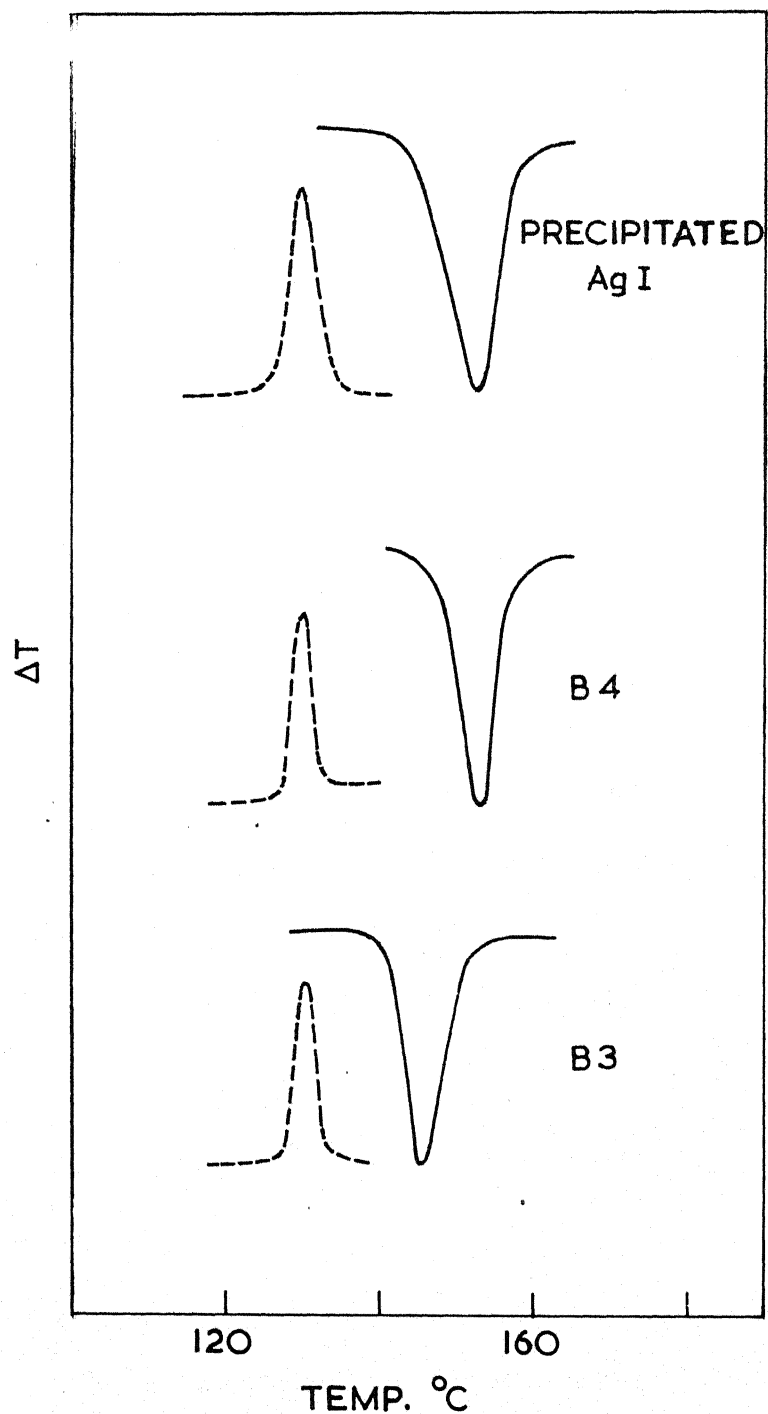


Fig.IV.2. DTA curves of pure B3, pure B4 and precipitated AgI (at 16°/minute heating rate). Full line indicates the forward transition while the broken line indicates the reverse transition.

indicate that the $B3 \rightarrow B4$ transformation is not a well-defined first order transformation. We are not even sure that $B3$ transforms to $B23$ through the $B4$ intermediate. It appears that the $B3 \rightarrow B4$ transformation is more likely to be higher order athermal transition as suspected by Schneer^{3,6}. Accordingly, the molar volumes of the $B3$ and $B4$ phases are quite close (41.23 and 41.22 c.c. respectively).

We have also followed the phase transitions of $B3$ and $B4$ by electrical conductivity measurements. The results (Fig. IV.3) clearly show that both $B3$ and $B4$ transform to the same phase ($B23$) although there is some indication of the $B3 \rightarrow B4$ transition prior to the transformation to the $B23$ phase. The energies of activation for conduction in the $B3$ and $B4$ phases are ~ 0.20 and ~ 0.60 eV respectively. The conductivity results are in general agreement with those reported by Takahashi and coworkers²². The lower energy of activation for conduction in the $B3$ phase is possibly associated with the larger concentration of defects in the cubic structure.

(b) Born treatment of the phase transitions of silver halides

In order to employ the Born model for the study of the phase transitions of silver halides it is necessary to have the appropriate repulsive parameters and other terms in the potential energy expressions for these solids. The repulsive parameters can be obtained by making use of the known physical data such as the lattice energies U , compressibilities β and thermal expansion coefficients, γ , of the stable phases. The repulsive parameters

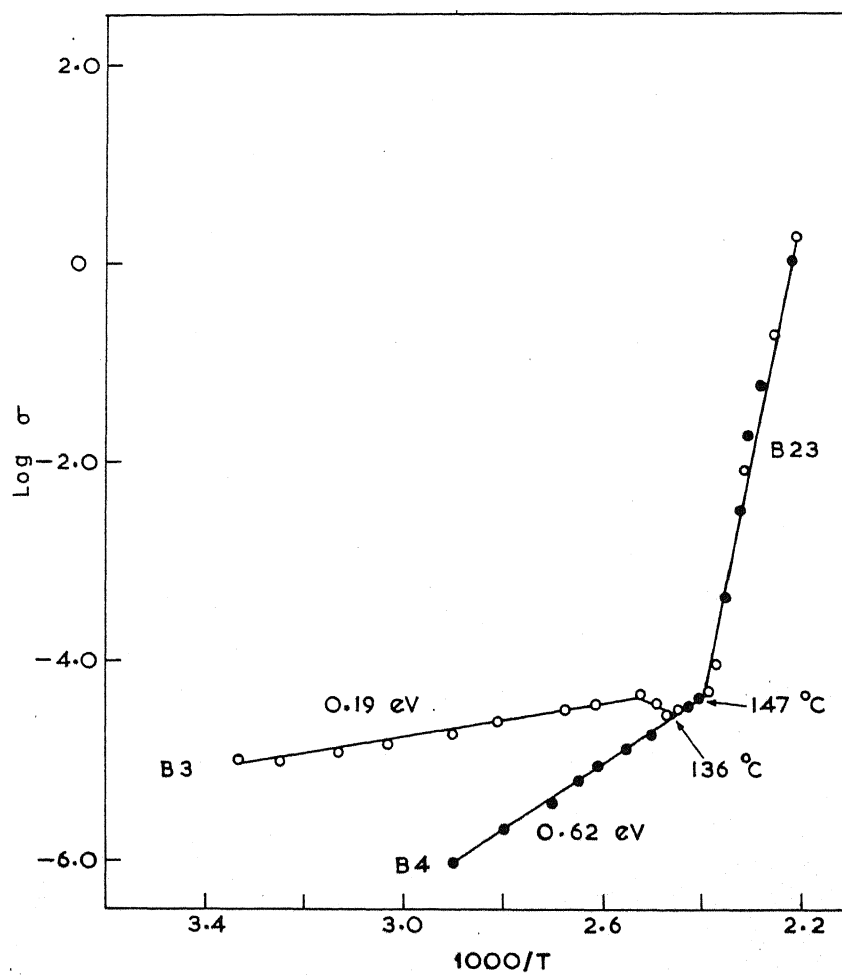


Fig. IV.3 Plot of the logarithm of a.c. conductivity of B3 and B4 AgI against the reciprocal of absolute temperature.

so calculated should account for the phase transitions of the silver halides as well. For this purpose, we have employed the two parameter repulsive term (including only the nearest neighbour interactions) in the Born expression for the potential energy of the solid:

$$U = \frac{Ae^2}{r} + K (C/r^6 + D/r^8) - M b \exp (-r/\rho) + \phi_0 \quad (1)$$

In equation (1) b and ρ are the two repulsive parameters, A is the Madelung constant, r is the equilibrium interionic distance, ϕ_0 is the zero point energy, C and D are the van der Waals constants for the dipole-dipole and dipole-quadrupole interactions respectively and M is the number of nearest neighbours. K is the van der Waals term multiplicand proposed earlier by Rao and coworkers^{10,11}; the need for employing $K > 1$ in many alkali halides has been established¹⁰⁻¹². Unlike in alkali halides, we could not employ the three or four-parameter repulsive terms due to the lack of sufficient data needed for the evaluation of these parameters.

The various terms as well as the physical data required for the calculation of the repulsive parameters of silver halides are given in Table IV.2. The van der Waals constants C and D are obtained from the values of the coefficients c_{++} , c_{+-} , c_{--} , d_{++} , d_{+-} and d_{--} and the corresponding lattice sums from Mayer²³. In the case of AgCl, the revised van der Waals constant proposed by Lynch²⁴ (with and without field correction) was also employed in addition to Mayer's value, to calculate the repulsive

TABLE IV.2

Data Employed for Evaluation of the
Repulsive Parameters of Silver Halides^(a)

	<u>AgCl (B1)</u>	<u>AgBr. (B1)</u>	<u>AgI (B3)</u>
Lattice energy, $U(\text{kcal/mole}^{-1})$	203	197	190
Interionic distance, r (Å)	2.772	2.884	2.812
c_{++} (10^{-60} ergs)	67	67	67
c_{--}	133	208	437
c_{+-}	89	109	151
d_{++} (10^{-76} ergs)	91	91	91
d_{--}	268	475	1228
d_{+-}	150	199	315
Compressibility, β (10^{-12} cm ² dyne ⁻¹)	2.4	2.75	4.11
Thermal exp. coefficient, γ (10^{-5} deg ⁻¹)	9.89	10.40	11.34

Structural Constants^(b)

		<u>B1</u>	<u>B2</u>	<u>B3</u>
Lattice Sums,	S'_6	6.5950	8.7088	4.3540
	S''_6	1.8070	3.5445	0.7620
	S'_8	6.1460	8.2077	4.1040
	S''_8	0.8000	2.1476	0.2530
Madelung Constant,	α	1.74756	1.76267	1.63805

(a) c_{++} , d_{++} etc., are from Mayer²³
 U and r are from Huggins⁹

(b) Structural constants are from Jones and Ingham²⁵.

parameters. The structural constants, viz., the lattice sums S_6^1 etc., and the Madelung constants were taken from Jones and Ingham²⁵.

In order to evaluate the repulsive parameters b and ρ we need another equation besides the lattice energy expression (1). We can obtain such relations by the differentiation of the lattice energy expression with respect to r as shown below:

$$r(dU/dr) = - \left[\alpha e^2/r + K(6C/r^6 + 8D/r^8) - (Mb/\rho) \exp(-r/\rho) \right] \quad (2)$$

$$r^2(d^2U/dr^2) = (2\alpha e^2/r) + K(42C/r^6 + 72D/r^8) - (r^2Mb/\rho^2) \exp(-r/\rho) \quad (3)$$

The left hand side of equation (2) is equal to $3V(P-T\eta/\beta)$, a result obtained from the vibrational Hildebrand relation and its volume derivative²⁶. The term $r^2(d^2U/dr^2)$ in equation (3) is given by $(9V/\beta) + 6V(P-T\eta/\beta)$ also obtained from the Hildebrand relations²⁶. These equations apply to the static crystal and so P and T refer to the normal pressure and temperature. β and η are the compressibility and coefficient of volume expansion of the stable phase and V is the molar volume of the solid. Equations (2) and (3) can be written in a convenient form as shown below:

$$1/\rho \left[rM b \exp(-r/\rho) \right] = S_1 \quad (4)$$

$$1/\rho^2 \left[r^2M b \exp(-r/\rho) \right] = S_2 \quad (5)$$

where

$$S_1 = \left[6e^2/r + K(6C/r^6 + 8D/r^8) - 3V(P-T\eta/\beta) \right]$$

$$S_2 = \left[24e^2/r + (48C/r^6 + 72D/r^8) - (9V/\beta) + 6V(P-T\eta/\beta) \right]$$

From equations (4) and (5) the value of ρ can be obtained since, $\rho = (S_2/S_1)r$. The value of ρ obtained can be fed into any one of the equations (1), (2) or (3) to calculate b . The values of ρ and b may thus be calculated for various assumed values of $K \gg 1$.

In the case of AgI, the van der Waals constants C and D are not available for the hexagonal structure; hence we have calculated b and ρ for the B3 phase of AgI (Table IV.2). An attempt to derive the repulsive parameters for AgI employing the thermal transformation data was difficult because of uncertainties in some of the physical data.

The repulsive parameters obtained for the B1 phases of AgCl and AgBr as well as for the B3 phase of AgI are listed in Table IV.3. In the case of AgCl, we have obtained the parameters for three different van der Waals coefficients. Mayer²³ long ago suggested the ρ (in 10^{-8} cm) values of AgCl, AgBr and AgI to be 0.247, 0.271 and 0.260 Å respectively. From our solutions in Table IV.3 we see that these ρ values of the silver halides are obtained when we employ Mayer's²³ van der Waals coefficients with K between 1.0 and 1.8. These results show the need for slightly increased van der Waals terms in the case of AgBr and AgI. In order

TABLE IV.3

Repulsive Parameters, b and ρ for Silver Halides
(b in 10^{-12} ergs mole $^{-1}$; ρ in 10^{-8} cm)

K	AgCl (a)				AgBr (b)		AgI (b)	
	MAYER		LYNCH I		b	ρ	b	ρ
	b	ρ	b	ρ				
1.0	20169	<u>0.245</u> ^(c)	25599	0.224	11914	0.278	21144	0.252
1.2	17832	0.253	25117	0.230	10614	0.287	18635	0.261
1.6	14589	0.272	22087	0.241	9188	0.302	15102	<u>0.275</u> ^(c)
1.8	13487	0.277	20628	<u>0.246</u> ^(c)	8797	0.307	13903	0.281
2.2	11939	0.286	18200	0.255	8338	0.317	12224	0.292
2.6	10954	0.290	16385	0.262	8180	0.324	11157	0.300
3.0	10310	0.297	15037	0.269	8142	0.330	10459	0.308
							16520	0.305

(a) The repulsive parameters are obtained by employing the van der Waals coefficients of Mayer and Lynch (I with field correction, II without field correction). In the case of Lynch II, we find $K \ll 1$ to obtain a ρ value close to Mayer's ρ value.

(b) Values employing van der Waals coefficients of Mayer.

(c) The underlined ρ values are pretty close to the values suggested by Mayer²³.

to pick unit sets of solutions for the silver halides we calculated the lattice energies of the stable phases and found that the parameters listed in Table IV.4 satisfactorily account for the experimental lattice energies reported by Tosi²⁷. We shall now examine whether these repulsive parameters also account for the phase transitions of silver halides.

The early studies of Bridgmann²⁸ showed that AgCl and AgBr transformed from the B1 structure to the B2 structure at ~ 88 and ~ 84 kbars respectively; there have been some modifications of Bridgmann's results recently^{29,30}. We have calculated the lattice energies of the B2 and B3 phases of AgCl and AgBr employing the repulsive parameters in Table IV.4 and the interionic distances of Huggins⁹. The lattice energies so calculated are shown in Table IV.5. The lattice energy differences between the B1 and B2 phases of AgCl and AgBr so calculated are 3800 ± 1000 and 9000 ± 1000 calories per mole respectively. These values are not unsatisfactory considering the large uncertainties in the experimental data reported in the literature.

The difference in the lattice energies of the B1 and B3 phases of AgI is calculated to be $2300 \text{ cal mole}^{-1}$. This is in good agreement with the experimental transition energy of $1500 \pm 500 \text{ cal mole}^{-1}$, calculated on the assumption that the transition pressure*

* There is some disagreement in the data on the pressure transitions of AgI as can be seen from the papers of Piermarini and Wier³², Shock and Jamieson³⁰, Basset and Takahashi¹, Adams and Davis² and Jacobs³¹.

TABLE IV.4

Repulsive Parameters Satisfying the Experimental
Lattice Energies of Silver Halides

		K	b (10^{-12} ergs mole $^{-1}$)	ρ (a) (10^{-8} cm)	Lattice Energy (b) (kcal mole $^{-1}$)
	Mayer	1.1	17832	0.250 (0.247)	214.1 (213.6)
AgCl (B1)	Lynch I ^(c)	1.2	18200	0.255	213.9
	Lynch II ^(c)	1.3	12305	0.267	213.8
AgBr (B1)	Mayer	1.3	16645	0.270 (0.271)	210.4 (210.2)
AgI (B3)	Mayer	1.3	47395	0.242 (0.260)	208.7 (208.1)

(a) ρ values in parentheses are from Mayer²³

(b) Tosi's reported experimental lattice energies are given in parentheses.

(c) See Table IV.3 foot note (a).

TABLE IV.5

Lattice Energies (in kcal mole⁻¹) of the
B1, B2 and B3 Phases of Silver Halides ^(a)

	<u>B1</u>	<u>B2</u>	<u>B3</u>
AgCl	214.1 (213.6) ^b	210.3	200.3
AgBr	210.4 (210.2) ^b	201.4	194.4
AgI	206.4	209.9	208.7 (208.1) ^b

(a) Values obtained with Mayer's van der Waals coefficients
(Table IV.2); Mayer's b and ρ are taken from Table IV.4.

(b) The values in parentheses are from Tosi²⁷.

is about 3-5 kilobars^{1,28,31}. We have calculated the lattice energy of the B2 phase of AgI assuming that this is close to the high temperature B23 structure. The lattice energy difference between the B3 and B2 phases of AgI is 1200 ± 200 cal mole⁻¹. Considering the gross assumptions made in these calculations, we feel that the Born treatment is fairly satisfactory in explaining the phase transitions of silver halides.

(c) Structures and phase transitions of AgI-AgBr solid solutions

The crystal structure data on the solid solutions of AgI and AgBr are given in Table IV.6. The diffractometer traces of a few solid solutions at 25°C, are shown in Fig. IV.4. It is seen that the lattice parameters of the B4 and B3 forms of AgI decrease (Table IV.6) upto 10-15% AgBr and remain constant for higher percentages of AgBr. This indicates that AgBr probably enters into solid solution with AgI either in the B3 or B4 form upto about 10-15% AgBr.* Above 15% AgBr, the x-ray lines due to the B1 phase start appearing, the intensities of the B1 reflections increasing with % AgBr. On the high AgBr side, incorporation of AgI increases the lattice constant of the B1 phase upto about 25-30% AgI (Table IV.6), possibly indicating the formation of a solid solution of B1 structure upto this composition. Extrapolation of the B1 lattice parameter of

* It is particularly interesting to see a drastic decrease in the c parameter of the solid solution containing $\sim 10\%$ AgBr; the cause for this is not clear.

We also obtained the lattice parameters of the B3 forms of the solid solutions by grinding the precipitates. We found that the formation of the B3 phase by grinding was more difficult in the case of solid solutions compared to pure AgI.

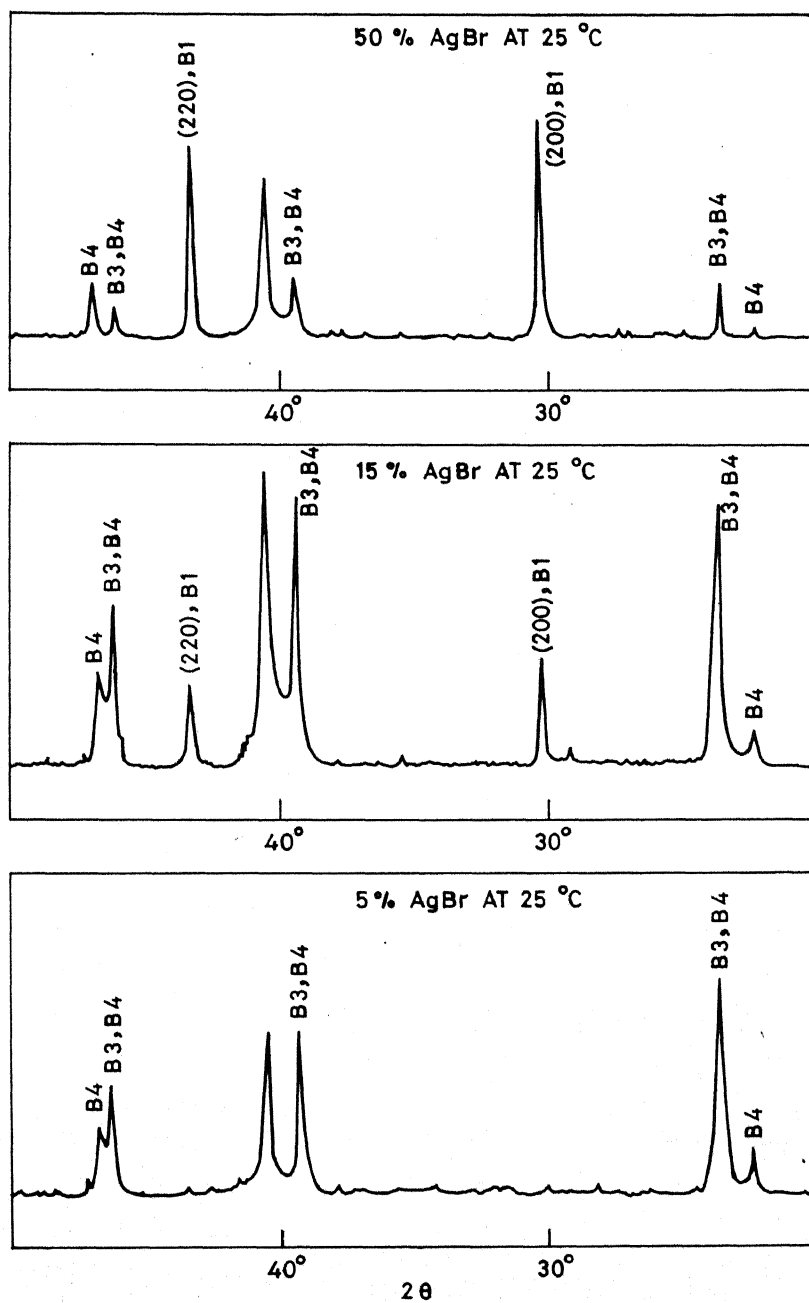


Fig. IV.4 X-ray powder diffraction patterns of AgI-AgBr solid solutions at 25°C, showing the appearance of B₁ phase above $\sim 10\%$ AgBr.

TABLE IV.6

Crystal Structure Data on the
Solid Solutions of AgI - AgBr

<u>Mole % AgBr</u>	B4		B3	B23 ^(a)	B1
	<u>a, Å</u>	<u>c, Å</u>	<u>a, Å</u>	<u>a, Å</u>	<u>a, Å</u>
0	4.591	7.498	6.495	5.074	(6.10) ^(b)
5	4.581	5.568	6.463	5.040	5.910
8	4.580	4.932	6.452	5.007	5.910
10	4.581	3.860	6.442	5.000	5.910
15	4.581	5.090	6.442	4.987	5.920
25	4.580	5.080	6.441	4.987	5.920
50	4.581	5.060	6.442	4.987	5.896
75	4.581	5.080	6.441	4.987	5.860

(a) At 170°C

(b) The value of 6.10 Å for pure AgI is the extrapolated value.

the solid solution gives a value of $a \sim 6.10 \text{ \AA}$ which is close to the expected value of the lattice constant of pure AgI in B1 form³².

The DTA curves of a few solid solutions are shown in Fig. IV.5 and the transition enthalpies are listed in Table IV.7. It can be seen that the DTA peaks appear distinctly at least upto 75% AgBr, the peak area decreasing with % AgBr. Obviously, the proportion of the AgI-AgBr solid solution (of the approximate composition $\text{AgI}_{0.9}\text{Br}_{0.1}$) decreases with increasing % AgBr. On the basis of the DTA peak areas we can roughly estimate the % solid solution of this composition as a function of % AgBr (Table IV.7). There is a slight increase in the thermal hysteresis with % AgBr; the volume change, ΔV , accompanying the $B3 \rightarrow B23$ transition also slightly increases with increasing AgBr content in the solid solutions. ΔV is maximum at $\sim 10\%$ AgBr.

X-ray diffraction patterns of the solid solutions distinctly show the reflections due to the B23 phase after the transition temperature (Fig. IV.6). The high temperature pattern consists of lines only due to the B1 and B23 phases as expected. The lattice parameter of the B23 phase of the solid solution decreases upto about 15% AgBr, again confirming that the solid solution limit persists in this high temperature phase as well.

We can readily construct a partial phase diagram of the AgI-AgBr system with the aid of the following experimental observa-

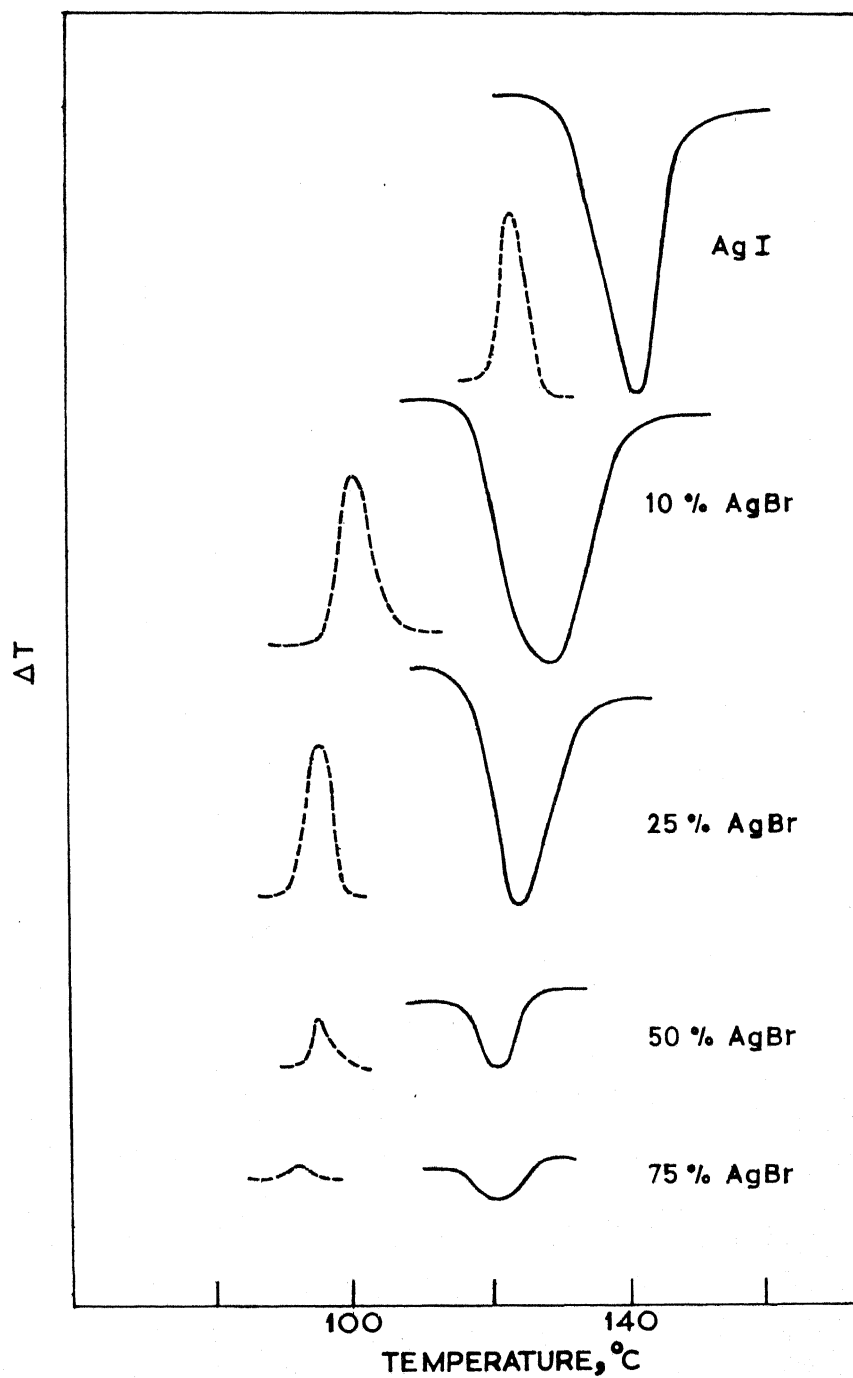


Fig. IV.5 DTA curves of AgI-AgBr solid solutions. Full line represents the forward transition while the broken line indicates the reverse transition.

TABLE IV.7

Transformation data on AgI - AgBr Solid Solutions

Mole % AgBr	T_t (forward), °C	ΔH (cals mole ⁻¹) ^(b)	Approximate ^(c) fraction of solid solution
0	146 (25) ^(a)	2000	-
5	132 (30)	1900	
10	130 (30)	1670	1.00
15	128 (30)	1560	0.93
25	128 (30)	1500	0.89
50	126 (30)	316	0.60
75	122 (30)	175	0.10

(a) The thermal hysteresis values are given in parentheses.

(b) ΔH values are for the composition $\text{AgI}_{(1-x)}\text{Br}_x$.

(c) The values are estimated from the ratio of the ΔH values with respect to the ΔH of 10% AgBr.

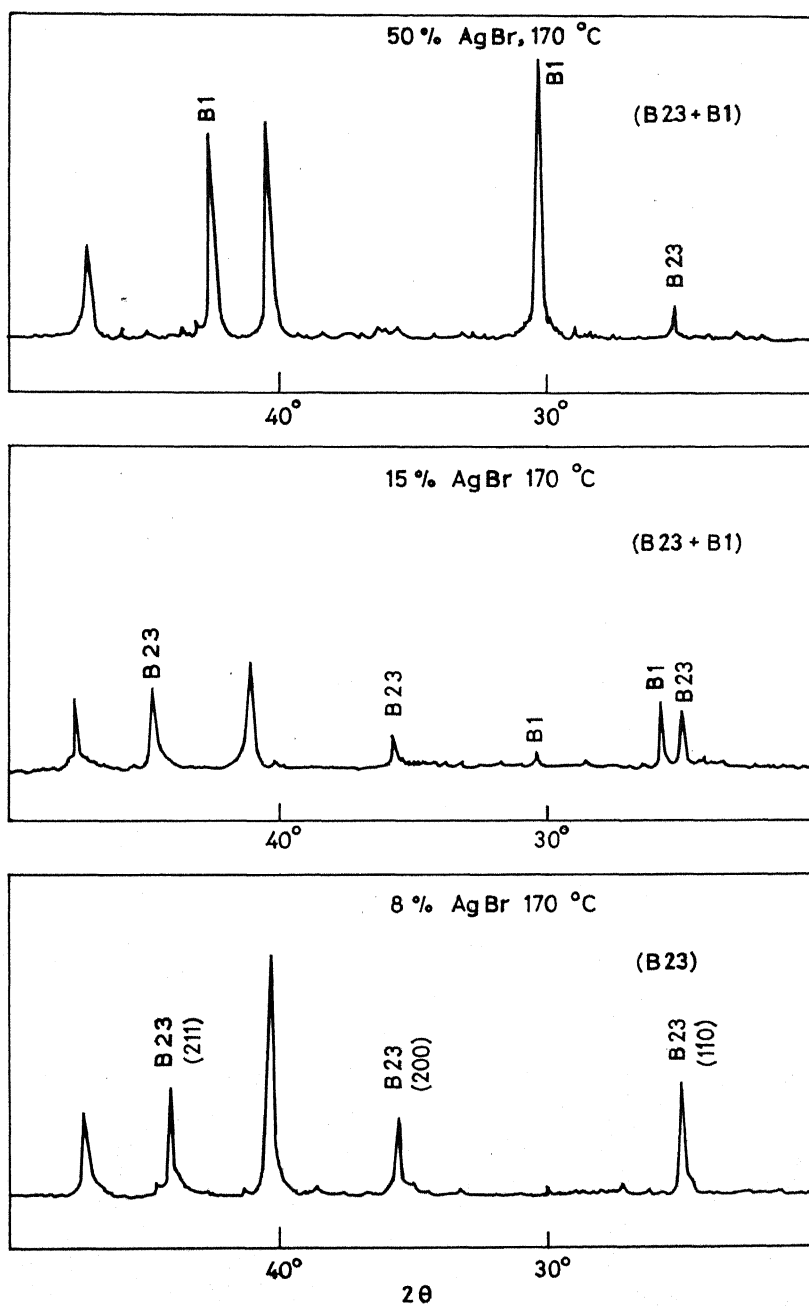


Fig. IV.6 X-ray powder diffraction patterns of AgI-AgBr solid solutions above transition temperature showing the presence of B1 and B23 structures.

tions: (i) AgBr enters into solid solution with AgI upto $\sim 15\%$ in the B3/B4 and B23 phases. (ii) AgI enters into solid solution with AgBr in the B1 phase upto $\sim 25\%$ (iii) the temperature of transition of the B3/B4 phase of the solid solutions (to the B23 phase) are available from the DTA curves. Above the transition temperature, B1 and B23 phases exist upto $\sim 80\%$ AgBr. There is a minor inconsistency in our observations from the DTA and x-ray studies in that at $\sim 75\%$ AgBr we still see the transition of B3/B4 to B23 (Fig. IV.5) even though x-ray patterns show formation of good solid solutions of B1 structure. The x-ray patterns however, have some weak reflections of B3/B4 phases of solid solutions, even at $\sim 75\%$ AgBr. These difficulties may be due the nonequilibrium nature of the precipitates. (iv) The percentage of the solid solution of the approximate composition $\text{AgI}_{0.9}\text{Br}_{0.1}$ estimated from the relative DTA peak areas may be employed to show the composition limits of the two solid solutions on the high and low AgBr sides of the phase diagram. (v) Melting points were determined by DTA curves and the eutectic temperature (minimum melting point) was found to be 340°C at $\sim 68\%$ AgBr.

The partial phase diagram constructed with the above data is shown in Fig. IV.7; the broken lines are shown in the diagram to indicate that we do not know the exact position of these lines. The phase diagram shown in Fig. IV.7 differs from that of Stasiw and Teltow¹⁵. We feel that the phase diagram by Stasiw and Teltow¹⁵, not only fails to conform to the experimental observations on the

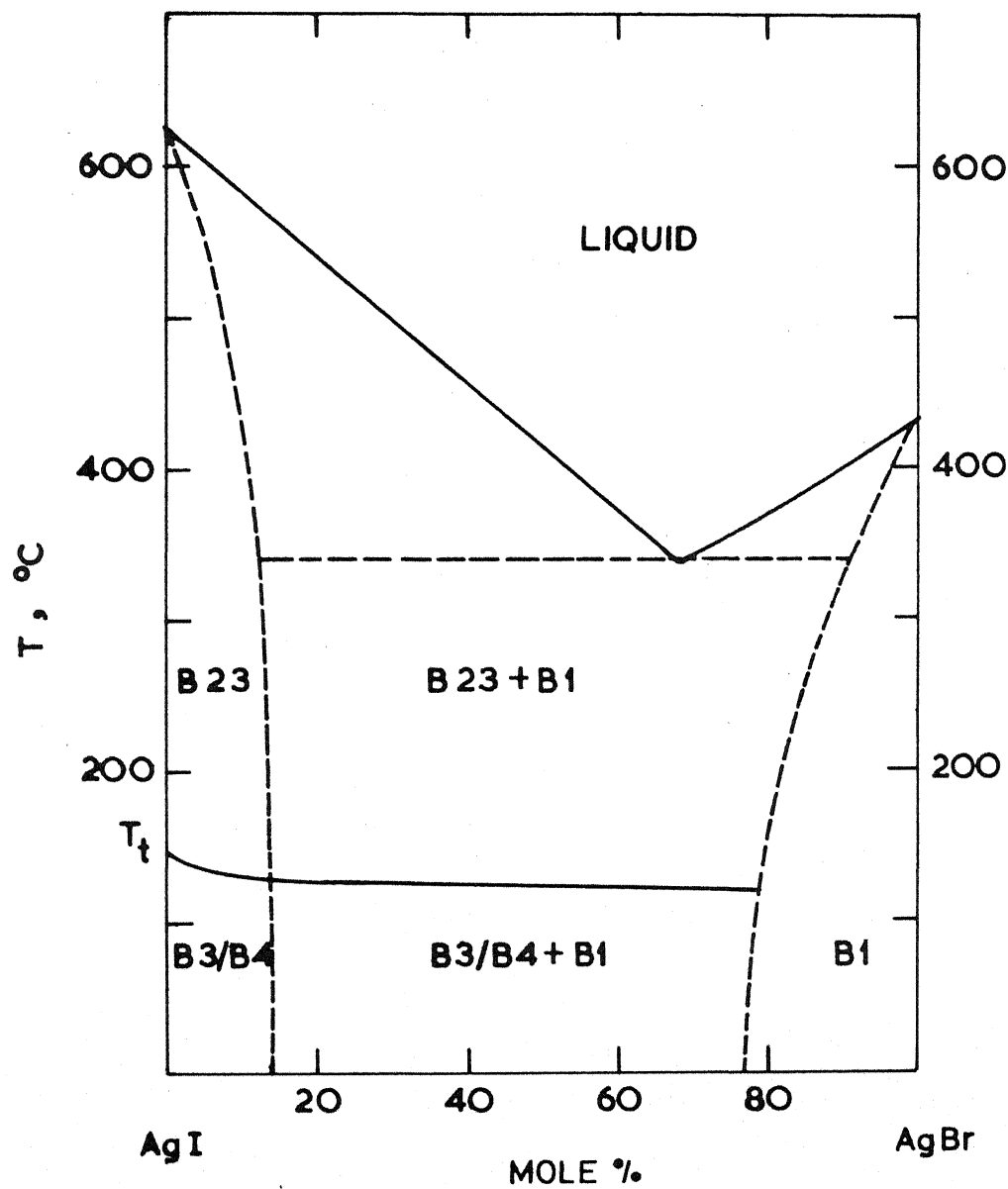


Fig.IV.7. Partial phase diagram of the AgI-AgBr system.

solid solutions, but also contradicts the accepted rules in constructing phase diagrams. The eutectic point reported by them is also in error.

(c) Born treatment of the AgI-AgBr solid solutions

The lattice energies of the B1, B2 and B3 structures of AgCl, AgBr and AgI were listed in Table IV.5. To a first approximation we can calculate the lattice energy of a solid solution, $U^{S.S.}$, as the weighted sum of the lattice energies of the components⁹:

$$U^{S.S.} = \left[f U_{AgBr} + (1-f) U_{AgI} \right], \quad (7)$$

where U_{AgBr} and U_{AgI} are the lattice energies of the two compounds in the same structure, and f is the mole fraction of AgBr in the solid solution. We calculated the lattice energies of the solid solutions in the B1 and B3 structures employing equation (7) (Table IV.8). The results show that at $\sim 15\%$ AgBr the B1 structure of the solid solution becomes more stable than the B3 structure. This is in good agreement with the experimental results discussed earlier (see Figures IV.4 and IV.7).

IV.3 EXPERIMENTAL

(a) Preparation of AgI and AgI-AgBr solid solutions

AgI was prepared by adding a 5% solution of $AgNO_3$, with stirring, to a solution of KI, the samples being of analytically

TABLE IV.8

Lattice energies (kcal mole⁻¹) of the
AgI-AgBr Solid Solutions in B1 and B3 forms^(a)

<u>Mole % AgBr</u>	<u>B1</u>	<u>B3</u>
0	206.4	208.7
5	206.6	208.0
10	206.8	207.3
15	207.0	206.8
25	207.2	205.1

(a) The lattice energies of AgBr and AgI for the corresponding structures are taken from Table IV.5

pure grade. Precipitation, washing, filtration and drying were done in dark enclose to prevent the action of light. The AgI thus prepared was a mixture of B3 and B4 forms as found by x-ray diffraction (Fig. IV.1) analysis.

The B4 form of AgI was prepared by dissolving the precipitated AgI in excess of KI solution and reprecipitating the AgI by addition of drops of water with stirring. The precipitate of B4-AgI was washed filtered and dried under similar conditions described earlier. The lattice constants were determined to be $a = 4.591 \text{ \AA}$, and $c = 7.498 \text{ \AA}$ (NBS values : $a = 4.592 \text{ \AA}$ and $c = 7.510 \text{ \AA}$)¹⁸.

The B3 form of AgI was prepared from the B4 form. The B4 sample initially maintained at $\sim 100^\circ\text{C}$ was ground continuously in a mortar, when the temperature was reduced to room temperature. This process of grinding while cooling, was repeated about three times to ensure complete conversion of B4 into B3 form. The B4 form which had a bright yellow colour changed to orange red indicating the $B4 \rightarrow B3$ conversion. The lattice constant of B3 form at 25°C , was found to be $a = 6.495 \text{ \AA}$ (NBS value: $a = 6.495 \text{ \AA}$)¹⁸.

The solid solutions were prepared by coprecipitating AgI and AgBr, by adding 5% AgNO_3 solution to a mixture of solutions (containing appropriate amounts) of KI and KBr. Solid solutions of AgI and AgBr were also prepared by fusing the pure components at $\sim 600^\circ\text{C}$. Solid solutions prepared by precipitation as well as

fusion yielded identical results in the x-ray and DTA investigations. The B3 forms for the solid solutions ($\text{AgBr} \leq 10\%$) were prepared by grinding the precipitated solid solution. We found it more difficult to obtain the B3 form by this procedure unlike in pure AgI . Apparently AgBr does not favour the formation of B3 form in solid solutions. The percentage B3 form was, however, greater in the ground samples.

(b) Differential thermal analysis

The phase transformations were studied by recording the differential thermal analysis (DTA) curves employing an Aminco thermoanalyzer, fitted with a programmed furnace, voltage stabilizer, deviation amplifier and an automatic X-Y recorder. Typical thermograms obtained under constant heating rate were given in Figs. IV.2 and IV.6. The applicability and limitations of DTA as a tool for the study of crystal structure transformations have been well examined in this laboratory^{21,33}. The procedure for obtaining the enthalpies and energies of activation from DTA curves, and the uncertainties in such results have been discussed by Rao and Rao²¹. Plots of $\log k$ versus $1/T$ (employing the procedure of Borchardt and Daniels³⁴) for evaluating E_a for the $\text{B3} \rightarrow \text{B23}$ and $\text{B4} \rightarrow \text{B23}$ transformations are given in Fig. IV.8; here k is given by $\Delta T/A-a$ where ΔT is the differential temperature and A and a represent the total amount and quantity transformed respectively. The melting points of the samples were determined by heating the samples in fusion cups in the thermoanalyzer.

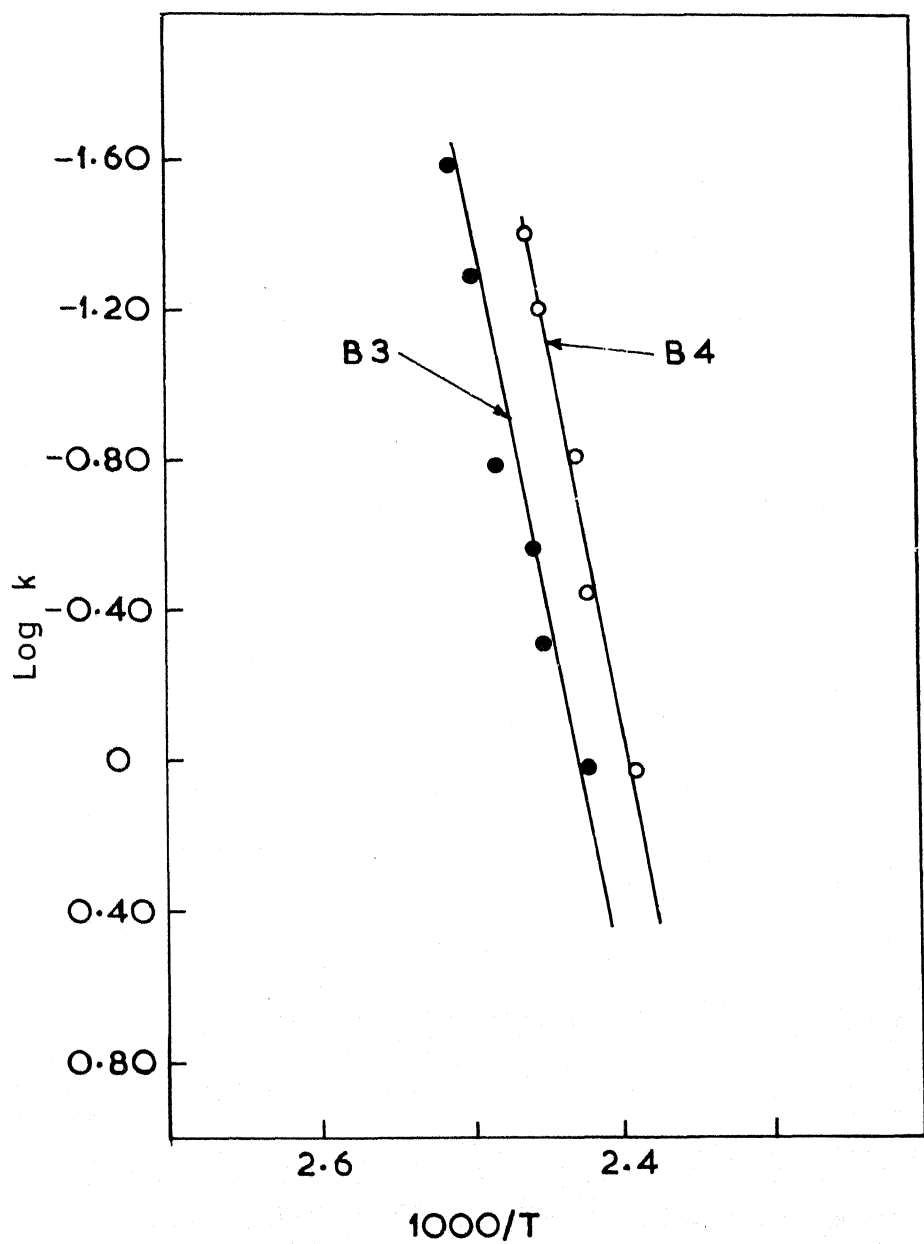


Fig. IV.8 Activation energy plots from DTA data ($\log k$ versus $1/T$) for the $B3 \rightarrow B23$ and $B4 \rightarrow B23$ transitions of AgI.

(c) X-ray diffraction

X-ray diffraction patterns were recorded employing a General Electric (XRD-6) diffractometer, $\text{CuK-}\alpha$ radiation ($\lambda = 1.5405 \text{ \AA}$). The high temperature patterns of pure AgI as well as that of solid solutions were recorded at $\sim 170^\circ\text{C}$, employing a sample holding furnace assembly fitted with a temperature programmer. Typical x-ray diffraction patterns were shown in Figs. IV.1,4 and 6. We are not able to explain the origin of the extra line at $2\theta = 40-41^\circ$ in all the patterns. The lattice dimension of the B23 form of pure AgI was found to be 5.074 \AA at $\sim 170^\circ\text{C}$. (Lit. value: $a = 5.04 \text{ \AA}$ at 25°C)¹⁷.

(d) Far infrared spectra

The far infra red spectra were recorded in the region 300 to 30 cm^{-1} in a Beckmann IR-11 spectrometer, in a polyethylene matrix, at 25°C .

(e) Electrical conductivity.

The AC resistivity (at 1KHz) of B3 and B4 forms (made into polycrystalline pellets, dia. 1.30 cm and thickness $\sim 0.2 \text{ cm}$) in a conductivity cell³⁵ with a metal spring load to support the pellet between platinum discs. The resistance was measured as a function of temperature with a General Radio Impedance bridge (1608-A).

Born calculations on silver halides were made on the IBM 7044/1401 computer of this Institute.

Acknowledgement

The author is thankful to Mr. J.K. Jain of the Mechanical Engineering Department for assistance in computer programming. The author's thanks are due to Dr. J.R. Ferraro of the Argonne National Laboratory for the far infrared spectra.

REFERENCES

1. W.A. Basset and T. Takahashi, *Am. Mineralogist*, 50(10), 1576 (1965).
2. L.H. Adams and B.L. Davis, *Am. J. Sci.*, 263, 359 (1965).
3. C.J. Schneer, *Acta Cryst.*, 8, 279 (1955).
4. G. Burley, *J. Phys. Chem.*, 68, 1111 (1964).
5. A.J. Majumdar and R. Roy, *J. Phys. Chem.*, 63, 1858 (1959).
6. C.J. Schneer and R.W. Whiting Jr., *Am. Mineralogist*, 48, 737 (1963).
7. L.W. Strock, *Z. Physik. Chem.*, B25, 441 (1934).
8. S. Hoshino, *J. Phys. Soc., (Japan)*, 12, 315 (1957).
9. M.L. Huggins in "Phase Transformations in Solids", (ed. by R. Smoluchowski, John Wiley & Sons, New York, 1951).
- 10a. K.J. Rao, G.V. Subba Rao and C.N.R. Rao, *Trans. Faraday Soc.*, 63, 1013 (1967).
- 10b. K.J. Rao and C.N.R. Rao, *Proc. Phys. Soc.*, 91, 754 (1967).
11. K.J. Rao, G.V. Subba Rao and C.N.R. Rao, *J. Phys. C. (Proc. Phys. Soc.)*, Ser., 2, 1, 1134 (1968).
12. M. Natarajan, K.J. Rao and C.N.R. Rao, *Trans. Faraday Soc.*, 65, 0000 (1969).
13. T. Barth and G. Lunde, *Z. Physik. Chem.*, 122, 293 (1926).
14. H. Chateau, M.C. Moncet and J. Pouradier, *Science et. indus. phot.*, 27, 402 (1956).
15. V.O. Stasiw and J. Teltow, *z. anorg. chem.*, 259, 143 (1949).
16. A. de Cugnac, H. Chateau and J. Pouradier, *Compt. rend. Acad. Sci., Paris*, Ser. C, 14, 264 (1967).
17. I.E. Knaggs, B. Kalik and C.F. Elam, quoted in 'Crystal Data' (ACA Monograph No.5), ed. by J.D.H. Donnay, USA, 1963.

18. 'Standard x-ray Diffraction Powder Patterns', ed. by H.S. Swanson, M.C. Morris, E.H. Evans and L. Ulmer, National Bureau of Standards Vols., 8, and 9 (1964).
19. C.R. Berry, Phys. Rev., 161, 848 (1967).
20. G.L. Bottger and A.L. Geddes, J. Chem. Phys., 46, 3000 (1967).
21. K.J. Rao and C.N.R. Rao, J. Material Sci., 1, 238 (1966).
22. T. Takahashi, K. Katusmi and Y. Osamu, J. Electrochem. Soc., 116, 357 (1969).
23. J.E. Mayer, J. Chem. Phys., 1, 327 (1933).
24. D.W. Lynch, J. Phys. Chem. Solids, 28, 1941 (1967).
25. J.L. Jones and A.E. Ingham, Proc. Roy. Soc., A107, 636 (1925).
26. F.G. Fumi and M.P. Tosi, J. Phys. Chem. Solids, 23, 295 (1962).
27. M.P. Tosi, 'Solid State Physics', Vol. 16, p. 1 (1964) (ed. by F. Seitz, Academic Press, New York).
28. P.W. Bridgmann, Proc. Am. Acad. Arts, Sci., 76, (1945).
29. P.W. Montgomery, Am. Soc. Mech. Engrs. Paper 64, WA/PT-18 (1964).
30. R.N. Shock and J.C. Jamieson, J. Phys. Chem. Solids, 30, 1527 (1969).
31. R.B. Jacobs, Phys. Rev., 54, 325 (1938).
32. G.J. Piermarini and C.E. Weir, J. Res. Natl. Bur. Std., A66, No. 4, 325 (1962).
33. M. Natarajan, A.R. Das and C.N.R. Rao, Trans. Faraday Soc., 65, 3081 (1969).
34. H.J. Borchardt and F. Daniels, J. Am. Chem. Soc., 79, 41 (1957).
35. G.V. Subba Rao, Ph.D. Thesis 1969 (Indian Institute of Technology, Kanpur).

CHAPTER V

PARTICLE SIZE EFFECTS AND THERMAL HYSTERESIS IN CRYSTAL STRUCTURE TRANSFORMATIONS

CHAPTER V

PARTICLE SIZE EFFECTS AND THERMAL HYSTERESIS IN CRYSTAL STRUCTURE TRANSFORMATIONS*

V.1 INTRODUCTION

The effect of particle size on crystal structure transformations has not been reported extensively in the literature¹. Buerger² has pointed out that small particle size may favour a crystal structure transformation if the transformation is aided by a fluid phase in which the parent phase is soluble. Thus, the reconstructive transformation of powdered wurtzite is slower than that of single crystals³. If the transformation is not aided by solution, it is expected to proceed by a cooperative mechanism and hence favoured by larger particles. In the quartz crystoballite transformation, the transitional non-crystalline phase has been found to grow and decay considerably faster in finely divided samples⁴. In the anatase-rutile

* Papers based on these studies have appeared in the Transactions of the Faraday Society, 65, 3081 (1969) and Journal of Materials Science, (1970).

transformation, particle size and surface area seem to have little effect on the transformation⁵; in the ferroelectric transformation of BaTiO_3 , small particles markedly affect the enthalpy⁶. In the case of ZrO_2 , the metastable tetragonal phase gets stabilized by the excess surface energy in samples of small particle size⁷.

We have presently investigated particle size effects on the temperature, thermal hysteresis and enthalpies of the following crystal structure transformations. The phase transformations studied are^{1,8} (i) the $\alpha - \beta$ inversion of quartz ($\sim 575^\circ\text{C}$) (ii) the orthorhombic \rightleftharpoons hexagonal transformation of K_2SO_4 ($\sim 580^\circ\text{C}$) (iii) the orthorhombic II \rightarrow rhombohedral I ($T_1 \sim 136^\circ\text{C}$) and rhombohedral I \rightarrow rhombohedral III ($T_2 \sim 118^\circ\text{C}$) transformations of KNO_3 (iv) $\text{Pm}\bar{3}\text{m} \rightleftharpoons \text{Fm}\bar{3}\text{m}$ transformations of NH_4Cl ($\sim 184^\circ\text{C}$) and NH_4Br ($\sim 165^\circ\text{C}$) and (v) hexagonal \rightleftharpoons cubic transformation of AgI ($\sim 147^\circ\text{C}$). Thermal hysteresis in KNO_3 transformation could not be studied because of the structural hysteresis in the transformation. We have examined the applicability and limitations of the technique of differential thermal analysis^{8,9} to the study of particle size effects on crystal structure transformations.

We have examined the thermal hysteresis⁹ in reversible crystal structure transformations in the light of Turnbull's theory of heterogeneous nucleation¹⁰ and also in terms of thermodynamics. Introducing some approximations, Turnbull's theory of nucleation has been employed to evaluate the interfacial energies between the

two phases of a solid undergoing a reversible phase transformation. The interfacial energies can also be obtained by the method suggested by Bruce¹¹ for solid-liquid and solid-gas interfaces. The results of the two methods have been compared for AgI, CsCl, quartz, NH_4Cl , NH_4Br and K_2SO_4 .

V.2 RESULTS AND DISCUSSION

(a) Effect of rate of heating and particle size on thermal hysteresis

The effect of particle size on the phase transformations of quartz, K_2SO_4 and KNO_3 under constant rate of heating are given in Table V.1. It can be seen that the transformation temperatures generally decrease with the increase in particle size. Chang¹² has similarly reported that for small particle sizes, T_t is higher in the $\alpha - \beta$ transition of cristoballite. What is more interesting to us is that the $\alpha - \beta$ transition of quartz which is traditionally believed to show almost no thermal hysteresis^{8,13}, exhibits appreciable hysteresis when the particle size is small. Observation of thermal hysteresis, ΔT , may be taken to indicate absence of thermodynamic equilibrium at all stages of the transformation. It has been suggested that ΔT is proportional to the volume change (and the strain energy) accompanying the transformation^{8,14,15}; it is possible that the strain energy would be greater in small particles. In Table V.1 we have given the values of $\Delta T_i (= T_i^f - T_i^r)$ as well as $\Delta T_p (= T_p^f - T_p^r)$; the former does not include kinetic factors

TABLE V.1

Variation of Transformation Temperatures, Thermal Hystereses and Enthalpies with Particle Size

Quartz		K_2SO_4		KNO_3							
Size, μ	$T_t, ^\circ\text{C}$	$\Delta T^{(a)}$	$\Delta H(\text{cals mole}^{-1})$	Size, μ	$T_t, ^\circ\text{C}$	$\Delta H(\text{cals mole}^{-1})$	$T_2, ^\circ\text{C}$				
5.5	582	12(5)	112	7.5	600	23(5)	1750	5.5	140	1450	110
13.0	580	10(5)	105	13.0	602	24(5)	1650	15.0	138	1400	108
18.0	578	10(5)	100	29.0	597	21(5)	1350	29.0	140	1300	120
29.0	572	7(5)	96	49.5	590	20(5)	1200	49.5	140	1200	118
93.5	576	6(5)	82	83.5	590	18(5)	1075	83.5	140	1175	120
210.0	576	5(5)	72	115.0	588	15(5)	1000	115.0	133	1000	118
258.5	573	3(5)	66	137.0	590	15(5)	950	137.0	130	1050	115

(a) ΔT_p values ($=T_p^{\text{forward}} - T_p^{\text{reverse}}$) are given here. The values in parenthesis refer to $\Delta T_i (=T_i^{\text{forward}} - T_i^{\text{reverse}})$

since the transformation temperatures T_i correspond to the initiation of transformations⁸. As such the ΔT_i values do not vary much with particle size (Table V.1).

Since thermal hysteresis in reversible transformation is likely to be a consequence of non-equilibrium conditions, we have examined the hysteresis as a function of heating rate in quartz and K_2SO_4 samples of different particle sizes. The results shown in Table V.2 indicate that ΔT decreases with decrease in the rate of heating. The extrapolated value of ΔT (Fig. V.1) at zero rate of heating is appreciably smaller (it is nearly zero in some cases) than that at finite rates of heating. This is understandable since we would be closer to the equilibrium conditions at slow rates of heating; we would therefore expect hysteresis to be minimal when particle size is large and heating rates are slow.

(b) Thermodynamic treatment of hysteresis

We could consider the work done due to change in volume in a transformation $P\Delta V$, as equal to the thermal energy $C_p \Delta T$. Here, ΔV is the change in molar volume accompanying the transformation, ΔT is the thermal hysteresis, and C_p is the heat capacity of the transformed nuclei. The increased pressure, P , experienced by the nuclei during the transformation can be approximated by $P = \Delta V / \beta V$, where β is the compressibility of the transforming phase. Thus, we find,

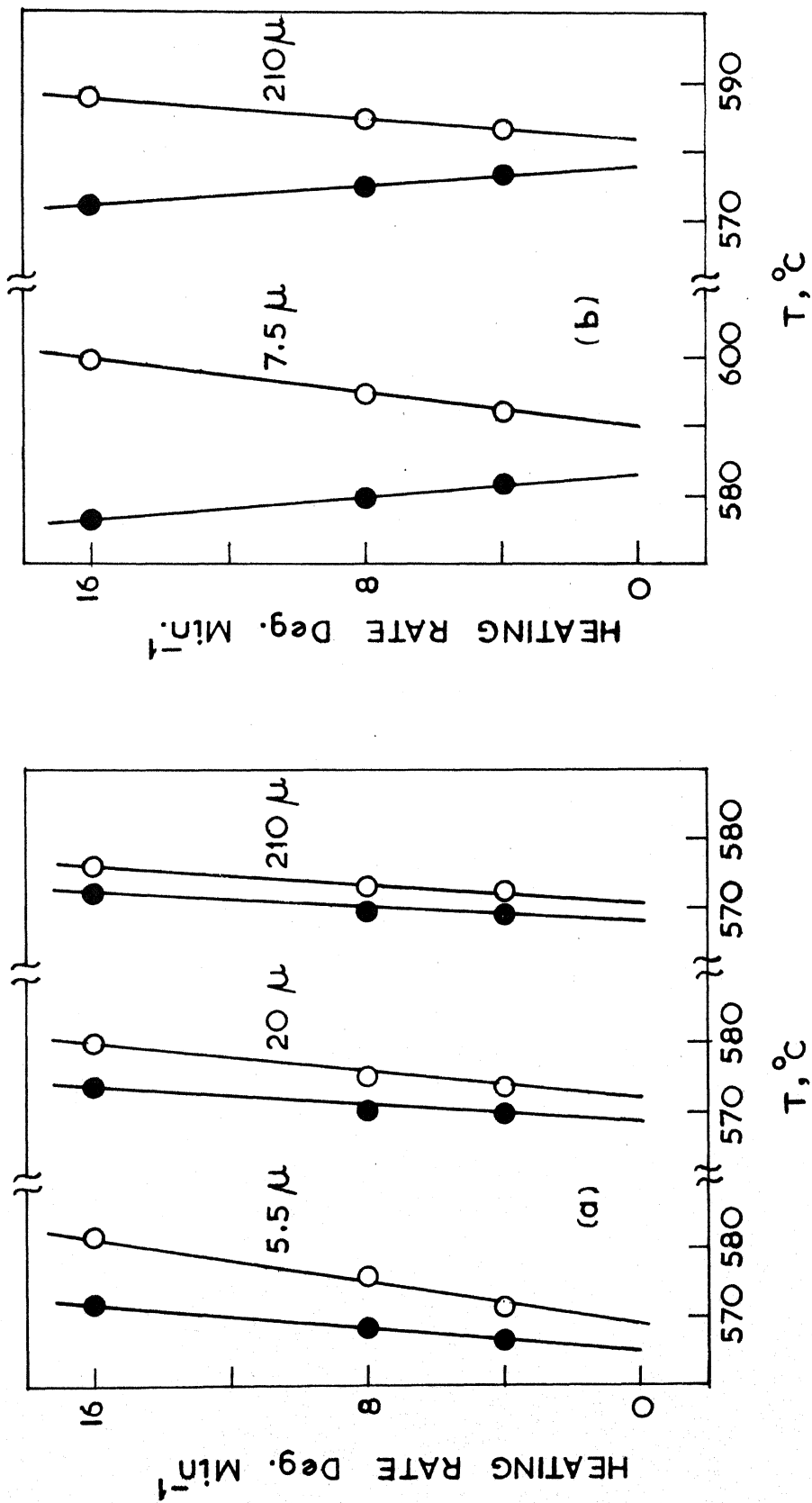


Fig. V.1. Variation of ΔT with rate of heating for different sizes of quartz (a) and K₂SO₄ (b). Open circles represent T_f (heating) and closed circles T_r (cooling).

TABLE V.2

Rate of Heating and Thermal Hysteresis

Heating rate (deg. min ⁻¹)	Quartz (a)			K ₂ SO ₄ (a)	
	<u>5.5 μ</u>	<u>20 μ</u>	<u>210 μ</u>	<u>7.5 μ</u>	<u>115 μ</u>
16	12.00	6.00	5(5)	23	15(5)
8	8.00	3.50	3(3)	15	10(4)
4	6.00	2.50	2(2)	11	6.5(3)
0 (b)	4.00	2.00	1(0-1)	7	5(1-2)

(a) Hysteresis data are based on DTA peak temperatures (ΔT_p). The ΔT_i values are given in paranthesis in one case; the values were similar with different particle sizes.

(b) Extrapolated value.

$$\Delta T = (1/c_p \beta) (\Delta V)^2 / V \quad (1)$$

Equation (1) assumes that the entire volume change of the crystal takes place under the same pressure. It is likely, however, that the transformation proceeds with relative ease after the nuclei reach a critical size. We may therefore need to multiply the right hand side of equation (1) by a factor $K (0 < K < 1)$. Since it is not possible to estimate the value of K , we have calculated the ΔT values assuming K to be unity (equation 1) for four phase transitions where data on β , c_p and ΔV are available; unfortunately, these data were not available for KNO_3 and K_2SO_4 . The calculated values are compared in Table V.3, with the experimental ΔT_i values (at zero rate of heating) obtained with samples of fairly large particle size ($> 150 \mu$). In spite of the gross assumptions made in deriving equation (1) we see that the calculated and the observed ΔT values vary in the same direction; the results are indeed encouraging.

(c) Thermal Hysteresis and Turnbull's theory of heterogeneous nucleation

The increase in ΔT with decrease in particle size is similar to the observation of Turnbull¹⁰ in the case of liquid-solid transformations in metals. According to Turnbull, the rate of heterogeneous nucleation, R_n , may be defined as the number of nuclei of the new phase appearing per unit area of the parent phase per second.

TABLE V.3

Experimental and Calculated Values of ΔT

	$\Delta V^2/V$	$\Delta T^{(a)}$ (calculated)	$\Delta T_i^{(b)}$
SiO ₂	0.08	4.3	< 1
AgI	0.07	2.9	< 1
NH ₄ Cl	1.21	24.7	6
NH ₄ Br	2.26	44.0	14

- (a) An average value of C_p of the bulk phase in the transformation region was taken for ΔT_p calculation.
- (b) Extrapolated values at zero rate of heating; experimental ΔT_i values were obtained at 16°, 8°, and 4° min⁻¹. ΔT_p values cannot be used here since they include kinetic factors.

$$R_n = R_o \exp \left\{ -(A/\Delta T^2) f(\theta) \right\} \exp (-\Delta F_D/k_T) \quad (2)$$

where R_o is a constant involving a vibrational frequency term and ΔF_D is the activation energy for material transport. The term $f(\theta)$ has value $0 < f(\theta) \leq 1$ and is determined by the contact angle, θ , between the parent phase and the new phase and A is given by,

$$A = \frac{16 \pi \gamma_{T_o}^3}{3kT \Delta H_v^2} \quad (3)$$

In equation (3), γ is the interfacial energy between the two phases, T_o and T are the equilibrium and observed transformation temperatures and ΔH_v is the volumetric heat of transformation. At the onset of nucleation, R_n will be sufficiently high so that we may take R_n to be equal to $(1/4\pi r^2)$ where r is the radius of the particle (assumed to be spherical). Thus, we get

$$1/r^2 \approx 4\pi R_n \approx 4\pi R_o' \exp \left\{ A' / (\Delta T)^2 \right\} \quad (4)$$

where $A' = Af(\theta)$ and R_o' includes the second exponential term in equation 2. Equation 4 can be simplified to the form:

$$\log \langle r \rangle^* = B + \left[C / (\Delta T)^2 \right] \quad (5)$$

where B and C are constants. It is indeed found that plots of $\log \langle r \rangle$ against $1/(\Delta T_p)^2$ are linear in the case of quartz and K_2SO_4 upto a particle size of about 100 microns (Fig. V.2). The linearity is found with the data at zero heating rate

* $\langle r \rangle$ refers to the average particle size given in Table V.1.

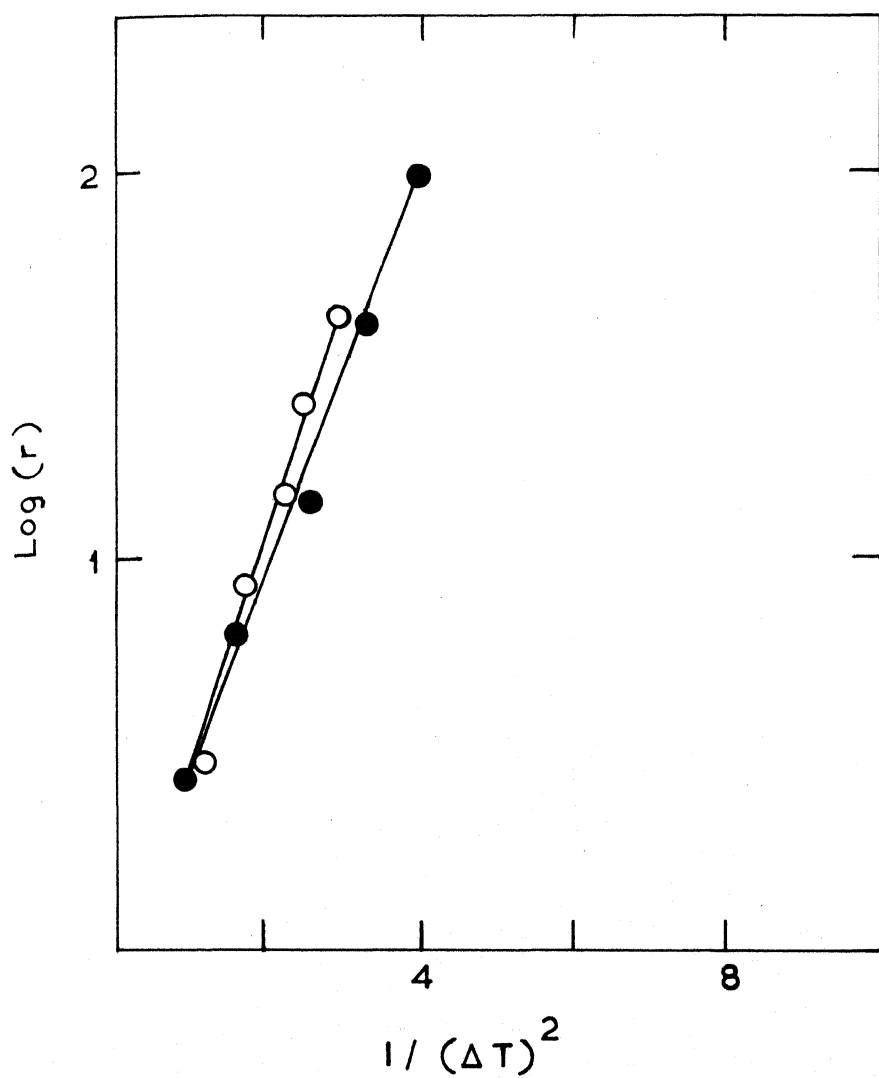


Fig.V.2. Plots of $\text{Log}(r)$ versus $1/(\Delta T)^2$ for quartz (shaded circles) and K_2SO_4 (open circles).

Table V.2) as well. With large particle sizes, equation (5) fails probably because of effects of grain boundaries and related factors. It may be noted that Rao and Rao⁸ had earlier found that particle size effects on ΔT and strain energies are negligible in the particle size range, 150-450 microns.

(d) Interfacial energies in solids

Interfacial energies have been estimated by Turnbull¹⁰ in liquid-solid transformations. We have attempted to estimate the interfacial energies of some solids studied here employing the nucleation theory. The nucleation rate of the solid phase (number cc^{-1}) in individual droplets (in liquid-solid transformations), R_n and ΔT are related by an expression similar to equation (2) and here the rate of transformation has been assumed to be proportional to the rate of nucleation. The quantities A , $f(\theta)$, ΔF_D have the same significance as mentioned earlier. Assuming homogeneous nucleation on the surface, $f(\theta)$ becomes equal to 1. Since $\Delta T = |T_0 - T|$, is not very large, the transport term, $\Delta F_D/kT \approx \Delta F_D/kT_0$ can be assumed to be a constant. These approximations lead to the expression $\ln \langle r \rangle = B + C \gamma^3 / (\Delta T^2)$ which is similar to equation (5), except that the slope of the linear plot of $\ln \langle r \rangle$ against $1/(\Delta T^2)$ will be equal to $C \gamma^3$. Since C is given by $C = 16 \pi T_0^2 / 3 k T \Delta H_V^2$, γ can be readily evaluated. Here, surface nucleation has been assumed to take place rather than bulk nucleation; if, however, bulk nucleation is

present, these conclusions will still be valid, but C will be given by $C = 16\pi T_0^2 / 9kT \Delta H_V^2$. The interfacial energy γ of quartz and K_2SO_4 estimated from the values of C are 1.30 and 1.40 ergs cm^{-2} respectively (Table V.5). The effect of particle size on the crystal structure transformations of AgI, NH_4Cl and NH_4Br could not be studied because of heavy agglomeration of particles (especially below 100 microns) which rendered the separation of various sizes difficult.

Interfacial energies can also be estimated from the DTA curves for the phase transformations (Fig. V.3) where the ordinate Y is taken to be proportional to R_n in equation (2). Even though the absolute value of R_n may change rapidly with ΔT during the transformation, Y may still be considered to be proportional to R_n :

$$Y = KR_n = KR_0 \exp \left\{ - A\gamma^3 / \Delta T^2 \right\} \quad (6)$$

In equation (6) K is unknown but is likely to be very small. If equation (6) is valid, then a plot of $\log Y$ versus $1/\Delta T^2$ should give a measure of the interfacial energy γ . A typical plot for CsCl is shown in Fig. V.4. The values of γ obtained by this procedure are given in Table V.5. We could not obtain γ for KNO_3 by this procedure due to the structural hysteresis in the transformation^{1,9}.

Bruce¹¹ has made theoretical estimates of the change in surface energy in solid-liquid and solid-vapour transformations of

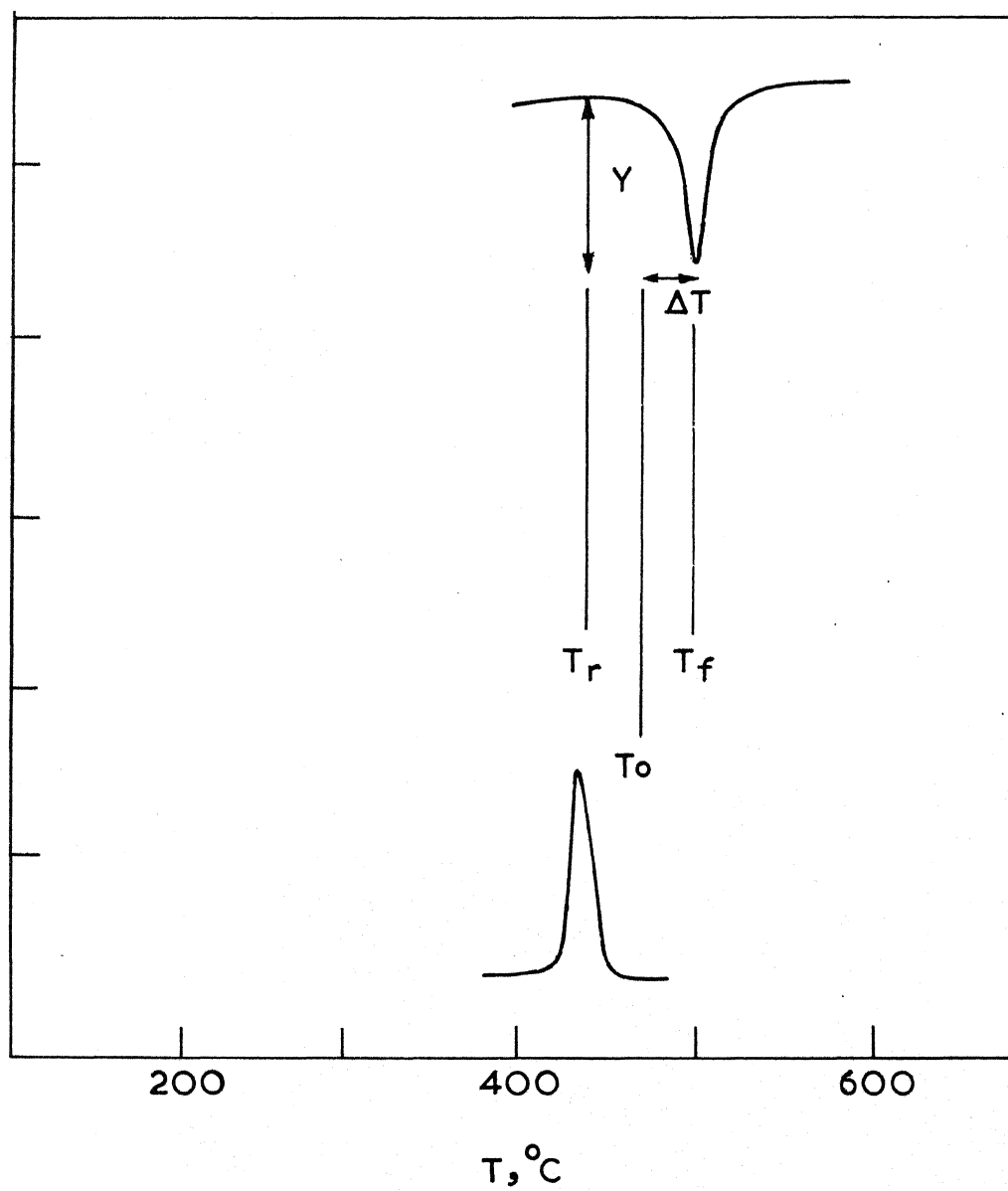


Fig.V.3. Typical DTA curve for CsCl transformation illustrating the relation between Y and ΔT ($T_f = 480^{\circ}\text{C}$ and $T_r = 448^{\circ}\text{C}$).

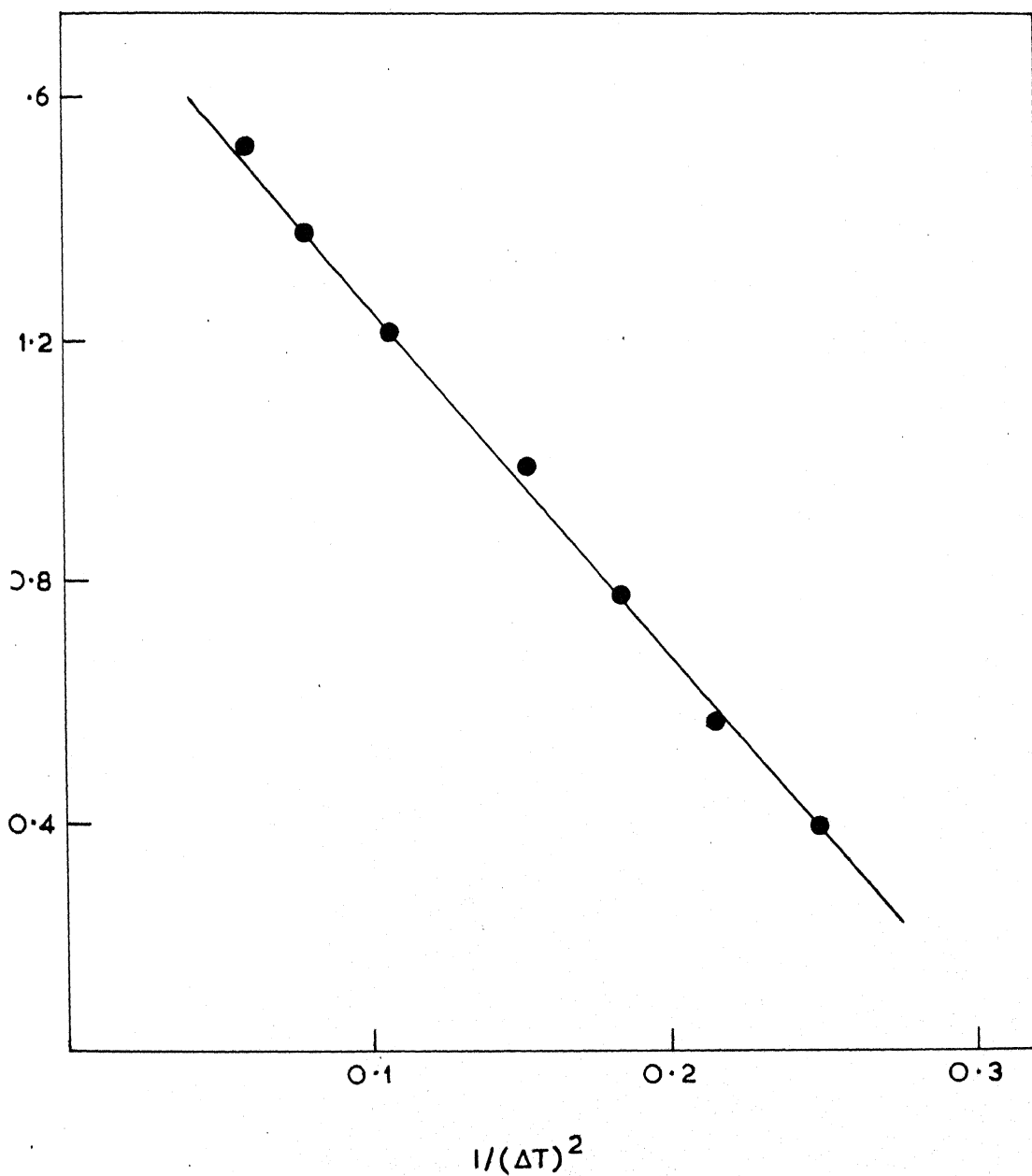


Fig.V.4. Straight line plot of $\log Y$ versus $1/(\Delta T)^2$ for CsCl transformation. The ordinate, Y , is the height of a point in the DTA curve from the base line (see Fig.V.3.).

inorganic crystalline materials. For solid-liquid transformations Bruce¹¹ employs the relationship,

$$\gamma = B/A (\Delta H_T \times J/N_O) \quad (7)$$

where γ is the change in surface free energy (which may be taken to be the interfacial energy), B is the ratio of "free bonds" to total coordination number per atom/molecule on the surface, $(1/A)$ is the number of atoms per unit area of the interface, ΔH_T is the gram atomic heat of transformation, N_O is the Avagadro number and J is the Joule constant. If such a procedure is to be extended to a solid-solid transformation (where there is a change from one crystal structure I to another structure II taking place) then the B/A term can be written as the average difference between the free bonds per unit area of the transforming interface. Thus

$$(B/A)_{\text{average}} = \left| (B/A)_I - (B/A)_{II} \right| \quad (8)$$

The (B/A) values on the right hand side of equation (8) are taken for the lowest B/A values corresponding to the lowest energy for the particular structure.

The B/A values for the crystal structures of AgI , NH_4Cl , NH_4Br and CsCl are given in Table V.4. Equation (7) may now be written as,

$$\gamma = (B/A)_{\text{average}} (\Delta H_T J/N_O) \quad (9)$$

Bruce's method of estimating the interfacial energy, γ , has been

TABLE V.4

(B/A) Values Employed for Calculation of γ for Various Solids(a) NH_4Cl , NH_4Br and CsCl

	<u>FCC structure (Fm$\bar{3}$m)</u>			<u>BCC structure (Pm$\bar{3}$m)</u>		
	(100)	(110)	(111)	(100)	(110)	(111)
B	1/6	1/3	1/2	1/2	1/4	1/2
(1/A)	$4/a^2$	$4/\sqrt{2}.a^2$	$4/\sqrt{3}.a^2$	$1/a^2$	$2/\sqrt{3}.a^2$	$2/\sqrt{2}.a^2$
(B/A)	$2/3.a^2$	$4/3\sqrt{2}.a^2$	$2/\sqrt{3}.a^2$	$1/2.a^2$	$1/2\sqrt{2}.a^2$	$1/\sqrt{3}.a^2$

(b) AgI

	<u>Wurtzite Structure</u>		<u>Zinc Blende</u>		
	<u>Hexagonal plane</u>	<u>Prism</u>	(100)	(110)	(111)
B	1/2	1/4	1/2	1/4	1/2
(1/A)	$2/\sqrt{3}.a^2$	$4/\sqrt{3}.1.6333a^2$	$2/a^2$	$2/\sqrt{2}.a^2$	$4/\sqrt{3}.a^2$
(B/A)	$1/\sqrt{3}.a^2$	$1/\sqrt{3}.1.6333a^2$	$1/a^2$	$1/2\sqrt{2}.a^2$	$2/\sqrt{3}.a^2$

TABLE V.5

Interfacial Energies, γ in ergs cm^{-2} of Some Solids

Solid	Transition employed	ΔH , cals gm ⁻¹ ion ⁻¹	γ from Bruce's method (equation 9)	γ from DTA curves (equation 6)	γ from $\log \langle r \rangle V_s 1/(\Delta T)$ (equation 5)
Quartz	$\alpha \rightleftharpoons \beta$	43	-	1.0	1.3
K ₂ SO ₄	Orthorhombic \rightleftharpoons hexagonal	1050	-	-	1.4
CsCl	Pm $\bar{3}$ m \rightleftharpoons Fm $\bar{3}$ m	300	1.5	1.0	-
NH ₄ Cl	Pm $\bar{3}$ m \rightleftharpoons Fm $\bar{3}$ m	550	3.4	2.1	-
NH ₄ Br	Pm $\bar{3}$ m \rightleftharpoons Fm $\bar{3}$ m	450	1.6	1.5	-
AgI	Hexagonal \rightleftharpoons B.C.C.	800	1.6	4.4	-

(a) ΔH values are taken from DTA observations reported in this thesis (in other chapters) and also from reference 8.

illustrated in Appendix I for the case of CsCl. The calculated values of γ for various solids, by Bruce's method are furnished in Table V.4. This method of calculation does not seem to be satisfactory to the $\alpha - \beta$ inversion of quartz which is a displacive type of transformation where the α - and β - crystal structures are almost alike except that the α -form is a slightly distorted version of the β -form.

The results of the various calculations of the interfacial energies are summarized in Table V.5. We note that the interfacial energies of these solids are only a few ergs cm^{-2} and the results of the three methods agree fairly well with one another. Our attempts to improve the calculated (by Bruce's method) values of γ , by introducing a parameter to account for the difference in bond strengths in the different crystal structures were not too useful.

(e) Particle size effects on the enthalpies of transformation

The enthalpies of transformations ΔH , decreases with increase in particle size in all the cases studied presently (Table V.1). The results show that by employing the $\alpha - \beta$ inversion peak of quartz as the reference¹³, one could arrive at erroneous conclusions if care is not taken to examine particle size effects. This result is in variance with some of the literature reports that the heats of transformation (obtained by DTA) of very small particles (< 10 microns) of kaolinite¹⁶ and quartz^{17,18} are

considerably smaller. Berkelhamer¹⁹, on the otherhand, found little change in DTA peak areas with particle size in the range 1-150 microns. The results of the present study are likely to be more reliable compared to early DTA studies and we feel that the decrease in ΔH with decrease in particle size reported earlier¹⁶⁻¹⁸ is likely to be due to impurities, packing problems or some other extraneous factors^{1,9}. The standard ΔH value of ~ 86 cal mole⁻¹ for the α - β inversion in quartz¹³, is found presently only when the particle size is $\sim 80 \mu$ or greater; in the II \rightarrow I transition of KNO_3 , the true value of ΔH (~ 1200 cal mole⁻¹) is found only when particle size is ~ 50 . In K_2SO_4 , the true value²⁰ of ΔH is not found at any particle size because of higher order components in the transformation²¹.

Assuming that the increased ΔH values of the transformation in samples of small particle size are due to excess surface energies, we can write,

$$\Delta H_{\text{obs}}^V = \Delta H_{\text{real}}^V + (\Delta \sigma A_s)/V \quad (10)$$

where ΔH_{obs}^V and ΔH_{real}^V are the observed and real volumetric heats of transformation, $\Delta \sigma$ is the difference in surface energy of the initial and final states, A_s is the surface area of the particles and V is the volume of a particle. Taking A_s to be constant and the particles to be spherical, equation (10) may be written as,

$$\Delta H_{\text{obs}}^V = \Delta H_{\text{real}}^V + 3\Delta \sigma/r \quad (11)$$

The observed variations (Fig. V.5) show that the situation is more complex. If we, however, assume the surface areas of the initial and the transformed phases to be different, we obtain the relation,

$$\Delta H_{\text{obs}}^V = \Delta H_{\text{real}}^V + 3\Delta\sigma(r_i + r_f) \Delta r / r_i^3 \quad (12)$$

where r_i and r_f are the initial and final radii of the particles and $\Delta r = (r_i - r_f)$. If $r_i \gg r_f$ the second term in equation (12) reduces to $3\Delta\sigma/r_i$ as in equation (11). If $r_i \approx r_f$, ΔH^V will be independent of r ; the situation when $r_i \ll r_f$ is unrealistic and may be ignored. The first two cases will give two straight lines, one with zero slope in the small particle range. While we may consider the variation of ΔH^V with particle size in Fig. V.5 as composed of two straight lines, it is not easy to explain why r_i should be greater than r_f . Equation (12) tacitly assumes a mechanism wherein particles break up during the transformation possibly in the nucleation step.

Another possible explanation for the behaviour shown in Fig. V.5 is that $\Delta\sigma$ [equation (10)] also varies with particle size. This is not unreasonable since in the finer particles produced by grinding, the surface composition of crystal faces may change in such a way as to increase the surface energy σ_i of the initial state. The curves in Fig. V.5 could then be interpreted as due to the combined effect of the variation of A_s and $\Delta\sigma$ with the particle size.

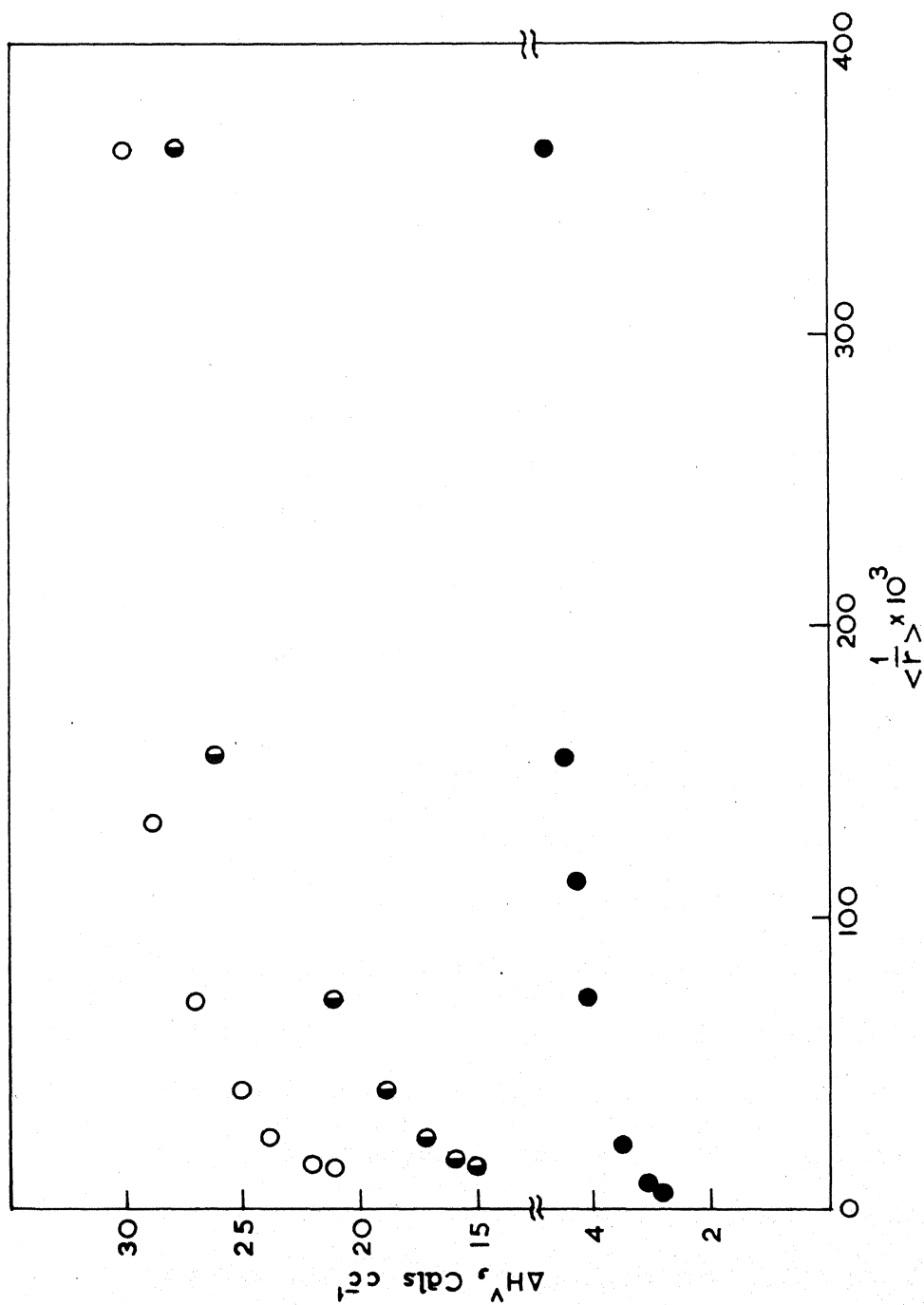


Fig. V.5. Volumetric heat of transformation, ΔH_v , as a function of $1/\langle r \rangle$ for quartz (shaded circles), K_2SO_4 (half-shaded circles) and KNO_3 (open circles).

V.3 EXPERIMENTAL

Quartz, K_2SO_4 , KNO_3 , AgI, NH_4Cl and NH_4Br of better than 99.99% purity or of spectroscopic grade (J & M or Alfa) were employed for the study. Samples of quartz, K_2SO_4 and KNO_3 of particle sizes down to 40 micron range were prepared by grinding the dry salts in a ball mill followed by sieving with the ASTM standard sieves.

To obtain particles of lower than 40 microns, an Aminco air elutriator (Roller particle size analyzer) was employed. The air elutriator functions on the principle of Stoke's law. Compressed air is passed at a known pressure through a chamber containing the particles of known density; by varying the air pressure particles of various sizes are collected in different receivers. The particles in the various size ranges were examined under an ordinary reflection microscope (August Ristelhueber Hamburg) fitted with a calibrated eye-piece. The number of particles belonging to various sizes were counted in each size range and histograms prepared. Typical histograms are shown in Fig. V.6. The standard deviation²² was calculated from the arithmetic mean; for the 5.5 and 93.5 μ samples of quartz, the standard deviations were 1.0 and 2.0 μ respectively. The radius of the particle $\langle r \rangle$, was taken to be half the particle size. Microscopic examination of the particles showed that in K_2SO_4 and KNO_3 there is some agglomeration of particles when the particle size is above 250 microns.

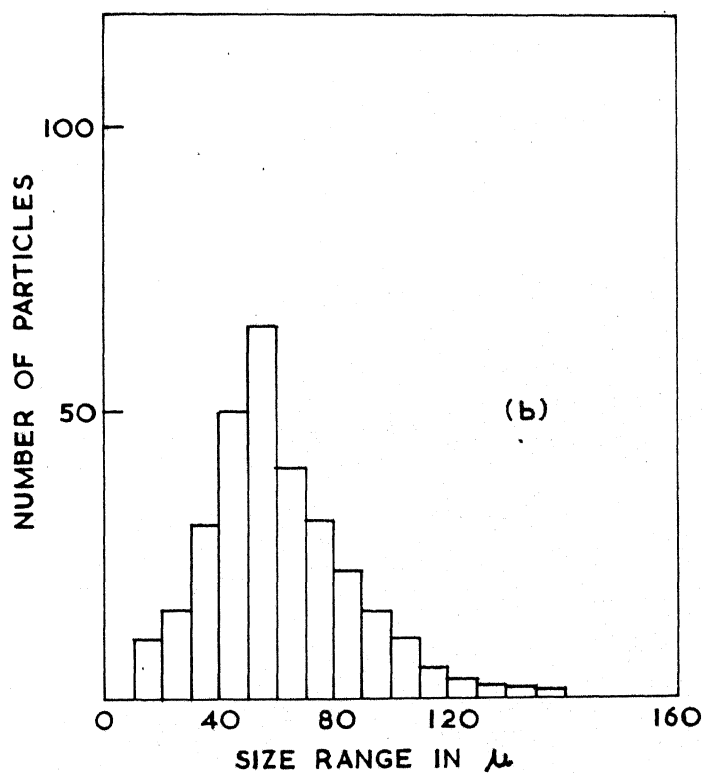
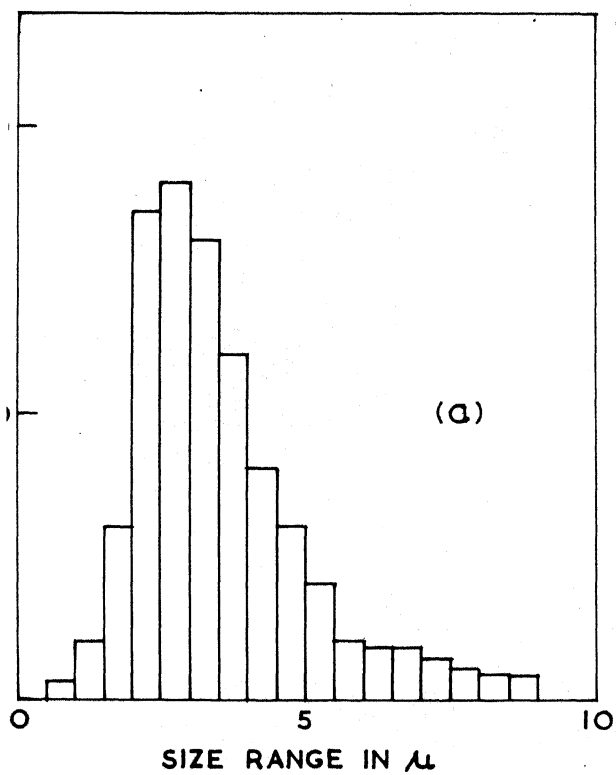


Fig. V.6. Typical histograms for two different sizes of quartz. The most probable particle sizes in these two cases were taken to be (a) 2.75μ and (b) 46.75μ .

All the transformations were studied by recording the differential thermal analysis (DTA) curves employing an Aminco thermoanalyzer fitted with a constant voltage stabilizer, temperature programmer and an x-y recorder. The limitations and applications of DTA to the study of crystal structure transformations have been discussed in earlier publications from this laboratory^{8,23,24}. Both the DTA peak temperatures, T_p , and the initiation temperatures, T_i , were recorded in all the cases; the enthalpies were obtained from peak areas employing external standards as reported earlier.

Acknowledgement

The author's thanks are due to Dr. A.R. Das of the Department of Metallurgical Engineering for helpful discussions with regard to the sections on Turnbull's theory and interfacial energies.

REFERENCES

1. C.N.R. Rao and K.J. Rao, in "Progress in Solid State Chemistry", ed. by H. Reiss, Pergamon Press, Oxford, 1967.
2. M.J. Buerger, in "Phase Transformations in Solids", ed. by R. Smoluchowski, John Wiley, New York, 1957.
3. F.A. Kroger, Z. Krist., A102, 136 (1939).
4. A.L. Roberts, in "Kinetics of High Temperature Processes", ed. by W.D. Kingery, John Wiley, New York, 1959.
5. S.R. Yoganarasimhan and C.N.R. Rao, Trans. Faraday Soc., 58, 1579 (1962).
6. M. Richard, L. Eyraud, M. Festivean and R. Riviere, Compt. Rend., 255, 2917 (1962).
7. R.C. Garvie, J. Phys. Chem., 69, 1238 (1965).
8. K.J. Rao and C.N.R. Rao, J. Materials Sci., 1, 238 (1966).
9. W.J. Smothers and Y. Chang, "Handbook of Differential Thermal Analysis", Chemical Publishing Company, New York, 1966.
10. D. Turnbull, J. Chem. Phys., 17, 71 (1949); *ibid.*, 18, 198, 768 and 769 (1950).
11. R.H. Bruce in "Science of Ceramics", Vol. 2, ed. by . . . G.H. Stewart, Academic Press, 1965.
12. S.C. Chang, C.F. Ho and C.C. Kiang, Akad. Sinica Mukden, 23, 462 (1957); CA, 52, 19339d.
13. A.J. Majumdar and R. Roy, J. Phys. Chem. Solids, 25, 1487 (1964).
14. A.R. Ubbelohde, Quart. Rev., 11, 246 (1957).
15. D.G. Thomas and L.A.K. Staveland, J. Chem. Soc., 1420, 2572 (1951).
16. R.E. Grim, Am. Mineral., 32, 493 (1947).
17. I.C. McDowall and W. Vose, Nature, 170, 366 (1952).
18. M. Fieldes, Nature, 170, 366 (1952).

19. L.H. Berkelhamer, U.S. Bur. Mines. Rept. Invest. 3762 (1944); CA, 38, 5696.
20. A. Arell, Ann. Acad. Sci. Fenn, AIV, 101 (1961).
21. A.J. Majumdar and R. Roy, J. Phys. Chem., 69, 1684 (1965).
22. R.D. Cadle, "Particle Size Determination", Interscience, New York, 1955.
23. K.J. Rao, G.V. Subba Rao and C.N.R. Rao, Trans. Faraday Soc., 63, 1015 (1967).
24. G.V. Subba Rao, M. Natarajan and C.N.R. Rao, J. Amer. Ceramic Soc., 51, 179 (1968).

APPENDIX I

Calculation of interfacial energy γ , of CsCl employing Bruce's method

In the Pn3m-Fm3m transformation of CsCl the anion arrangement changes from simple cubic to F.C.C; the average B/A value can be determined in the following manner. In the F.C.C. structure, of the three faces, (100), (110) and (111), the (100) face has the least value of B/A (Table V.4). This ^Cconclusion _Aarises from the following considerations. The area of a face is a_1^2 where a_1 is the lattice constant. Number of ions on this face is 4 (two cations + two anions); value of B (the ratio of free bonds to total coordination bonds) for the (100) face is 1/6. Thus $1/A = 4/a_1^2$ and $B/A = 2/3a_1^2$. For the B.C.C. structure the (110) face can similarly be shown to have the lowest value of B/A. The area is $\sqrt{2} a_2^2$ where a_2 is the lattice parameter. The number of ions in this area is 2 (cations or anions) and $1/A$ is equal to $2/\sqrt{2} a_2^2$. $B = 2/8 = 1/4$ and hence $B/A = 1/2\sqrt{2} a_2^2$. The interfacial energy γ is then given by equation (8)

$$\gamma = (B/A)_{\text{average}} \times (\Delta H_T J/N_o)$$

$$\gamma = (2/3a_1^2 - 1/2\sqrt{2}a_2^2) 300 \times 4.2 \times 10^7 / 6.023 \times 10^{23}$$

where $a_1 = 4.12 \text{ \AA}$, $a_2 = 6.91 \text{ \AA}$ and $\Delta H_T = 300 \text{ cal/gm ion}^{-1}$.
(references 9 and 13). γ is thus found to be about 1.5 ergs cm^{-2} .

CHAPTER VI

CRYSTALLIZATION AND PSEUDOCRYSTALLIZATION IN OXIDES

CHAPTER VI

CRYSTALLIZATION AND PSEUDO- CRYSTALLIZATION IN OXIDES*

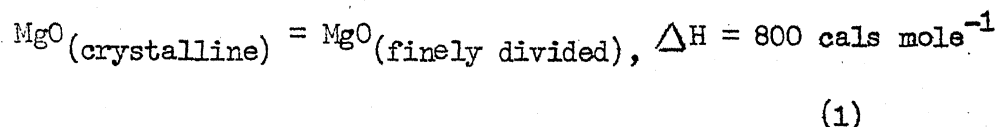
VI1 INTRODUCTION

Exothermic crystallization reactions associated with large heats have been observed in the differential thermal analysis curves of amorphous ferric oxide and chromia^{1,2}, titania³ and alumina⁴. After the exothermic reactions these oxides show high crystallinity as evidenced by x-ray analysis. An examination of the literature indicated that there was little information on quantitative aspects of crystallization reactions, and it was considered worthwhile to examine the crystallization reactions in a few oxides. Such a study would be of importance in surface chemistry as well as solid state chemistry, particularly in understanding pseudocrystallization (disorder-order) reactions in oxides^{5,6}. In this chapter the crystallization of a few amorphous oxides (viz., Fe_2O_3 , Al_2O_3 , Cr_2O_3 and TiO_2) and the pseudocrystallization in magnesium oxide have

*Papers based on this work have appeared in the Transactions of the Faraday Society, 65, 3088 (1969) and Journal of Chemical and Engineering Data, 13, 235 (1968).

been discussed. At this stage it would be pertinent to review the background of the MgO problem investigated presently.

Giauque⁷ showed that the heats of solution of finely divided and crystalline samples of MgO are considerably different and presented his findings in terms of the thermochemical equation



Giauque⁷ as well as Taylor and Wells⁸ suggested that this heat content anomaly could be due to particle size effects since the particle size of MgO increases appreciably with the temperature of preparation; however, these workers did not have any quantitative measure of the particle sizes of their samples. Since crystalline MgO samples are generally prepared by the decomposition of the hydroxide at relatively high temperatures compared to the finely divided samples, Rao and Pitzer⁵ as well as Rao, Yoganarasimhan and Lewis⁶, attributed the major part of such heat content anomalies to pseudocrystallization involving the removal of internal defects. As mentioned earlier, crystallization of amorphous oxides is known to be associated with large evolution of heat.

The increased energy content of finely divided MgO was shown to be primarily due to crystallite size effects by Thomas and Baker⁹, who measured the crystallite sizes (from x-ray line widths) of samples prepared by the dehydration of brucite at different temperatures. These workers showed that the energy content of the

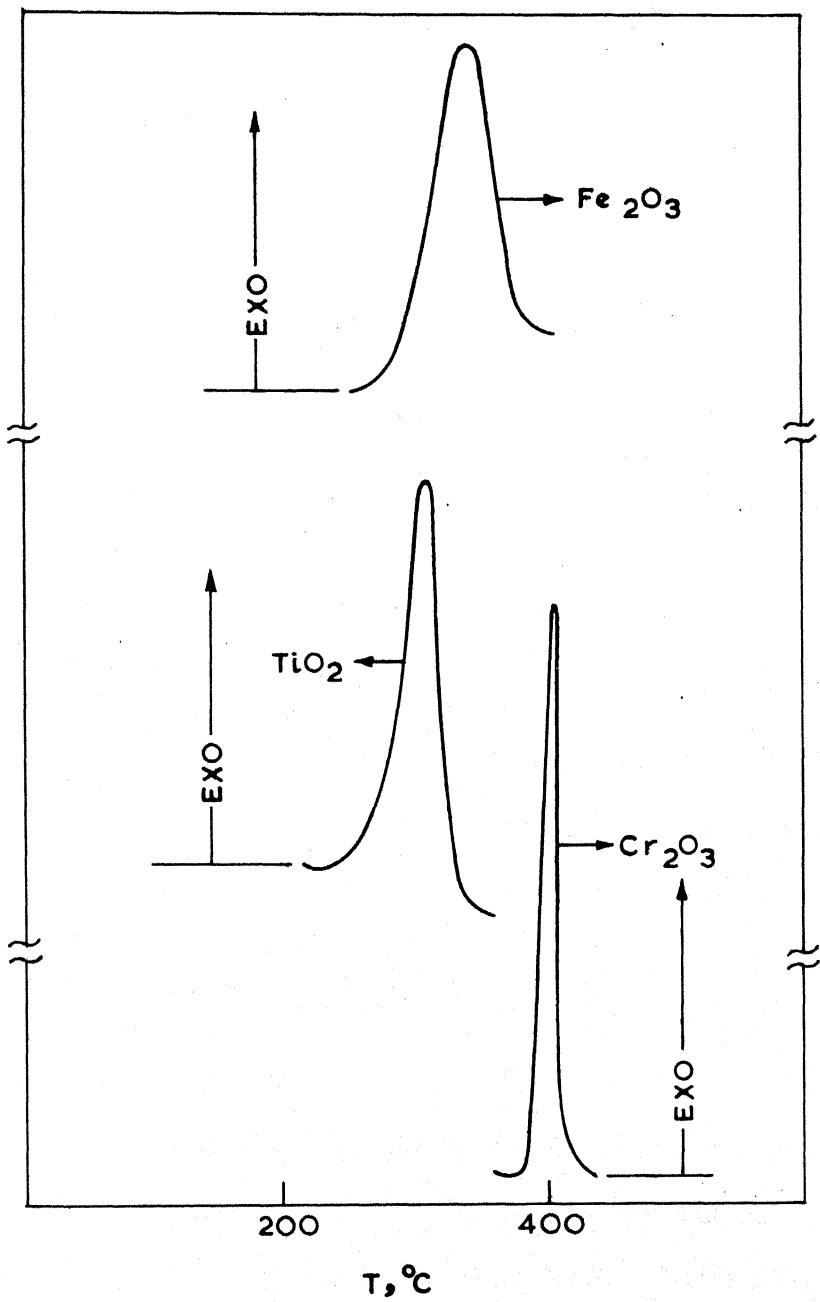
crystallites calculated by the Weissenbach relation¹⁰ agree well with the experimental results of Livey and coworkers¹¹ on the heats of solution. There is also some evidence that microstresses in MgO samples may contribute to the energy content of small particles produced by the decomposition of various magnesium compounds¹².

While the reduction in surface area (or increase in crystallite size) is expected to produce energy changes continuously over a wide temperature range^{9,13}, the pseudocrystallization reaction would occur sharply in a narrow temperature range^{5,6}. Even though a smooth variation of the heats of solution of MgO with the temperature of preparation of the oxide has been suggested^{9,11}, a closer examination of the experimental data reveals that the data could as well be shown to indicate a "transition" around 600°C. We have presently investigated thermal and particle size effects on MgO in order to examine the relative importance of these different factors in causing increased energy content of finely divided MgO samples. For this purpose, we have prepared several samples of MgO by the dehydration of $\text{Mg}(\text{OH})_2$ at different temperatures between 350° and 1200°C, and measured their x-ray line profiles, surface areas and heats of solution in 0.1N HCl.

VI.2 RESULTS AND DISCUSSION

(a) Crystallization of Al_2O_3 , Cr_2O_3 , Fe_2O_3 and TiO_2

The temperatures corresponding to the initiation and the peak in the DTA curves (Fig. VI.1) for the crystallization reactions are



DTA curves for the crystallization of oxides.

listed with the enthalpies, ΔH_{cryst} , and energies of activation, E_a , in Table VI.1. The ΔH_{cryst} values are large. The ΔH_{cryst} for Fe_2O_3 found in this study agrees with that of Friek and Klenk¹⁴ who estimated the lower limit for the heat of crystallization to be 13 kcal. mole⁻¹ by measurements of heats of solution in HF.

The ΔH_{cryst} values reported here should be of value, since there seems to be no other data or estimates available in the literature; further, it is difficult to measure the heats of solution of crystalline oxides owing to their high insolubility even in very strong acids. The E_a values for the crystallization reactions are not very high in comparison with the activation energies for phase transformations in solids¹⁵, indicating that the crystallizations of amorphous oxides take place with relative ease.

The description of the initial states of the oxides as "amorphous" is not decisive or exact, since many amorphous states may be possible with different energies and therefore different heats of crystallization. Thus, the enthalpies of annealing of disordered oxides produced by neutron irradiation or ion bombardment would be considerably different^{15a}. The present study, however, shows that the low-temperature removal of water from hydroxides or oxygen from peroxides leaves the oxides in "relic" structures which will then crystallize at higher temperatures releasing energy. The data reported here should clearly indicate the magnitude of the heats of such crystallization reactions. It is possible that the amorphous

TABLE VI.1

Heats of Crystallization of Oxides^(a)

	Cryst. Temp., °C		kcal. Mole ⁻¹	
	Initial	Peak	$-\Delta H_{\text{cryst}}$	E_a
Al_2O_3	170	265	14	12
Cr_2O_3	390	410	12	40
Fe_2O_3	260	335	32	20
$\text{TiO}_2^{(b)}$	250	305	15	18

(a) The data are for freshly prepared samples.

(b) Freshly prepared TiO_2 (anatase) gives a single exothermic peak at $\sim 305^\circ\text{C}$. With aging another peak appears at $\sim 230^\circ\text{C}$. If the area under the latter peak is also considered, the ΔH_{cryst} becomes much larger. The final product after crystallization is anatase in both the cases.

state may actually be similar to the glassy state. While this is all conjecture it would be interesting to explore such possibilities.

(b) Thermal and particle size effects in MgO

The experimentally determined values of the crystallite size, ϵ_{200} , the surface area, A_s , and the heats of solution, ΔH_s , are given in Table VI.2. It can be seen that the ΔH_s shows little variation upto $\sim 450^\circ\text{C}$ but suddenly decreases in the temperature range $450\text{--}650^\circ\text{C}$. The results differ from those of Livey and coworkers¹¹ who found a progressive decrease of ΔH_s with the temperature of preparation. The excess energy in small particles of MgO can be expressed in terms of $\Delta(\Delta H_s)$ (with respect to the sample at 950°C); the $\Delta(\Delta H_s)$ values are plotted against temperature in Fig. VI.2. The figure clearly shows the sharpness of the energy decrease in MgO particles between 450° and 650°C .

The excess energy, ΔE , of MgO particles was calculated by the relation of Weissenbach¹⁰:

$$\Delta E = 111/n + 1035/n^2 - 1944/n^3 + 1350/n^4 \quad (2)$$

where n is the number of atomic diameters on the particle edge and is approximately given by $\epsilon_{hkl}/2$. This relation assumes that MgO powder consists of cube-shaped particles of uniform size bounded by (100) faces. The values of ΔE are given in Table VI.2 and the $\Delta(\Delta E)$ values (with respect to the 950°C sample) are shown in Fig. VI.2.

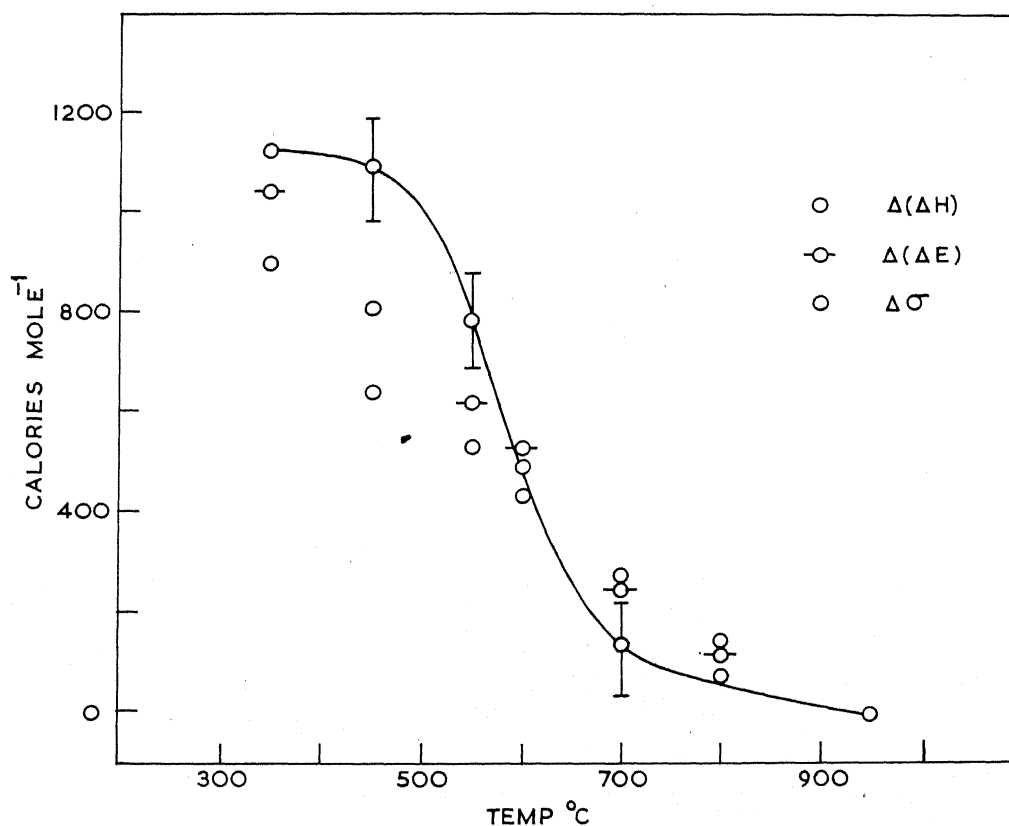


Fig. VI.2. Variation of $\Delta(\Delta H_s)$ (reference, 950°C. sample) obtained from experimental heats of solution of MgO samples prepared by the decomposition of $Mg(OH)_2$, at different temperatures. Values of $\Delta(\Delta E)$ and $\Delta\sigma$ are also shown in the figure for purposes of comparison.

TABLE VI.2

Crystallite Sizes, Surface Areas and Heats of Solution of MgO Samples

Temp. °C	$\epsilon_{(200)}, \text{\AA}^{(a)}$	ΔE cals mole ⁻¹	$\Delta(\Delta E)$ cals mole ⁻¹	A_s m ² g ⁻¹ (b)	σ cals mole ⁻¹ (c)	ρ g c.c. ⁻¹	ΔH_s kcal mole ⁻¹ (d)	$\Delta(\Delta H_s)$ cals mole ⁻¹
350	210	1150	1040	90	1176	3.2	34.11	1120
450	260	910	800	70	919	3.2	34.08	1090
550	320	730	620	62	814	3.0	33.78	790
600	370	630	520	53	696	3.1	33.48	490
700	510	360	250	42	552	2.8	33.12	130
800	920	220	110	32	420	2.0	33.07	80
950	2200	110	0	22	280	1.2	32.99	0

(a) The 1200°C sample was taken as the reference for instrumental broadening.

(b) A_s of 1200°C was 10 m²g⁻¹.

(c) Calculated from the surface energy of Lennard Jones and Taylor (Ref.16).

(d) At 35°C.

Giauque⁷ attempted to estimate the surface energy of finely divided MgO by applying the thermodynamic relation,

$$\Delta G = \Delta H - T\Delta S = 2\sigma^F V/r \quad (3)$$

where ΔG is for reaction (1), r is the radius of the particle and V is the molar volume ($11.10 \text{ cm}^3 \text{ mole}^{-1}$). Giauque⁷ could not, however, arrive at an estimate of the surface free energy, σ^F , due to the lack of particle size data. Assuming that for very finely divided MgO, $r \approx \epsilon_{200}/2$, $\Delta H = \Delta(\Delta H_s)$ in Table VI.2, and that ΔS is about $0.30 \text{ calories deg}^{-1} \cdot \text{mole}^{-1}$, σ^F can be estimated to be approximately $1850 \text{ ergs cm}^{-2}$ for the 350°C sample. On the otherhand, by multiplying Giauque's value for the internal pressure* ($35 \times 10^8 \text{ dynes cm}^{-2}$) by $r/2$ we get σ^F as $\sim 1840 \text{ ergs cm}^{-2}$. These estimates are only approximate and are considerably higher than the value of Lennard-Jones and Taylor¹⁶.

By making use of the $\Delta(\Delta H_s)$ values of the 350°C sample and the surface areas of the 350°C and 1200°C samples, the surface enthalpy, σ^H , of the MgO was calculated to be $\sim 1470 \text{ ergs cm}^{-2}$. The surface energy, σ , was estimated to be $\sim 1600 \text{ ergs cm}^{-2}$ by employing the $\Delta(\Delta E)$ value at 350°C . These values of σ^H and σ compare favourably with the value of $1362 \text{ ergs cm}^{-2}$ proposed by Lennard-Jones and Taylor¹⁶. The σ values of the various MgO samples in Table VI.2, were calculated by assuming the surface energy of

* Internal pressure is given by $2\zeta/r$ where ζ is the surface tension of the particles.

Lennard-Jones and Taylor¹⁶. The $\Delta\sigma$ values (with respect to the 950°C sample) are plotted in Fig. VI.2. It can be seen that the values of σ are quite close to the ΔE from Weissenbach's relation¹⁰ upto about 600°C; apparently the Weissenbach relation¹⁰ is fairly satisfactory in estimating surface energies.

An examination of the data in Table VI.2 and Fig. VI.2 indicates that the surface energy ($\Delta(\Delta E)$ as well as $\Delta\sigma$) decreases steadily as a function of temperature unlike $\Delta(\Delta H_s)$ which shows an abrupt decrease in a narrow temperature range (450-600°C). Beyond 600°C, the $\Delta\sigma$, $\Delta(\Delta E)$ and $\Delta(\Delta H_s)$ are about the same within experimental error of the last quantity (Fig. VI.2). Apparently, there are other factors besides surface area or particle size responsible for the observed variation of $\Delta(\Delta H_s)$. While lattice microstresses¹² might contribute to some extent to the abrupt decrease in $\Delta(\Delta H_s)$ with temperature, the major contribution may be due to a pseudocrystallization or the so-called order-disorder or defect-annealing^{5,6} reaction. The magnitude of the heat evolution in such a reaction would be much smaller than that found in the usual crystallization reaction of amorphous oxides.

The energy difference $\Delta(\Delta H_s) - \Delta\sigma$ or $\Delta(\Delta H_s) - \Delta(\Delta E)$ which may be attributed to the pseudocrystallization reaction decreases sharply between 450° and 600°C. Above 600°C, the increase in crystallite size becomes much more marked (Fig. VI.3; Table VI.2) probably due to the onset of sintering. These results are in

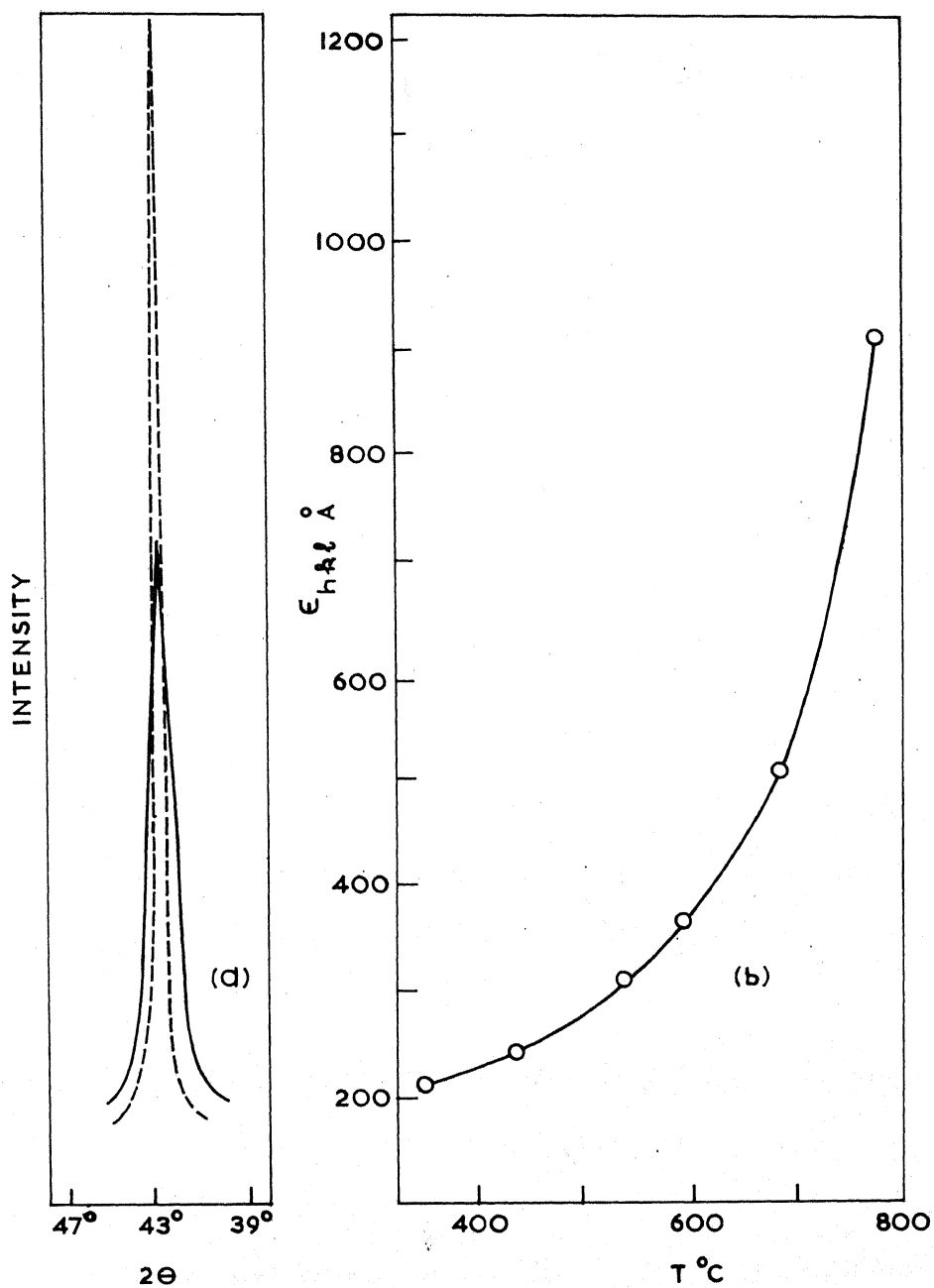


Fig. VI. 3. (a) X-ray profiles of the (200) reflection of MgO heated to 1200°C (dotted line) and 450°C (full line) (b) Variation of particle size of MgO samples with the temperature of preparation.

general agreement with the surface area studies of Razouk and Mikhail¹³ who have suggested that three processes may occur when MgO is heated: (i) recrystallization (ii) crystal growth and (iii) sintering. The processes apparently take place at different temperatures with different rates.

By making use of the surface areas and the crystallite sizes obtained in these studies, we can calculate the apparent packing densities, ρ^{app} , by the relation, $A_s = 3/r \rho^{\text{app}}$, where r is the radius of the particles (assumed to be spherical in shape). The ρ^{app} values indicate that there is a marked decrease in ρ^{app} starting at $\sim 600^\circ\text{C}$ possibly due to the onset of sintering. It is seen that even with the smallest crystallites of MgO (at 350°C), the value of ρ^{app} (3.2 g cc^{-1}) is less than the true density (3.58 g cc^{-1}) indicating that the packing of particles is not perfect. The ρ^{app} should become equal to the true density when $A_s r \approx 0.85 \text{ cm}^3 \text{ g}^{-1}$; looking at the present data, it appears that this may be realised in samples prepared between $250\text{--}300^\circ\text{C}$.

The $\Delta(\Delta H_s)$ curve in Fig. VI.2 is in some ways reminiscent of a glass transition; as mentioned earlier, it may not be inappropriate to think of finely divided active solids or amorphous solids as akin to the glassy state. In finely divided solids prepared by precipitation or low temperature decomposition of compounds, crystal imperfections may be "frozen in" as suggested by Kobayashi¹⁷ and Rao and coworkers⁶. A more plausible explanation for the excess

energy of the finely divided particles of MgO can be offered on the basis of surface and bulk defects discussed by Nelson, Tench and coworkers¹⁸⁻²⁰ in their studies of irradiated MgO. These workers have shown that the concentration of point defects on or close to the surface (s-centres) as well as that of the bulk centres (F and V) may decrease with decrease in particle size. Small amounts of impurities present in MgO may also affect the properties of the surface but their role is not clear at present.

The present results regarding the anomalous behaviour of finely divided MgO samples find indirect support from the recent studies on the heats of argon adsorption by Anderson and Horlock²¹. These workers find that microcrystalline oxides prepared from $\text{Mg}(\text{OH})_2$ yield higher heats of adsorption. Theoretical calculations do not predict this behaviour on the basis of surface heterogenieties or adsorption on surfaces other than (100); their results are, however, consistent with adsorption in very small pores or at points of crystal-crystal contact where the adsorbate atom is close to the more lattice ion neighbours than on the plane surface. The variations in the heats of adsorption among different MgO samples, are also consistent with changes in microstructure caused by different calcination treatment.

VI.3 EXPERIMENTAL

(a) Preparation, and thermal analysis of Al_2O_3 , Cr_2O_3 , Fe_2O_3 and TiO_2

The crystallization reactions of Al_2O_3 , Cr_2O_3 , Fe_2O_3 and TiO_2 have been studied by quantitative differential thermal analysis (DTA)

employing the phase transformations of lithium sulphate (monoclinic \rightleftharpoons cubic; 590°C; ΔH , 6.9 kcal. mole⁻¹), potassium sulphate (orthorhombic \rightleftharpoons hexagonal; 579°C; ΔH , 2.1 kcal. mole⁻¹) and potassium nitrate (II \rightarrow I; 136°C; ΔH , 1.2 kcal. mole⁻¹) as external standards¹⁵. The values of the ΔH_{cryst} reported here are based on three independent measurements of the DTA peak areas with respect to all the three standards; the ΔH_{cryst} values from the three standards agreed very well with each other. In this laboratory, the applicability and limitations of the DTA technique to the study of quantitative energy aspects of phase transformation have been examined in detail¹⁵. Since the crystallization reactions are associated with large heats, the technique is considered to be suitable to provide fairly reliable values for the heats of crystallization.

The DTA curves (Fig. VI.1) were recorded by employing an Aminco thermoanalyzer fitted with a voltage stabilizer, deviation amplifier, programmed furnace and an x-y recorder. The uncertainty in the ΔH_{cryst} values is $\sim 10\%$. The values of the energy of activation, E_a , calculated from the procedure of Borchardt and Daniels²² are, however, likely to be associated with larger uncertainties¹⁵. In order to ascertain that there is no mass change in the neighbourhood of crystallization, thermogravimetric analysis of the oxides was also carried out; the TGA curves (Fig. VI.4) show that there is no appreciable mass loss in the crystallization region. In the case of Al_2O_3 the loss was almost negligible.

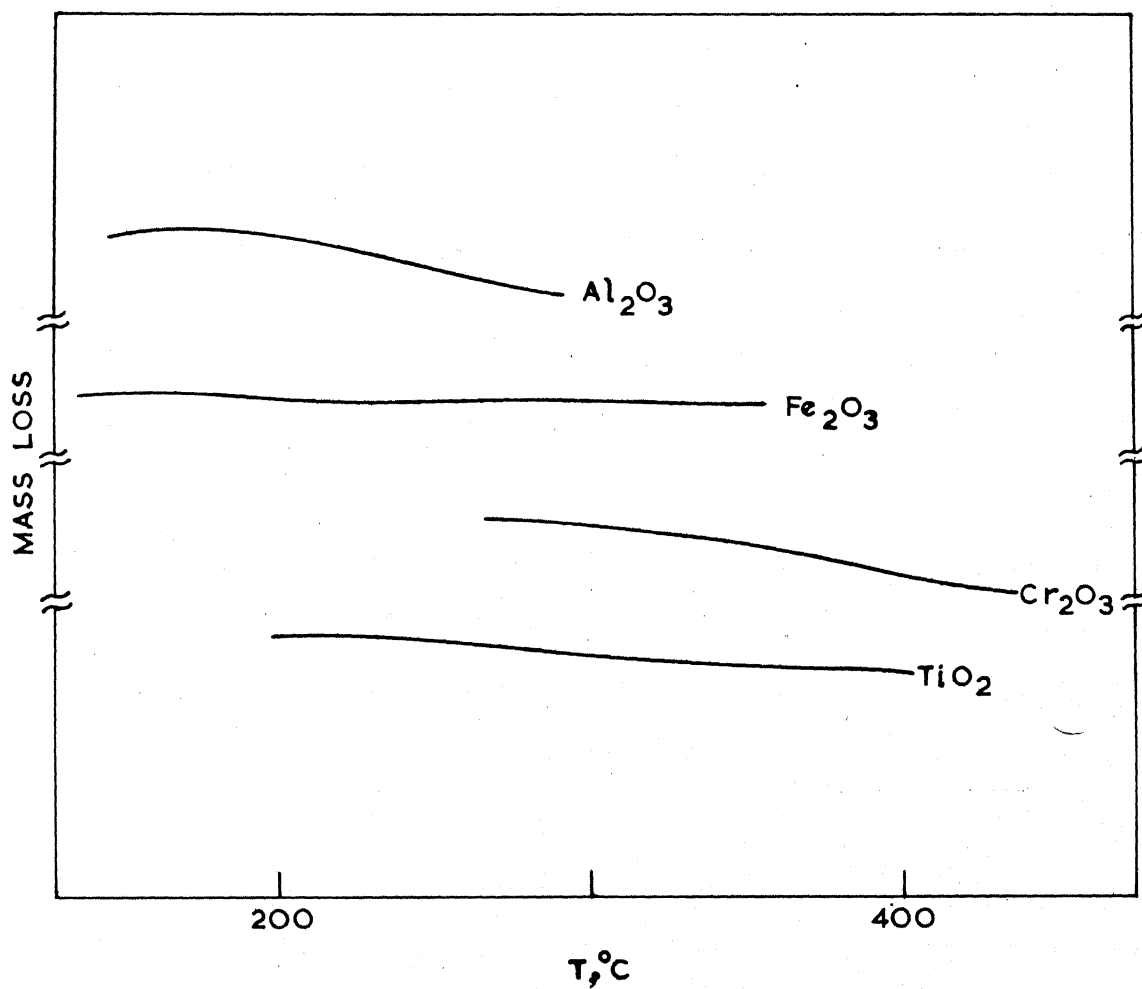


Fig. VI.4. TGA curves of oxides showing negligible mass loss in the region of the crystallization reaction.

Amorphous alumina was prepared by ammoniacal hydrolysis of AlCl_3 followed by drying in vacuum at $\sim 100^\circ\text{C}$. Fe_2O_3 and Cr_2O_3 were prepared by the ammoniacal hydrolysis of the nitrates followed by drying in air-oven at $\sim 120^\circ\text{C}$. Titanium peroxide was prepared by the procedure reported in the literature^{23,24}; the crystallization peak of TiO_2 appears after the endothermic peak owing to the decomposition of peroxide³. All the oxides were crystalline after the exothermic reactions as found by x-ray analysis. Cr_2O_3 and Fe_2O_3 had the rhombohedral structures while Al_2O_3 was in the γ -form. TiO_2 had the anatase structure.

(b) Preparation of MgO and measurements of ΔH_s , A_s and ϵ_{200}

Magnesium oxide precipitated by the dropwise addition of 6N ammonia solution to a solution of MgCl_2 was allowed to settle overnight, filtered, washed and dried in an oven at $\sim 110^\circ\text{C}$ for ~ 8 hrs. The hydroxide was heated at 350°C in vacuo (10^{-5} torr) for ~ 200 hrs to produce the finely divided MgO. Two gram portions of the oxide thus prepared were heated at 450° , 550° , 600° , 700° , 800° , 950° and 1200°C in vacuo (10^{-5} torr) for 3 hrs. and then sealed in pyrex bulbs. It was ascertained that the samples thus prepared had no water (or hydroxide) in them.

X-ray diffraction patterns^{9,25} of the MgO samples were recorded employing a Northern American Philips x-ray diffractometer with copper $K\alpha$ -radiation. The sample was taken in a perspex sample holder and pressed evenlyⁿ with a glass plate so that the MgO

packed was flush with the surface of the sample holder. The crystal structure and the lattice dimensions of all the MgO samples were the same, but the line widths varied with the temperature of preparation (Fig. VI.3). Line broadening, β , due to the particle size is related to the mean particle size ϵ_{hkl} for the particular reflection (hkl) by the equation²⁶,

$$\beta = \lambda K / \epsilon_{hkl} \cos \theta \quad (4)$$

where θ is the Bragg angle and K is the shape factor normally assumed to be close to unity. In order to allow for the instrumental broadening^b, a sample of MgO heated to 1200°C was taken as the reference²⁷ since the half line width of the sample was comparable to that of standard unstrained quartz. From the observed half-line widths, B, of MgO samples, the instrumental broadening b was then subtracted employing the Warren²⁶ correction. Warren²⁶ correction is given by the relation

$$\beta^2 = B^2 - b^2 \quad (5)$$

where B is the observed broadening of the line for the sample and b is the half-line width of the MgO sample heated to 1200°C. By making use of β values, the ϵ_{hkl} values for the samples of MgO were obtained. The ϵ_{hkl} values have an uncertainty of $\pm 10\%$.

B.E.T. surface areas of samples were measured from nitrogen adsorption at low temperatures employing a volumetric apparatus. The molecular area of 16.2 Å² was assumed for nitrogen.

The submarine calorimeter used for the measurement of heats of solution was essentially similar to that described in the literature^{28,29}. The calorimeter was calibrated by measuring the heats of solution of KCl; good agreement (within 0.2%) was obtained with the standard values obtained by Gunn³⁰. Outgassed samples of MgO in sealed bulbs were opened under the acid solution in the calorimeter. The heats of solution of the MgO samples in 0.1N HCl were determined at $35.0 \pm 0.10^\circ\text{C}$. The heat of solution of the 700°C sample of MgO was also determined at 25°C , and found to be 35.07 ± 0.05 kcal mole⁻¹; the value at 35°C was 33.11 ± 0.05 kcal mole⁻¹. Further, the heats of two sintered MgO samples with particle sizes of $\leq 37 \mu$ and $\geq 125 \mu$ were found to be identical (35.81 ± 0.05 kcal mole⁻¹) at 25°C .

Acknowledgement

The author's thanks are due to Dr. G.V. Chandrashekhar for preparing pure TiO_2 and to Mr. T.S. Sarma and Dr. J.C. Ahluwalia for the measurements of the heats of solution of the MgO samples.

REFERENCES

1. S.K. Bhattacharyya, V.S. Ramachandran and J.C. Ghosh, Adv. Catalysis, 9, 114 (1957).
2. C.N.R. Rao and C.W.W. Hoffman, J.Sc. Ind. Res.(India) 15B, 663 (1956).
3. S.R. Yoganarasimhan and C.N.R. Rao, Trans. Faraday Soc., 58, 1579 (1962).
4. S.K. Bhattacharyya, G. Srinivasan and N.D. Ganguli, J. Indian Chem. Soc., 41, 233 (1964).
5. C.N.R. Rao and K.S. Pitzer, J. Phys. Chem., 64, 282 (1960).
6. C.N.R. Rao, S.R. Yoganarasimhan and M.P. Lewis, Canadian J. Chem., 38, 2359 (1960).
7. W.F. Giaque, J. Am. Chem. Soc., 71, 3192 (1949).
8. K. Taylor and L.F. Wells, Bur. Stds. J. Res., 21, 133 (1938).
9. D.K. Thomas and T.W. Baker, Proc. Phys. Soc., (London), 74, 673 (1959).
10. B. Weissenbach, Radex Rundschau, 6, 257 (1951).
11. D.T. Livey, B.M. Walklyn, M. Hewitt and P. Murray, Trans. Brit. Cer. Soc., 56, 217 (1957).
12. Z. Librant and R. Pampuch, J. Amer. Ceram. Soc., 51, 109 (1968).
13. R.I. Razouk and R. Sh. Mikail^K, J. Phys. Chem., 63, 1050 (1959).
14. R. Friek and J. Klenk, Z. Electrochem., 41, 617 (1935).
15. K.J. Rao and C.N.R. Rao, J. Materials Sci., 1, 238 (1966).
- 15a. R. Kelly and C. Jech, Proc. Brit. Ceramic Soc., 9, 243 (1967) and R. Kelly, Private Communication to Professor C.N.R. Rao.
16. J.E. Lennard Jones and G.I. Taylor, Proc. Royal Soc., (London), A109, 476 (1925).
17. K. Kobayashi, Sci. Reports Tohoku Univ., 35, 173, 283 (1951).
18. R.L. Nelson, A.J. Tench and B.J. Hamsworth, Trans. Faraday Soc., 63, 1427 (1967).

19. R.L. Nelson and A.J. Tench, Trans. Faraday Soc., 63, 3039 (1967).
20. R.L. Nelson, J.W. Hale, B.J. Hamsworth and A.J. Tench, Trans. Faraday Soc., 64, 2521 (1968).
21. P.J. Anderson and R.F. Horlock, Trans. Faraday Soc., 65, 251 (1969).
22. R.J. Borchardt and F. Daniels, J. Am. Chem. Soc., 79, 41 (1957).
23. G.V. Gere and C.C. Patel, Z. Anorg. Allegem. Chem., 319, 176 (1962).
24. D.P. Kharkar and C.C. Patel, Current Sci.(India) 24, 413 (1955).
25. H.E. Swanson and E. Tatge, U.S. National Bureau of Standards, Circular 539, 1953.
26. H.P. Klug and L.E. Alexander, "x-Ray Diffraction Procedures", John Wiley & Sons, Inc., New York, 1954.
27. L.S. Birks and H. Friedman, J. Appl. Phys., 17, 687 (1946).
28. J.C. Ahluwalia and J.W. Cobble, J. Am. Chem. Soc., 86, 5377 (1964).
29. S. Subramanian and J.C. Ahluwalia, J. Phys. Chem., 72, 2525 (1968).
30. S.R. Gunn, J. Phys. Chem., 69, 2902 (1965).

CHAPTER VII

PHASE TRANSITIONS IN THE SOLID SOLUTIONS OF

VO_2 WITH TiO_2 , NbO_2 AND MoO_2

CHAPTER VII

PHASE TRANSITIONS IN THE SOLID SOLUTIONS OF VO_2 WITH TiO_2 , NbO_2 AND MoO_2 *

VII.1 INTRODUCTION

One of the widely investigated semiconductor-to-semimetal transitions is that of Vanadium oxide, VO_2^1 . Crystallographic², magnetic³⁻⁵ optical⁶ and electrical transport⁷⁻¹⁰ properties of VO_2 have been examined by various workers and the nature of the transition is fairly well understood. VO_2 is monoclinic at room temperature and transforms to tetragonal rutile structure at $\sim 68^\circ\text{C}^2$. This first order phase transition is associated with a marked change in the magnetic susceptibility^{5,6}, χ , but no long range magnetic order has been found in the low and high temperature phases. VO_2 exhibits an abrupt increase in the electrical conductivity, σ , by a factor of 10^4 - 10^5 in pure stoichiometric single crystalline samples¹⁰. Below the transformation temperature, T_0 (68°C), VO_2 is an n-type intrinsic

* A communication based on part of this work will be appearing in Solid State Communications (1970).

semiconductor^{8,11,12} and various theoretical models have been put forward to explain the nature of the semiconductor-to-metal transition^{13,14}.

Niobium oxide, NbO_2 , possesses a distorted rutile structure at room temperature¹⁵; the presence of Nb-Nb bonds has been suspected in this oxide. Sakata and coworkers^{16,17} have examined the phase transition in NbO_2 by high temperature x-ray and differential thermal analysis (DTA). These workers have noted that NbO_2 transforms from distorted rutile to normal rutile structure at $\sim 800^\circ\text{C}$. The presence of strong Nb-Nb bonds causes the order to persist at least upto 850°C at which temperature there is discontinuity in the tetragonal lattice parameters. The electrical properties of polycrystalline NbO_2 have been studied by a few workers; however, the results are conflicting. Jannick and Whitmore¹⁸ found that NbO_2 was semiconducting below $\sim 720^\circ\text{C}$ exhibiting a ten-fold increase in the conductivity around 800°C ., σ , however, remained constant above this temperature. The measured Seebeck coefficient was high at ordinary temperatures ($\sim 1 \text{ mv}/^\circ\text{C}$) but decreased gradually to a low constant value ($\sim 70 \mu\text{v}/^\circ\text{C}$) above 800°C . These results are in general agreement with those reported recently by Roberson and Rapp¹⁹ who only noted an anomalous behaviour in the conductivity above 800°C . Investigations of Sakata²⁰ reveal that even though a ten fold increase in σ occurs at $\sim 800^\circ\text{C}$, the behaviour upto $\sim 1200^\circ\text{C}$ is that of a typical semiconductor with an activation energy, E_a , of 0.34 eV; Sakata²⁰ also noticed that the magnetic susceptibility

shows a slight temperature dependence above 800°C. Thus, it can be concluded that the existing data do not lead to any definite conclusion regarding the electronic nature of the transition in NbO_2 .

The crystallography of the $\text{V}_{1-x}\text{Ti}_x\text{O}_2$ system has been examined by Ariya and Grossman²¹ for the range $0.4 \leq x \leq 1.0$ and by Sakata and Sakata²² for the range $0.8 \leq x \leq 1.0$. Both these groups of workers proposed a rutile structure for the solid solutions; no data are reported for the range $0.0 < x < 0.4$. The temperature dependence of the magnetic susceptibility (χ) and the room temperature electrical conductivity of a few $\text{V}_{1-x}\text{Ti}_x\text{O}_2$ solid solutions have been reported by Ariya and Grossman²¹ and Rüdorff and coworkers⁴. These workers noted that the solid solutions exhibit higher σ and χ than pure VO_2 at room temperature; the jump in σ as well as χ at the transition temperature, T_t ($T_t < T_o$ for $x \neq 0$) was, however, smaller in the solid solutions. For composition $x > 0.6$, no susceptibility anomaly seems to be present. The room temperature conductivity apparently goes through a maximum around $x = 0.5$. The temperature variation of conductivity in these systems has not been investigated in the literature.

Rüdorff and Marklin²³ have reported the crystallography, temperature dependence of χ and room temperature conductivities of a series of solid solutions $\text{V}_{1-x}\text{Nb}_x\text{O}_2$. According to these workers, the compositions $0.1 \leq x \leq 0.9$ all possess the tetragonal

rutile structure. Further, the jump in χ at T_t ($< T_0$) in the solid solutions is apparently smaller; the room temperature conductivity is lowest when $x = 0.5$. Rüdorff and Marklin²³ suggest that the rutile phases of the system $V_{1-x}Nb_xO_2$ are composed of variable valence states of vanadium and niobium.

Presently we have carried out a detailed investigation of the crystallography, differential thermal analysis and electrical conductivity of pure VO_2 , NbO_2 and of the solid solutions $V_{1-x}Ti_xO_2$ ($0.0 \leq x \leq 0.4$) and $V_{1-x}Nb_xO_2$ ($0.0 \leq x \leq 1.0$). It was of interest to us to find out whether the nature of the semiconductor-to-metal transition of VO_2 gets modified by addition of Ti^{+4} and Nb^{+4} ions. The literature data^{4,21} on the variation of χ with T indicate that the transition may become a semiconductor-to-semiconductor type with progressive substitution by Ti^{+4} ion. Further, the nature of the χ - T curves reported by Rüdorff and coworkers⁴ and Ariya and Grossman²¹ are also slightly different suggesting therefore different mechanisms for the transitions. A proper study of the conductivity behaviour was expected to clarify the situation. Besides these VO_2 - TiO_2 and VO_2 - NbO_2 systems, we have also investigated the $V_{1-x}Mo_xO_2$ system upto $x = 0.05$ employing DTA, x-ray and conductivity measurements.

VII.2 RESULTS AND DISCUSSION

(a) Structure of $\text{VO}_2\text{-TiO}_2$, $\text{VO}_2\text{-NbO}_2$ and $\text{VO}_2\text{-MoO}_2$ Systems

Pure VO_2 is monoclinic⁴ whereas TiO_2 is tetragonal²² (rutile) at room temperature; pure NbO_2 has a distorted rutile structure but can be indexed on the basis of a rutile pattern^{16,17}. We have investigated the crystal structures of a few solid solutions of $\text{V}_{1-x}\text{Ti}_x\text{O}_2$ ($0.0 \leq x \leq 0.4$) and $\text{V}_{1-x}\text{Nb}_x\text{O}_2$ ($0.0 \leq x \leq 1.0$) by powder x-ray diffraction and the results are presented in Tables VII.1 and 3. Our data on pure VO_2 is in agreement with those reported by Minomura and Nagasaki² and other workers²³.

The results in Table VII.1 show that the $\text{V}_{1-x}\text{Ti}_x\text{O}_2$ solid solutions are monoclinic even when $x = 0.4$, the monoclinicity decreasing with increasing x . It is thus possible that the solid solution at $x \gtrsim 0.6$ may possess the rutile structure as reported by Sakata and Sakata²². The present results of the composition $x = 0.4$, however, differ from Ariya and Grossman²¹, who have reported a rutile structure for this solid solution. The DTA and high temperature x-ray studies (Tables VII.1 and 2 and Fig.VII.1) reveal that all the phases with the composition $0 \leq x \leq 0.4$ undergo a phase transformation. The x-ray patterns at 80°C can be completely indexed on the basis of the rutile structure. The enthalpy of transition (Table VII.2), ΔH , decreases with x just as the monoclinicity of the low temperature structure. This

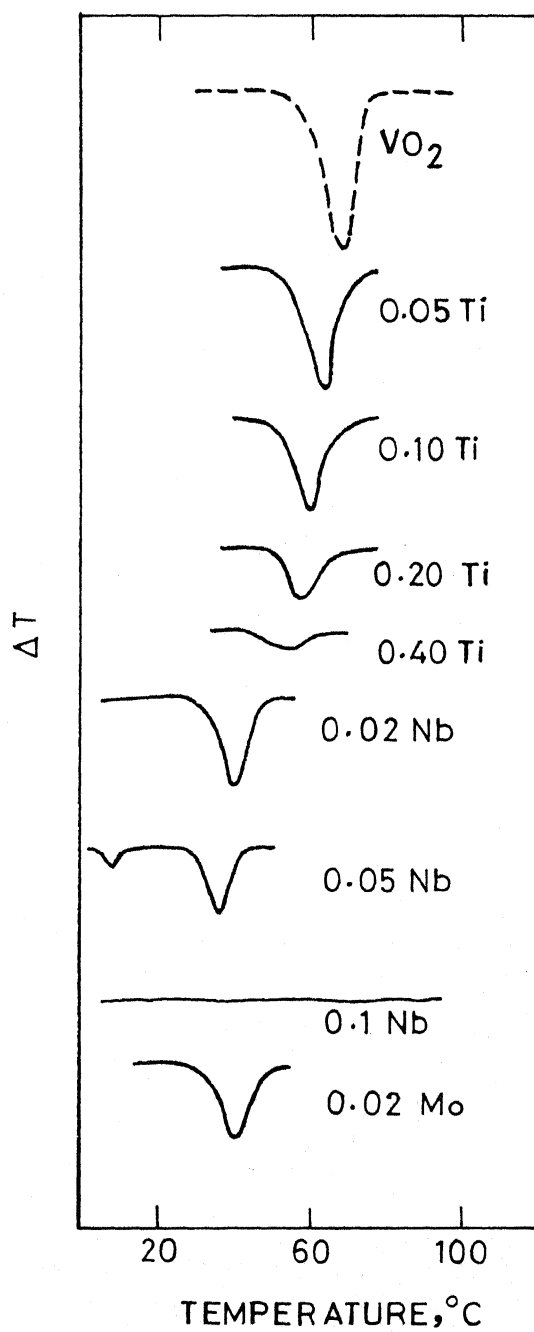


Fig. VII.1. DTA curves (heating rate $16^\circ \text{ min.}^{-1}$) of VO_2 and $\text{V}_{1-x}\text{Z}_x\text{O}_2$ ($\text{Z} = \text{Ti}, \text{Nb}$ or Mo); \underline{x} values are shown next to the curves.

TABLE VII.1Crystallographic Data on $V_{1-x}Ti_xO_2$ Solid SolutionsAt 25°C

<u>x</u>	<u>a, Å</u>	<u>b, Å</u>	<u>c, Å</u>	<u>β, °</u>
0.00	5.744	4.520	5.376	122.6
0.02	5.729	4.530	5.364	122.3
0.05	5.727	4.560	5.390	122.5
0.10	5.716	4.499	5.424	122.0
0.20	5.704	4.490	5.448	121.3
0.40	4.833	4.380	5.530	97.9

At 80°C

<u>x</u>	<u>a, Å</u>	<u>c, Å</u>
0.00	4.559	2.801
0.05	4.545	2.844
0.10	4.537	2.868
0.20	4.539	2.891
0.40	4.546	2.894

TABLE VII.2DTA Studies on $V_{1-x}Ti_xO_2$ Solid Solutions

x	$T_t, ^\circ C$	ΔH_{tr} (cals mole ⁻¹)
0.00	69 ^(a)	750
0.02	65	630
0.05	63	600
0.10	60	400
0.20	58	190
0.40	48	100

(a) DTA peak temperatures; thermal hysteresis of $\sim 15^\circ$ is observed with all samples.

TABLE VII.3

Crystallographic Data on $V_{1-x}Nb_xO_2$ Solid SolutionsAt 25°C

x ^(a)	<u>a, Å</u>	<u>c, Å</u>	<u>c/a</u>
0.02 ^(b)	4.510	2.890	0.64
0.05 ^(c)	4.540	2.880	0.63
0.10	4.569	2.880	0.63
0.30	4.647	2.870	0.62
0.50	4.682	3.033	0.65
0.70	4.728	3.040	0.66
0.90	4.788	3.009	0.63
1.00	4.820	2.980	0.62

(a) For $x = 0$ (pure VO_2) $a = 4.559$ Å and $c = 2.801$ Å at $\sim 80^\circ\text{C}$.

(b) Rutile structure with monoclinic distortion at room temperature.

(c) This solid solution is a distorted rutile at room temperature; below 7°C , this is probably like 2% NbO_2 (monoclinically distorted rutile).

appears intuitively reasonable since the magnitude of crystal distortion in a phase transition should, in principle, determine the magnitude of energy change. The electrical conductivity behavior to be discussed later also seems to support a non-rutile (monoclinic) structure for the low temperature phase of $V_{0.6}Ti_{0.4}O_2$. The magnetic susceptibility anomaly⁴ of this phase ($\sim 47^\circ C$) can only be explained on the basis of the present findings. In the high temperature rutile phases of $V_{1-x}Ti_xO_2$ the c/a value increases with x ; when $x \approx 0.6$, the c/a value appears to become close to that of rutile.

The room temperature lattice parameters of the solid solutions $V_{1-x}Nb_xO_2$ ($0.0 \leq x \leq 1.0$) are presented in Table VII.3. The lattice parameters for pure NbO_2 (distorted rutile structure) and some of the solid solutions (rutile structure) are in good agreement with the data available in the literature^{16,17,23}. We could not examine the high temperature x-ray pattern of NbO_2 (above $800^\circ C$), but there seems to be little doubt that the structure is that of rutile¹⁷. DTA curves clearly show a sharp peak corresponding to the distorted rutile \rightarrow rutile transition in NbO_2 around $800^\circ C$ with a ΔH of 250 cal/mole (Table VII.4). The ΔH value differs from that reported by Kusenko and Gel'd²⁴. We also note that contrary to the findings of Sakata¹⁷, there is a thermal hysteresis of $\sim 10^\circ$ in the DTA curve indicative of a first order transition.

TABLE VII.4

DTA Results on $V_{1-x}Nb_xO_2$ and $V_{1-x}Mo_xO_2$ Systems

$V_{1-x}Nb_xO_2$	$T_t, ^\circ C^{(a)}$	$\Delta H_{tr} \text{ (cals mole}^{-1}\text{)}$
$x = 0.00$	69	750
0.02	42	250
0.05 ^(b)	40	200
0.10	-	-
0.50	-	-
0.90	-	-
1.00	800	250
$V_{1-x}Mo_xO_2$		
$x = 0.02$	45	350

- (a) DTA peak temperatures; considerable thermal hysteresis is observed in all the solid solutions as in VO_2 ($\Delta T \sim 15^\circ$) as well as in pure NbO_2 ($\Delta T \sim 10^\circ$).
- (b) Another transformation at $7^\circ C$ with ΔH_{tr} of about $\sim 50 \text{ cal mole}^{-1}$ is also noticed.

It is interesting that eventhough the room temperature structures of pure VO_2 and NbO_2 differ considerably from the rutile structure, the solid solutions can be indexed on the basis of the rutile structure. Whereas the a parameter increases regularly with increasing values of x , the c parameter goes through a maximum in the range $0.5 \leq x \leq 0.6$ (Table VII.3), an observation made by Rudorff and Marklin. It appears that the ionic radii play a prominent role in stabilizing the rutile structure in the solid solutions, since $r_{\text{Ti}^{+4}} \approx \frac{1}{2} (r_{\text{V}^{+4}} + r_{\text{Nb}^{+4}})$. There seems to be a compromise between the monoclinicity of VO_2 and the deformed rutile lattice of NbO_2 to give rise to a normal rutile structure (which is the structure of the high temperature 'metallic' phase of VO_2 as well as NbO_2) throughout the composition range, $0.05 < x < 1.0$, approaching the ideal structure at the composition $x \approx 0.5$. When $x = 0.02$ the room temperature (25°C) phase seems to possess the rutile structure with monoclinic distortion; at $x = 0.05$ the room temperature structure is probably distorted rutile (as in NbO_2); this may change to a monoclinic structure at lower temperatures (see the section on conductivity). The stabilization of the rutile structure above $x > 0.05$ is reflected also in the electrical properties of these solid solutions which will be discussed later. The possibility exists that at low temperatures, distorted rutile structures may be present upto $x = 0.1$. The susceptibility data of Rudorff and Marklin²³ give some indications of this behaviour; these workers

find discontinuities in χ at low temperatures for compositions $0.1 \leq x \leq 0.4$ and no discontinuity when $x > 0.5$. DTA studies carried out in an inert atmosphere, of solid solutions $V_{1-x}Nb_xO_2$ ($0.1 \leq x \leq 0.9$) failed to show the phase transformation of either VO_2 ($\sim 70^\circ C$) or NbO_2 ($\sim 800^\circ C$) (Table VII.4 and Fig. VII.1). When $x = 0.02$ there is transformation to the rutile structure at $\sim 42^\circ C$, a temperature much lower than in pure VO_2 . When $x = 0.05$, there is transition at $\sim 40^\circ C$ with a ΔH of ~ 200 cal mole $^{-1}$ and another at $7^\circ C$ with a ΔH of less than 100 cal mole $^{-1}$.

The solid solution $V_{0.98}Mo_{0.02}O_2$ possesses a distorted rutile structure, the exact nature of distortion not being clear (Table VII.5). It undergoes a transition to the rutile structure at $45^\circ C$ (Table VII.4), with an enthalpy of about 350 cal mole $^{-1}$. All these transformations are accompanied by appreciable hysteresis.

(b) Semiconductor-to-Semimetal Transition in VO_2

The four probe conductivity data on pellets of pure VO_2 clearly show a transition at $68^\circ C$ although it is not as abrupt as in single crystal materials (Fig. VII.2). At T_0 the conductivity jumps only by a factor of 10^2 compared to 10^4 reported by Ohashi and Watanabe²⁵ on polycrystalline samples of VO_2 . It is, however, gratifying to note that the observed room temperature conductivity is in excellent agreement with the data on single crystals and polycrystalline pellets reported by other workers^{8,10,25}. We find

TABLE VII.5

X-ray Data (2θ values in degrees) on $V_{0.98}Mo_{0.02}O_2$

VO_2 (monoclinic)	$V_{0.98}Mo_{0.02}O_2$ (a) (at 25°)	VO_2 (rutile)
at 25°C		at 80°C
26.92	-	-
27.85	27.63	* 27.73 28.05
33.44		-
36.96	37.08	37.28
42.08	40.61	40.72 42.52
42.20	42.13	-
44.68	47.28	44.56 47.22
52.98	-	-
55.52	55.43	55.68
-	57.53	-

(a) Assuming a distorted rutile we find, $a=4.560 \text{ \AA}$ and $c=2.863 \text{ \AA}$
($c/a \approx 0.63$).

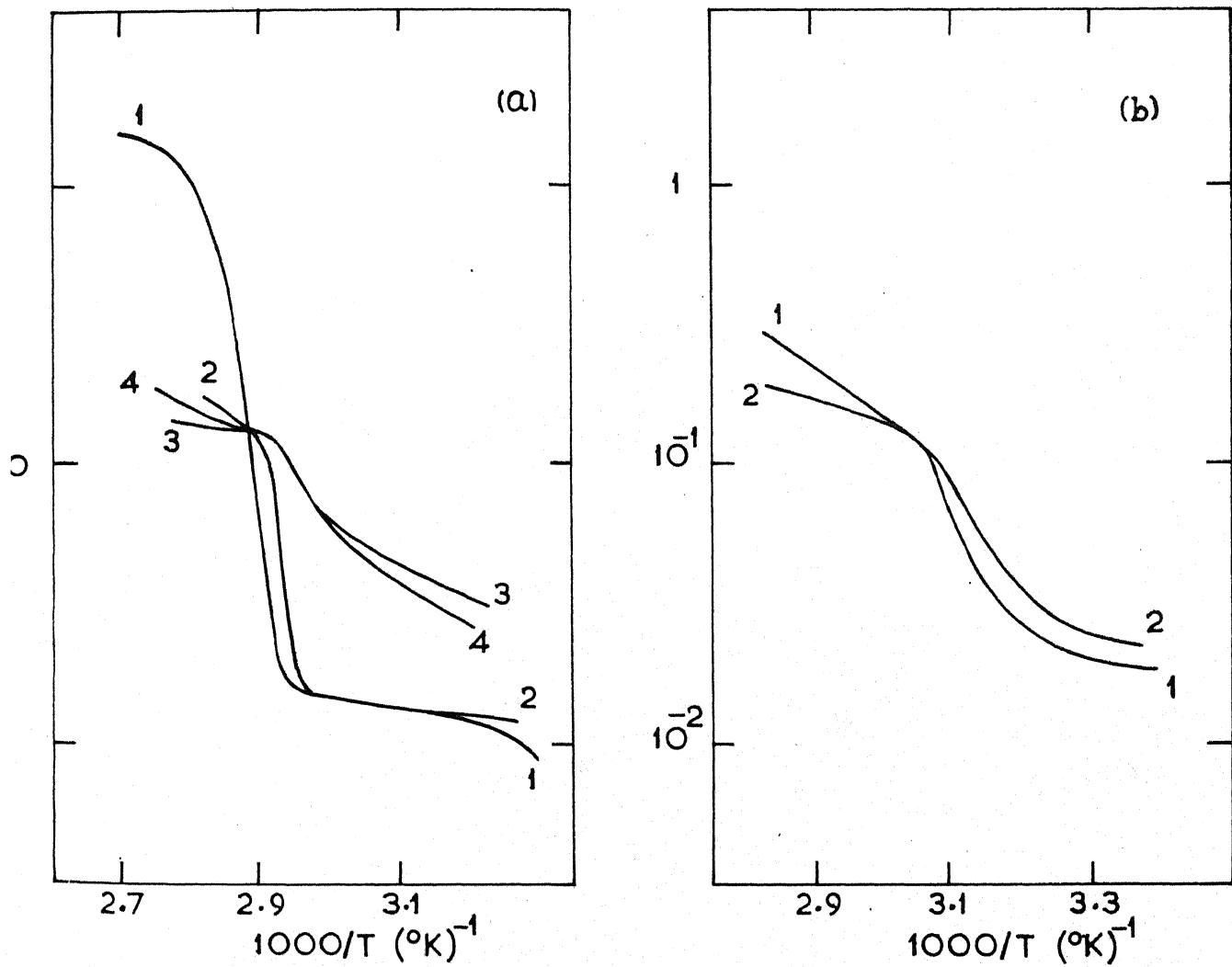


Fig. VII.2. Plot of electrical conductivity ($\text{ohm}^{-1}\text{cm}^{-1}$) versus reciprocal of absolute temperature (heating curves):
 (a) $\text{V}_{1-x}\text{Ti}_x\text{O}_2$; (1) $x=0$; (2) $x=0.02$; (3) $x=0.1$;
 (4) $x=0.20$; (b) $\text{V}_{1-x}\text{Nb}_x\text{O}_2$; (1) $x=0.02$; (2) $x=0.05$.

that the conductivity behavior of VO_2 does not improve significantly by taking the material through heating and cooling cycles through the transition temperatures several (more than three) times.

Neuman and coworkers⁸ have found that the conductivity at room temperature for VO_2 increases rapidly as x deviates from 2.0 in VO_x . The agreement of our conductivity data for VO_2 with those for the single crystal and polycrystalline samples reported by other workers^{8,10,25} indicates that the stoichiometry of the samples presently investigated is likely to be close to VO_2 . Further, the E_a value of 0.15 eV evaluated from the $\log \sigma$ versus $1/T$ plot (not shown in the Figure) in the low temperature region of VO_2 is in excellent agreement with that of Ladd and Paul¹⁰ on single crystals of pure VO_2 . In the immediate vicinity of the transition, E_a increases to ~ 0.3 eV, slightly lower than the values of Ladd and Paul¹⁰ (0.5 eV) and Ohashi and Watanabe²⁵ (0.42 eV). Further, we have noted a thermal hysteresis of 3-5°C in VO_2 transition while cooling the sample.

(c) Conductivity Anomalies in $\text{V}_{1-x}\text{Z}_x\text{O}_2$ ($\text{Z} = \text{Ti, Nb or Mo}$)

The room-temperature σ of $\text{V}_{1-x}\text{Ti}_x\text{O}_2$ with $x = 0.02 - 0.20$ is higher than that of pure VO_2 , σ being maximum when $x \approx 0.10$; when $x \approx 0.40$, however, the room temperature σ is lower than in pure VO_2 . The T_t values determined from the $\sigma - T$

data (Table VII.6) agree well with the DTA results (Table VII.2). The jump in conductivity, $\Delta\sigma$, at T_t is always smaller in the solid solutions than in pure VO_2 , $\Delta\sigma$ is largest when $x = 0.02$ and lowest when $x = 0.40$. The values above T_t are of the same magnitude for $0.02 \leq x \leq 0.20$ even though the σ values at $T < T_t$ are appreciably different (Fig. VII.2a). In this regard, the σ - T curves of the present study are similar to the χ - T curves of Rudorff and coworkers⁵ rather than those of Ariya and Grossman²¹. Rudorff and coworkers⁵ find that χ values of the solid solutions are similar above T_t , but considerably different below T_t . All the solid solutions presently studied, $0.02 \leq x \leq 0.40$ (as well as the composition with $x = 0.01$ studied by MacChesney and Guggenheim²⁶) show semiconductor behavior above T_t with activation energies (E_a) in the range 0.25 - 0.43 eV (Table VII.6). Our results support the observation of MacChesney and Guggenheim²⁶ that the incorporation of Ti^{4+} in VO_2 reduces the T_t , but are in disagreement with the data of Futaki and Aoki²⁷. Futaki and Aoki²⁷ also report that T_t in such solid solutions increases with c -axis of the (high-temperature) rutile phase. The present results on the series of $\text{V}_{1-x}\text{Ti}_x\text{O}_2$ solid solutions, however, show the opposite trend.

In the monoclinic structure of VO_2 , addition of Ti^{4+} creates holes in the valence band and decreases the energy gap thereby causing higher σ at $T < T_t$ and lower $\Delta\sigma$ at T_t . In pure

TABLE VII.6

Electrical Conductivity Data on $V_{1-x}Z_xO_2$ Systems ($Z = \text{Ti, Nb or Mo}$)

<u>Composition</u>		<u>Electrical conductivity</u>		
		40°C		
x		ohm ⁻¹ cm ⁻¹ $x(10^2)$	$T_t, ^\circ\text{C}$	E_a, eV
				$T < T_t$ $T > T_t$
0.00		0.80	69	0.15 ^(b) (0.28) -
<u>$V_{1-x}\text{Ti}_x\text{O}_2$ (a)</u>				
0.02		1.20	65	0.18 -
0.05		-	-	- -
0.10		5.80	63	0.15 0.25
0.20		4.70	58	0.23 0.43
0.40		0.25	45	0.16 0.31
<u>$V_{1-x}\text{Nb}_x\text{O}_2$</u>				
0.02 ^(c)		4.5	35	0.13 0.41
0.05 ^(d)		5.9	34	0.12 0.33
0.10 ^(e)		2.8	-	0.06 -
<u>$V_{1-x}\text{Mo}_x\text{O}_2$</u>				
0.02 ^(c)		4.6	40	0.12 0.41

(a) Monoclinic at 25°C.

(b) Value in parenthesis indicates just before transformation.

(c) These have monoclinic distortion but have been indexed as rutile structure.

(d) Shows another transition at 7°C (Monoclinic distorted rutile as in NbO_2) with a $\Delta H \sim 50$ cals mole⁻¹ (Fig. VII.); The 40°C transformation may be from distorted rutile to rutile. At 7°C, we observe a change in the slope of $\log \sigma$ vs $1/T$.

(e) Rutile structure at room temperature.

VO_2 , the homopolar $\text{V}^{4+}-\text{V}^{4+}$ bond can trap conduction electrons in the low-temperature phase²⁸. Apparently heteropolar bonds present in the solid solutions are not as effective in the trapping of charge carriers. The σ (just as the ΔH) in the solid solutions decreases with the monoclinicity of the low temperature phase (Table VII.1 and Fig. VII.2a). This is reasonable since the magnitude of crystal distortion should in principle determine these changes. The c/a ratio of the high-temperature rutile phase approaches the value in pure TiO_2 at high x . This would cause a decrease in σ above T_t with increase in x as observed experimentally. Above T_t it is possible that the Δ_{cc} and Δ_{cac} are much lower than the critical overlap²⁹ necessary to make them metallic.

In the solid solutions, $\text{V}_{1-x}\text{Nb}_x\text{O}_2$, the T_t and $\Delta\sigma$ are both lower when $x = 0.02$ and 0.05 (Table VII.6 and Fig. VII.2b); the conductivities of the low-temperature phases are higher compared to pure VO_2 . It is interesting that T_t is about the same when $x = 0.02$ and 0.05 . The high-temperature rutile phases are semiconducting with E_g in the range $0.3 - 0.4$ eV. When $x = 0.05$, we have noticed a change of slope in the σ - T curve at $\sim 7^\circ\text{C}$ in addition to the transition at 40°C . This is in accord with the DTA curve (Fig. VII.1), which shows two phase transitions, the one at $\sim 7^\circ\text{C}$ being associated with much lower ΔH . When $x = 0.10$, the rutile structure is stabilized and we do not see any transition corresponding to pure VO_2 or pure NbO_2 ; instead

it is semiconducting with a very low E_a of 0.06 eV in the range 20 - 85°C.

The solid solution with 2% MoO_2 shows a higher σ of the low-temperature phase compared to pure VO_2 , lower T_t and $\Delta\sigma$. Here again, the high-temperature phase shows semiconducting behavior with an E_a of 0.4 eV. The 5% MoO_2 sample appears to be metallic³⁰.

VII.3 EXPERIMENTAL

The methods of preparation of pure VO_2 , NbO_2 and the solid solutions are available in the literature³¹. The phase transformations were studied by recording the differential thermal analysis (DTA) curves employing an Aminco Thermoanalyzer³². The ΔH values were obtained from DTA peak areas³² employing the value of 750 cal mole⁻¹ for pure VO_2 as standard.

The x-ray patterns were recorded on a XRD-6 General Electric diffractometer attached to a sample holding furnace assembly with a temperature programmer and a voltage stabilizer. Cu K_α -radiation ($\lambda = 1.5405 \text{ \AA}$) was used.

DC conductivity measurements (both by two and four probe techniques) were made on polycrystalline pellets. The description of the conductivity set up and the procedure for conductivity measurements are described elsewhere³³.

Acknowledgement

The author is thankful to Dr. G.V. Subba Rao for his assistance with the conductivity measurements.

REFERENCES

1. D. Adler, Rev. Mod. Phys., 40, 714 (1968).
2. G. Andersson, Acta Chem. Scand., 10, 623 (1956); S. Minomura and H. Nagasaki, J. Phys. Soc. Japan, 19, 131 (1964).
3. K. Kosuge, T. Takada and S. Kachi, J. Phys. Soc. Japan, 18, 318 (1963); T. Kawakubo and T. Nakagawa, J. Phys. Soc. Japan, 19, 517 (1964).
4. W.G. Rudorff, G. Walter and J. Stadler, Z. anorg. allgem. Chem., 297, 1 (1958).
5. J. Omeda, H. Kusumoto, K. Narita and E. Yamada, J. Chem. Phys., 42, 1458 (1965).
6. A.S. Barker, Jr., H.W. Verleur and H.J. Guggenheim, Phys. Rev. Letters, 17, 1286 (1966); H.W. Verleur, A.S. Barker, Jr., and C.N. Berglund, Phys. Rev., 172, 788 (1968).
7. F.J. Morin, Phys. Rev. Letters, 3, 34 (1959).
8. C.H. Neuman, A.W. Lawson and R.F. Brown, J. Chem. Phys., 41, 1591 (1964).
9. K. Kosuge, J. Phys. Soc. Japan, 22, 551 (1967).
10. L. Ladd and W. Paul, Solid State Comm., 7, 425 (1969).
11. I. Kitahiro, T. Ohashi and A. Watanabe, J. Phys. Soc. Japan, 21, 2422 (1966).
12. I. Kitahiro and A. Watanabe, J. Phys. Soc. Japan, 21, 2423 (1966).
13. J.B. Goodenough, Bull. Soc. Chim. France, 4, 1200 (1965).
14. D. Adler and H. Brooks, Phys. Rev., 155, 826 (1967).
15. A. Magneli, G. Andersson and G. Sundkvist, Acta Chem. Scand., 9, 1402 (1955).
16. T. Sakata, K. Sakata and I. Nishida, phys. status solidi, 20, K155 (1967).
17. K. Sakata, J. Phys. Soc. Japan, 26, 582 (1969).
18. R.F. Janninck and D.H. Whitmore, J. Phys. Chem. Solids, 27, 1183 (1966).

19. J.A. Roberson and R.A. Rapp, J. Phys. Chem. Solids, 30, 1119 (1969).
20. K. Sakata, J. Phys. Soc. Japan, 26, 867 (1969).
21. S.M. Ariya and G. Grossmann, Sov. Phys. Solid State (English Transl.), 2, 1166 (1960).
22. K. Sakata and T. Sakata, Japan J. Appl. Phys., 6, 112 (1967).
23. W. Rüdorff and J. Marklin, Z. anorg. allgem. Chem., 334, 142 (1964).
24. F.G. Kusenko and P.V. Gel'd, Izv. Vysshikh Uchch Zavendenii, Tsvetna'ya Met., 3, 102 (1960); CA., 55, 3141d (1961).
25. T. Ohashi and A. Watanabe, J. Am. Ceram. Soc., 49, 519 (1966).
26. J.B. MacChesney and H.J. Guggenheim, J. Phys. Chem. Solids, 30, 225 (1969) and the references cited therein.
27. H. Futaki and M. Aoki, Japan J. Appl. Phys., 8, 1008 (1969).
28. J.B. Goodenough, Phys. Rev., 117, 1442 (1960).
29. J.B. Goodenough, Czech, J. Phys., 17B, 304 (1967).
30. J.B. Goodenough, in "Transition Metal Compounds", Gordon and Breach, New York, 1964.
31. R.E. Loehman, C.N.R. Rao, J.M. Honig and C.E. Smith, J. Sci. Ind. Res. (India), 28, 13 (1969).
32. K.J. Rao and C.N.R. Rao, J. Materials Sci., 1, 238 (1966).
33. G.V. Subba Rao, Ph.D. Thesis, 1969, Indian Institute of Technology, Kanpur, India

CHAPTER VIII

PHASE TRANSFORMATIONS IN SOME HALIDE SYSTEMS

CHAPTER VIII

PHASE TRANSFORMATIONS IN SOME HALIDE SYSTEMS*

VIII.1 INTRODUCTION

An examination of the recent crystallographic literature, particularly the monographs on x-ray diffraction patterns published by the U.S. National Bureau of Standards¹ revealed that some of the compounds of the general formula, $ABCl_3$ where A is Cs or Rb and B is Pb or Cd, exhibit interesting phase transitions. The reported space groups suggested the possibility of ferroelectricity in some of these halides. Since the observation of ferroelectricity in such simple compounds is of considerable interest, we considered it worthwhile examining the phase transitions in these compounds. While the phase transitions in some of the chlorides have not been completely described in the literature, there is little or no information on the phase transitions of the corresponding

* A communication based on part of this work has appeared in Physics Letters, 29A, 528 (1969).

bromides or iodides. We have presently investigated the crystallography and phase transitions of the chlorides, $ABCl_3$, as well as of the corresponding bromides and iodides. In addition, we have studied the phase transition in $CsCuCl_3$ which has not been reported in the literature.

VIII.2 RESULTS AND DISCUSSION

(a) Phase transition in $CsPbX_3$ ($X = Cl, Br, \text{ or } I$)

$CsPbCl_3$:

Møller² reported the crystal structure of $CsPbCl_3$ to be tetragonal ($C_{4v}^1 - P4mm$; $a = 5.590 \text{ \AA}$, $c = 5.477 \text{ \AA}$)²; he has also reported a phase transformation of $CsPbCl_3$ at $\sim 47^\circ C$ from a tetragonal structure to a cubic perovskite structure ($a = 5.605 \text{ \AA}$ above $47^\circ C$). The volume change, ΔV , accompanying the transformation is negligible and on this basis the transformation was reported to be a second order one. The hysteresis, ΔT is also negligible accordingly. Recently, Sakudo and coworkers³ have identified a new phase transition around $40^\circ C$ based on x-ray, elastic and acoustic measurements; they observed superstructure at this transition temperature. Tooborg⁴ has investigated two phase transformations in $CsPbCl_3$ by NQR measurements and finds that the transformation at $47^\circ C$ is first order while that at $\sim 40^\circ C$ is a second-order one.

DTA (Fig. VIII.1) studies show that the transition at 47°C is associated with a very low enthalpy (~ 20 calories mole⁻¹); DTA curves, however, failed to show any transformation around 40°C as reported by Sakudo and coworkers³. The transition at 47°C is accompanied by a change of colour from light yellow to dark yellow. The low enthalpy and the absence of thermal hysteresis indicate a second or higher order transition at 47°C ⁵. The dielectric constant of CsPbCl_3 (Fig. VIII.2a) shows an anomaly at 47°C . There is also a marked increase in the dielectric constant in the $35\text{--}40^{\circ}\text{C}$ region possibly due to the new transformation reported by Sakudo and coworkers³. No dielectric hysteresis was observed in CsPbCl_3 in the transformation region ($25 - 60^{\circ}\text{C}$).

The present findings along with the observation of superstructure³ indicate that below 47°C CsPbCl_3 is possibly antiferroelectric. The tetragonal to cubic transformation probably corresponds to a change from the antiferroelectric phase to the paraelectric phase. We find that the tolerance factor for the perovskite CsPbCl_3 is 0.826; this would favour the distortion from the nonpolar cubic phase to the antipolar tetragonal phase. Such tolerance factors of less than unity are also found in other antiferroelectrics such as PbZrO_3 ⁶ and PbHfO_3 ⁷.

CsPbBr_3 :

CsPbBr_3 crystallizes in the distorted perovskite structure⁸ (orange colour); an orthorhombic form (colourless)

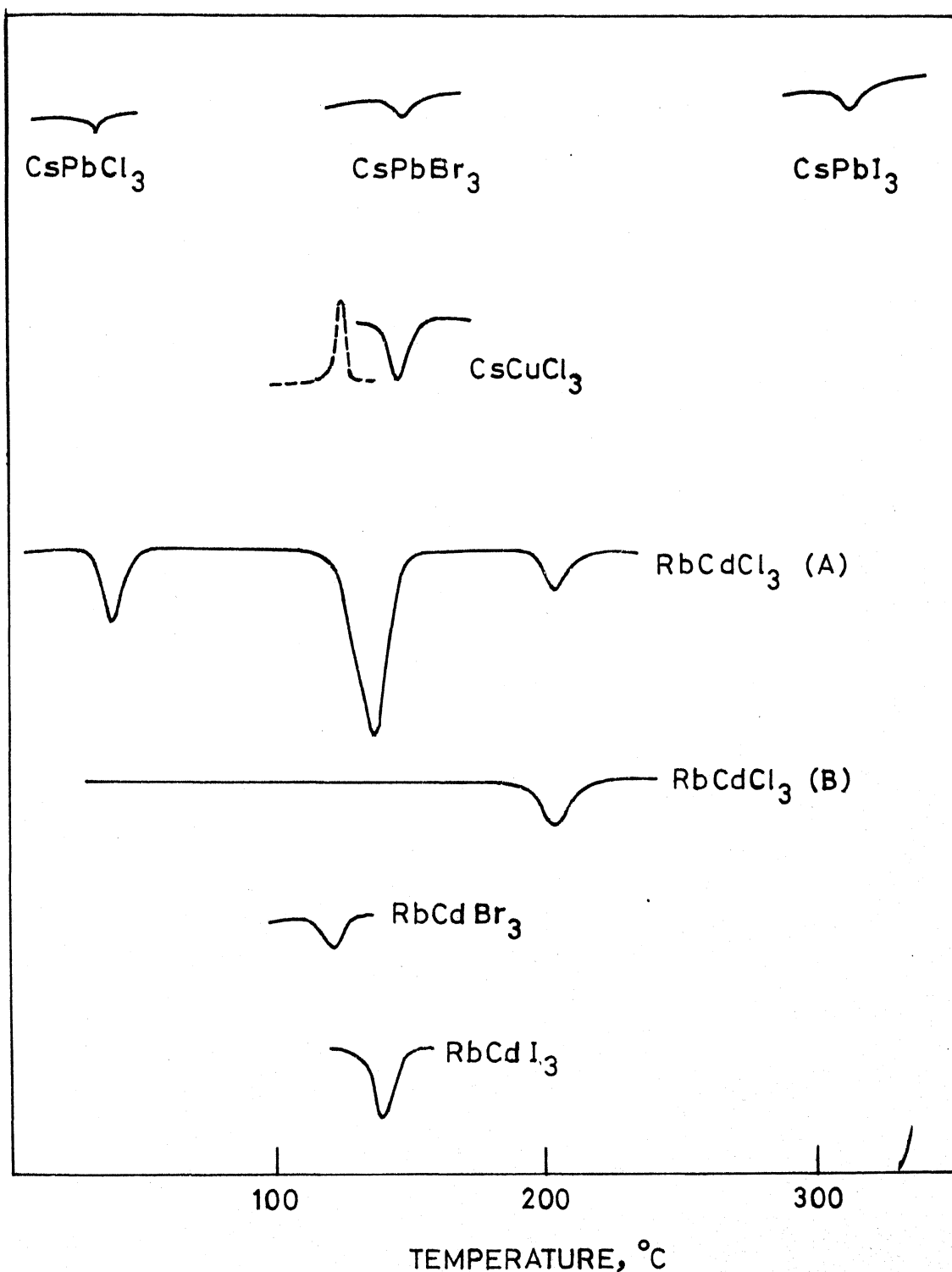


Fig. VIII.1 DTA curves of the mixed halides. RbCdCl_3 (A) prepared from aqueous solution; RbCdCl_3 (B) prepared from the melt. The transition at $\sim 28^\circ\text{C}$ was not reproducible in subsequent runs with fresh samples.

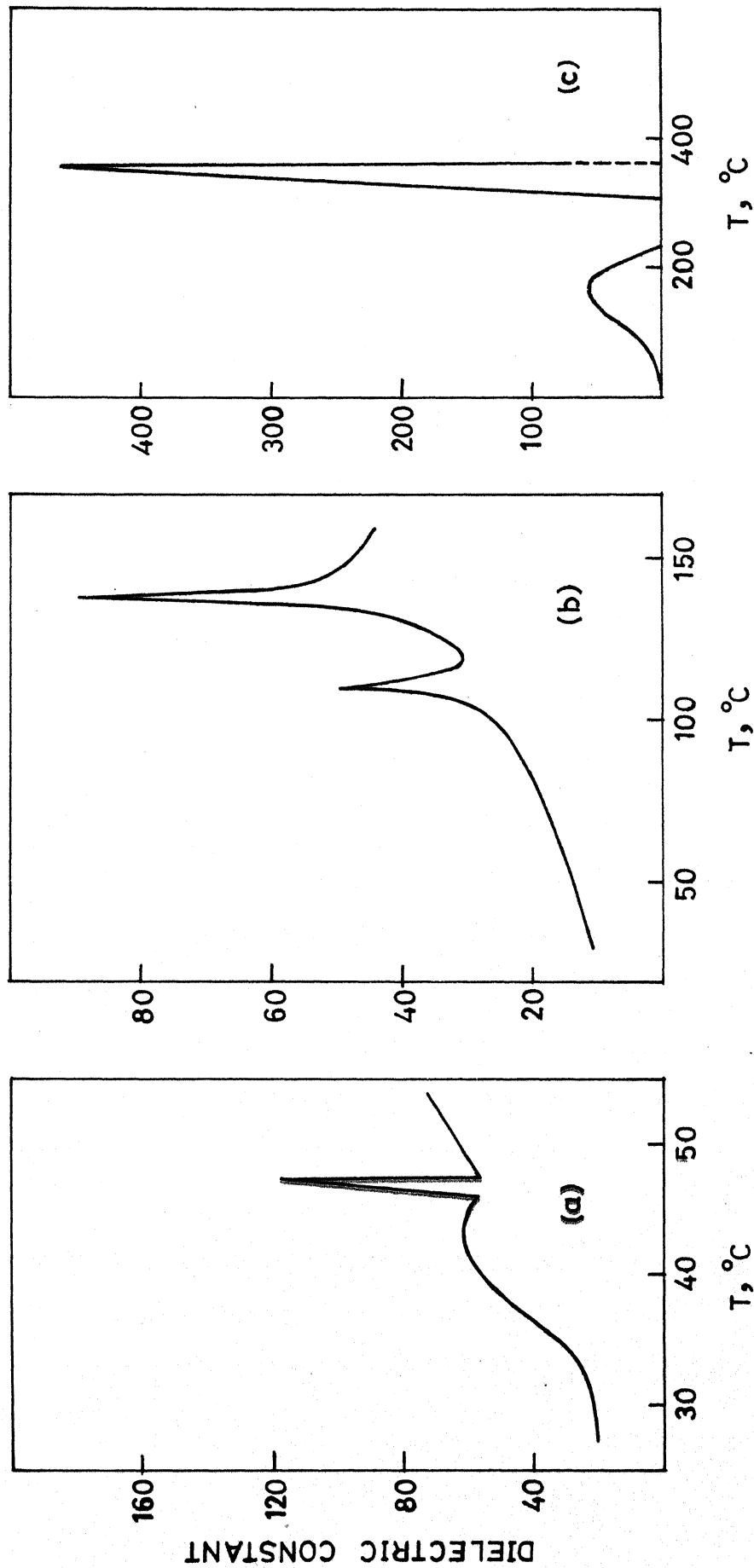


Fig. VIII.2 Dielectric constant as a function of temperature of (a) CsPbCl_3 , (b) CsPbBr_3 and (c) CsPbI_3 . Note that an anomaly precedes the transformation point in all the three cases.

isostructural with NH_4CdCl_3 is also known to exist at 25°C . CsPbBr_3 is reported to transform at $\sim 130^\circ\text{C}$ to a cubic perovskite structure ($a = 5.874 \text{ \AA}$). The volume change, ΔV , accompanying the transformation as well as the thermal hysteresis, ΔT , are negligible suggesting that the transition is likely to be a second order one⁵. NQR investigation by Volkov and coworkers⁹ indicate another transition around -106°C which is likely to be a second order one. Volkov and coworkers suggest that the transition at 130°C is first order transition contrary to the report by Möller⁸.

Our DTA studies show a reversible peak (Fig. VIII.1) at $\sim 130^\circ\text{C}$ with an enthalpy of $\sim 250 \text{ cal mole}^{-1}$. The hysteresis is negligible and the transformation is likely to be a higher order one. The measurement of dielectric constant as a function of temperature indicates two anomalies, one at $\sim 110^\circ\text{C}$ and the other at $\sim 139^\circ\text{C}$ (Fig. VIII.2b). The dielectric anomaly at 110°C may be akin to the one in CsPbCl_3 at $\sim 40^\circ\text{C}$. No ferroelectric hysteresis loop was observed in the region $25 - 140^\circ\text{C}$. It is possible that the transition at $\sim 139^\circ\text{C}$ is from an antiferroelectric phase to a paraelectric phase just as in CsPbCl_3 . The tolerance factor calculated for CsPbBr_3 is ~ 0.8123 .

CsPbI_3 :

Möller⁸ reported a monoclinic structure ($a = 6.23 \text{ \AA}$, $b = c = 6.15 \text{ \AA}$; $\beta = 91^\circ, 45'$) for CsPbI_3 (brownish yellow) below 305°C .

Above 305°C it is monoclinically distorted perovskite structure (in which the material is black in colour) with the space group PmCn; the lattice constants are known to be:

$$a = b = 6.15 \text{ \AA}; c = 6.23 \text{ \AA}; \beta = 88^\circ, 15'.$$

Recently Volkov and coworkers⁹ have reported that the structure of CsPbI₃ below 305°C is orthorhombic and that it is isostructural with the colourless (orthorhombic) form of CsPbBr₃; above 305°C, the material possesses a distorted perovskite structure as well as an (yellow form) orthorhombic structure.

Our DTA investigations showed an endothermic peak $\sim 340^\circ\text{C}$ (Fig. VIII.1). The transformation is reversible and the enthalpy is $\sim 1000 \text{ cal mole}^{-1}$. Dielectric constant measurements show an anomaly (Fig. VIII.2c) at $\sim 150^\circ\text{C}$ (probably akin to those at $\sim 40^\circ\text{C}$ in CsPbCl₃ and at $\sim 110^\circ\text{C}$ in CsPbBr₃) and another at $\sim 350^\circ\text{C}$ corresponding to the DTA peak (Fig. VIII.1). DTA, however, does not indicate the 150°C transition. No ferroelectric hysteresis loop is observed in the 25° - 350°C range. It is possible that the transition at $\sim 340^\circ\text{C}$ of CsPbI₃ is similar to the 47°C transition in CsPbCl₃ or/and the 130° transition in CsPbBr₃.

(b) Phase Transformations in RbCdX₃ (X = Cl, Br or I)

RbCdCl₃:

RbCdCl₃ is known to transform from an orthorhombic structure, I, (D_{2h}¹⁶ - Pnam; $\underline{a} = 8.959 \pm 0.001 \text{ \AA}$, $\underline{b} = 14.976 \pm 0.002 \text{ \AA}$

and $c = 4.0346 \pm 0.0004 \text{ \AA}$) to a tetragonal structure, II, $a = 10.304 \text{ \AA}$ and $c = 10.399 \text{ \AA}$) around 140°C^1 . The tetragonal structure then transforms to an undistorted cubic perovskite (III) around 190°C^1 . The dimension of the cubic unit cell has not been reported in the literature. While the cubic form rapidly reverts to the tetragonal form on cooling, the tetragonal form is reported to persist for an extended periods of time even at room temperature¹.

The sequence of transformations reported in RbCdCl_3 is similar to that in BaTiO_3 where the orthorhombic and tetragonal phases are ferroelectric¹⁰. This similarity in the phases as well as the fact that many of these halides mentioned before do have a common structure namely a distorted perovskite (in some temperature range) tempted us to examine the possible ferroelectricity in some of these materials particularly in RbCdCl_3 . We have presently examined the phase transitions of RbCdCl_3 employing high-temperature x-ray diffraction differential thermal analysis, dielectric constant measurements and hysteresis loop observations. We were particularly interested in the reverse transformation of the high temperature structure.

RbCdCl_3 prepared from aqueous solution transforms from structure I to II around 140°C . Structure II is stable upto $\sim 200^\circ\text{C}$ above which it transforms to a cubic perovskite structure (III) with a cell constant, $a = 10.3280 \pm 0.005 \text{ \AA}$ at 225°C . The DTA

curves corresponding to these transformations are shown in Fig. VIII.1. While III readily reverts back to II on cooling, structure II transforms to I only slowly depending on the temperature of quenching (Fig. VIII.3). If the quenching temperature is $\sim 35^{\circ}\text{C}$, it takes nearly four hours for II to come back to I (Fig. VIII.3). However, if samples heated to temperatures above 140°C are quenched to 0°C or -190°C , II transforms back to I almost immediately (Fig. VIII.4). Further there was evidence, in the x-ray patterns, for the presence of small proportions of II (Fig. VIII.5) after 4 or 5 hours when quenching at room temperatures.

RbCdCl_3 prepared by the fusion method, when suddenly quenched to room temperature exhibits the tetragonal structure II, as evidenced by x-ray diffraction patterns. The DTA curves (Fig. VIII.1) thus show only the $\text{II} \rightarrow \text{III}$ transformation. Sample of RbCdCl_3 obtained by fusion method comes back to I only on long standing, at room temperature, extending over a few days. Quenching at low temperature of this sample also stabilizes RbCdCl_3 in I, at room temperature. These studies clearly bring out the metastable nature of structure II. The enthalpies of $\text{I} \rightarrow \text{II}$ and $\text{II} \rightarrow \text{III}$ transformations estimated from DTA peak areas are 2300 and $200 \text{ cal mole}^{-1}$ respectively. The ΔH value of $\text{I} \rightarrow \text{II}$ is considerably smaller unless care is taken to see that the starting material is in orthorhombic structure (I). This is particularly true of the sample prepared by fusion. Besides $\text{I} \rightarrow \text{II}$ and $\text{II} \rightarrow \text{III}$

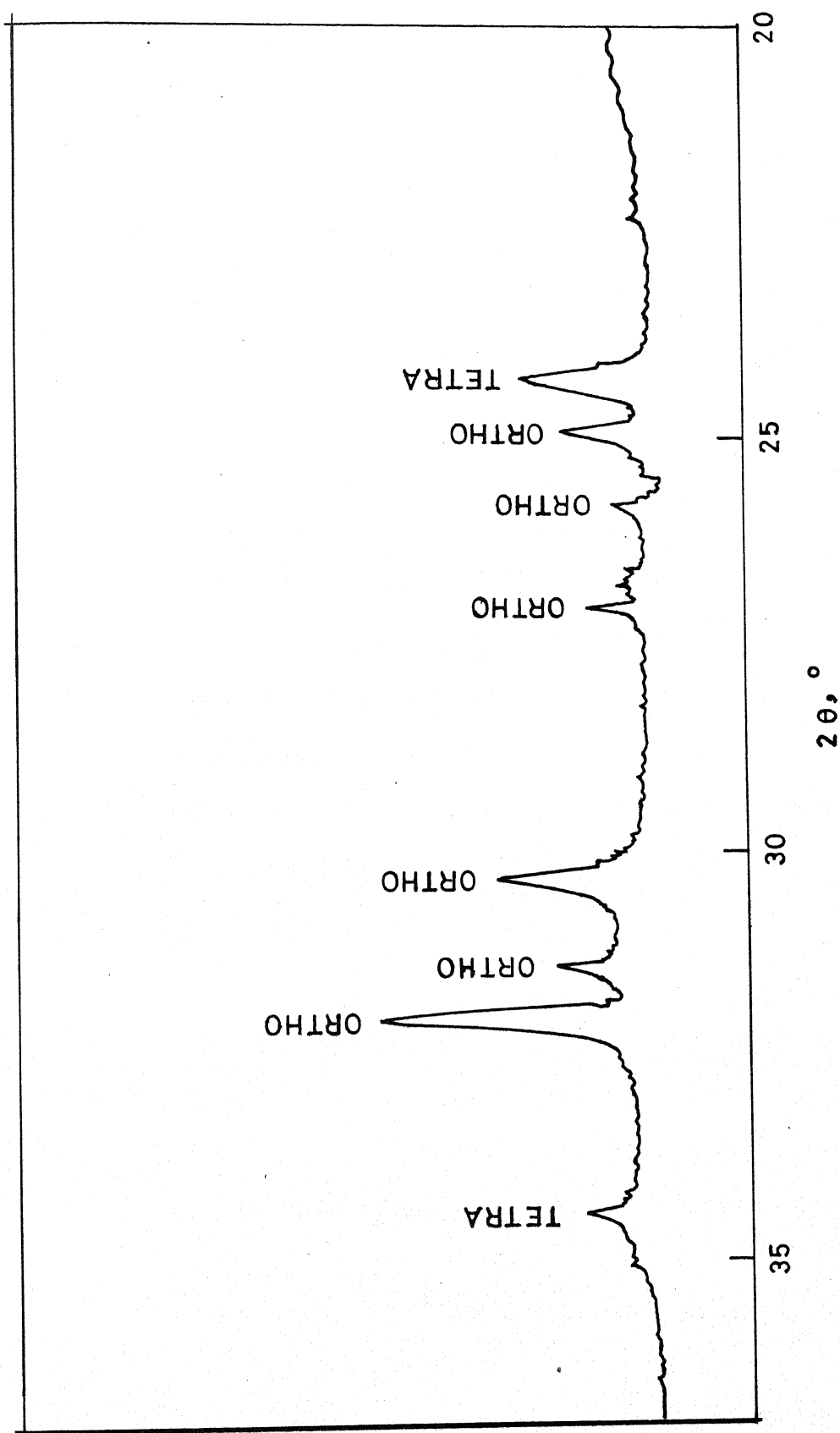


Fig. VIII.5 Coexistence of the lines due to the tetragonal and orthorhombic phases in RbCdCl_3 quenched to room temperature.

transitions, RbCdCl_3 prepared by solution showed another peak in the DTA curves at $\sim 28^\circ\text{C}$ (Fig. VIII.1)*.

Dielectric constant measurements were made from -150°C to 250°C to characterise the various phase transitions. Dielectric anomalies are clearly seen at $\sim 28^\circ\text{C}$, $\sim 140^\circ\text{C}$ and $\sim 200^\circ\text{C}$ (Fig. VIII.6a) consistent with the phase transformations observed in the DTA curves (Fig. VIII.1).

Although we have noticed some ferroelectric loops disappearing at the transition temperature, 140°C and at $\sim 200^\circ\text{C}$, we are not sure of these observations since many of these were not exactly reproducible. Looking at the dielectric constants, we do not expect ferroelectricity in this material. More detailed investigations of the crystallography and dielectric hysteresis are necessary before arriving at conclusions regarding the phase transitions in RbCdCl_3 .

RbCdBr_3 and RbCdI_3 :

The preparation and characterization of RbCdBr_3 and RbCdI_3 are not reported in the literature. Our preliminary investigations show that RbCdBr_3 is orthorhombic ($a = 8.950 \text{ \AA}$, $b = 15.380 \text{ \AA}$ and $c = 3.954 \text{ \AA}$) and is probably distorted. DTA shows an endothermic peak at $\sim 120^\circ\text{C}$ with an enthalpy of about

* We have not fully investigated this transformation. The crystal structure of RbCdCl_3 below this temperature ($\sim 28^\circ\text{C}$) is yet to be established.

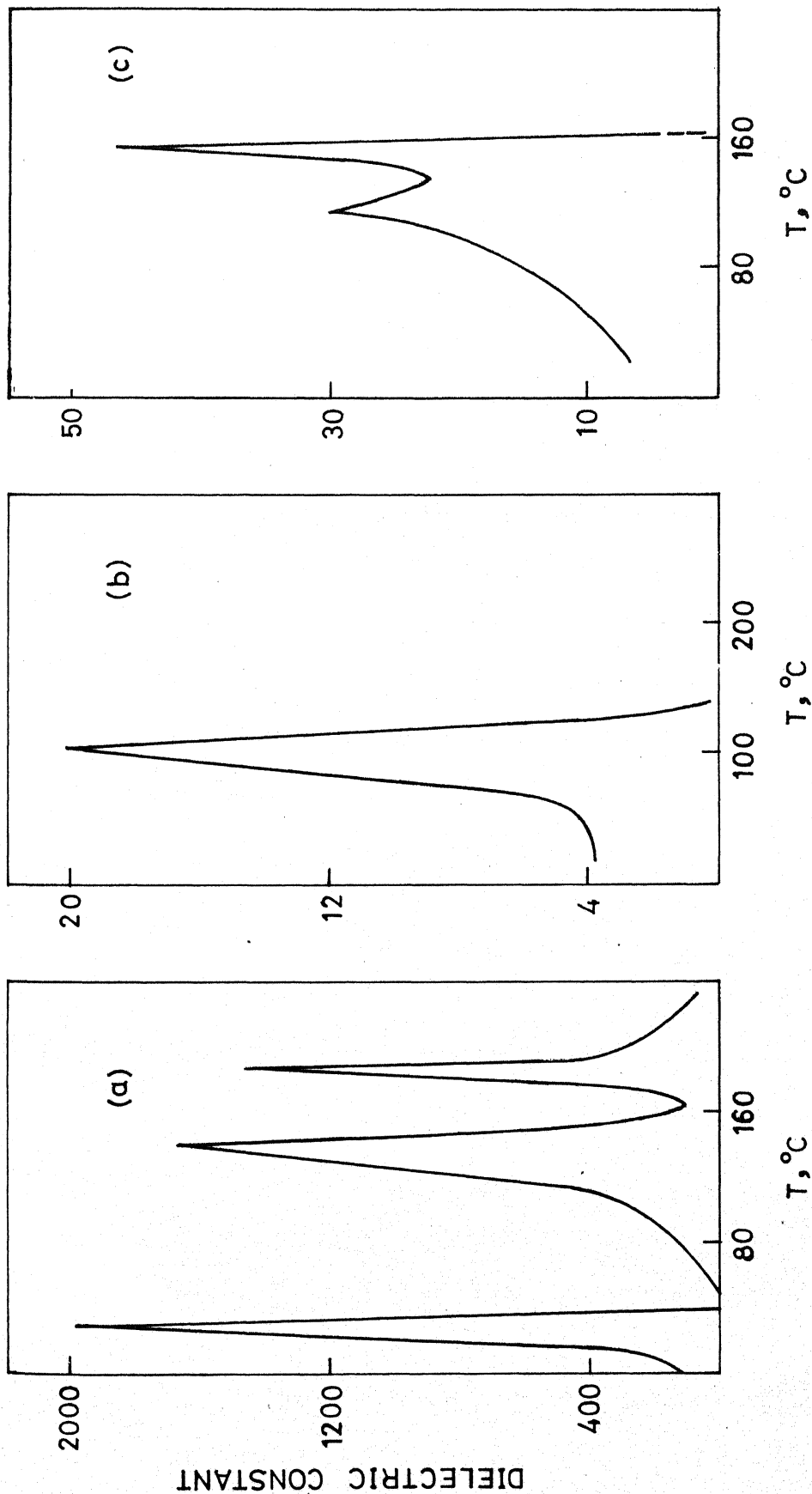


Fig. VIII. 6 Dielectric constant anomalies for (a) RbCdCl_3 , (b) RbCdBr_3 and (c) RbCdI_3 samples. The anomaly at 28°C for RbCdCl_3 was reproducible while the DTA peak corresponding to this was not.

1100 cal mole⁻¹ (Fig. VIII.1). The transformation is not readily reversible and is likely to be similar to the I - II transition in RbCdCl₃. The transformation is also indicated by the dielectric anomaly (Fig. VIII.6b) at ~ 105°C. The large transition enthalpy suggests that transition is likely to be of first order.

RbCdI₃ is found to possess distorted rutile structure ($a = 10.4 \text{ \AA}$, $c = 10.82 \text{ \AA}$), isostructural with CsPbCl₃. DTA shows an endothermic peak (Fig. VIII.1) at ~ 130°C with a large enthalpy of transition (~ 2250 cal mole⁻¹) suggesting a first order transition. The transformation is not readily reversible. Two dielectric anomalies at ~ 128° and also at ~ 160°C (Fig. VIII.6c) have also been noticed. No satisfactory and reproducible ferroelectric hysteresis loops were observed either in RbCdBr₃ or in RbCdI₃. The tolerance factors of RbCdX₃ are less than unity.

(c) Phase transition in CsCuCl₃:

CsCuCl₃ is hexagonal ($D_6^2 - P6_122$; $a = 7.2165 \text{ \AA}$ and $c = 18.1800 \text{ \AA}$) and no transformation has been reported for this compound in the literature¹. The crystals of CsCuCl₃ formed as dark red hexagonal prisms terminated by bipyramids. On grinding to powder the colour of the sample changed to dark orange yellow.

Our DTA investigations showed an endothermic transition at ~ 140°C (Fig. VIII.1) with an enthalpy of about 450 cal mole⁻¹. The transformation is reversible and is accompanied by an appreciable thermal hysteresis of about 10°. The fairly large ΔH value

and the presence of hysteresis suggest that the transformation is a first order one. The high temperature structure was ascertained by x-ray investigations and found to be face-centered cubic with a lattice constant, $a = 6.2205 \pm 0.005 \text{ \AA}$ (at 190°C).

(d) Concluding remarks :

The important results obtained on the phase transformations of the halides of the general formula, ABX_3 are summarized in Table VIII.1. The phase transformations are undoubtedly interesting and further studies are required to understand the detailed nature of these transitions.

VIII.3 EXPERIMENTAL

The samples were prepared by either mixing the aqueous solutions of the constituent halides and subsequent evaporation (where they are freely soluble in water), or by fusing the two halides at $\sim 500^\circ\text{C}$ (if they are sparingly soluble in water). RbCdBr_3 and RbCdI_3 were prepared by evaporation of aqueous solutions.

The phase transformations were examined by differential thermal analysis (DTA) employing an Aminco Thermoanalyzer and the procedure for estimating ΔH values etc., have been described in the earlier chapters.

X-ray diffraction measurements were made on a General Electric XRD-6 diffractometer fitted with a sample holding furnace

TABLE VIII.1

DTA Results on Mixed Halides

Halides	Transformation temperature, °C	ΔH_{tr} (cals mole ⁻¹)	Tolerance factor
CsPbCl ₃	47	20	0.826
CsPbBr ₃	130	250 ± 25	0.813
CsPbI ₃	310	1000 ± 100	0.806
RbCdCl ₃ (a)			
(?)	28	350 ± 50	0.835
(I → II)	137	2300 ± 250	
(II → III)	190	200 ± 25	
RbCdBr ₃ (b)	120	1060 ± 100	0.828
RbCdI ₃ (c)	130	2250 ± 250	0.820
CsCuCl ₃ (d)	140(130)	450 ± 50	-

(a) RbCdCl₃ I is orthorhombic, II is tetragonal and III is perovskite cubic.

(b) Orthorhombic at 25°C (a = 8.95 Å, b = 15.38 Å, c = 3.954 Å).

(c) Distorted perovskite at 25°C (a = 10.4000 Å, c = 10.8200 Å).

(d) T_{reverse} is given in parentheses.

attached to a temperature programmer. $\text{CuK}\alpha$ -radiation was used.

Dielectric constant measurements (at 1 kHz) of the samples were made on polycrystalline pellets, supported by a spring load between platinum discs in a conductivity cell, employing a General Radio 1650-A bridge.

Acknowledgement

The author is thankful to Dr. B. Prakash for help in some of the measurements.

REFERENCES

1. 'Standard x-ray Diffraction Patterns', U.S. National Bureau of Standards, Monograph No. 25 Section 5, ed. by H.E. Swanson, H.F. McMurdie, M.C. Morris and E.H. Evans, August (1967).
2. C.K. Møller, Mat. Fys. Medd. Dan Vid. Selsk., 32, No. 2 (1959).
3. T. Sakudo, H. Unoki, F. Fujii, J. Kobayashi and M. Yamoda, Phys. Letters, 23A, 542 (1969).
4. N. Tooborg, J. Chem. Phys., 50, 559 (1969).
5. C.N.R. Rao and K.J. Rao in "Progress in Solid State Chemistry", ed. by H. Reiss, Vol. 4 (Pergamon Press, Oxford, 1967).
6. G. Shirane, H. Danner, A. Pavlouic and R. Pepinsky, Phys. Rev., 95, 672 (1954).
7. W. Kanzig, 'Ferroelectrics and Antiferroelectrics', (Academic Press, London 1957).
8. C.K. Møller, Nature, 182, 1436 (1958).
9. A.F. Volkov, YU. N. Venetsev and G.K. Semin, phys. stat. solidi., 35, K167 (1969).
10. F. Jona and G. Shirane, 'Ferroelectric Crystals' Pergamon Press, New York, 1962.

SUMMARY

SUMMARY

Cesium chloride transforms from the CsCl structure ($Pm\bar{3}m$) to the NaCl structure ($Fm\bar{3}m$) at $\sim 480^\circ\text{C}$; the transition is accompanied by considerable thermal hysteresis ($\Delta T \sim 35^\circ$); the molar volume change, ΔV , accompanying the transformation is ~ 7.34 c.c. Addition of KCl to CsCl reduces the temperature of the $Pm\bar{3}m$ - $Fm\bar{3}m$ transformation and at $\sim 30\%$ KCl the solid solution is stabilized in the $Fm\bar{3}m$ phase. Addition of CsBr to CsCl, however, increases the transition temperature as well as the enthalpy of transition. Thus, KCl and CsBr produce opposite effects on the $Pm\bar{3}m$ - $Fm\bar{3}m$ transformation of CsCl.

The ΔV of the $Pm\bar{3}m$ - $Fm\bar{3}m$ transition increases slightly with the addition of KCl, while the ΔV shows a marked decrease in the CsBr solid solutions. Apparently, the first order characteristics of the CsCl transformation are still maintained in KCl solid solutions while in CsBr solid solutions higher order components seem to be present. Accordingly, we have found evidence for the coexistence of the $Pm\bar{3}m$ and $Fm\bar{3}m$ phases in some CsBr solid solutions in the neighbourhood of the transition temperature. These divergent behaviours of the CsCl-KCl and CsCl-CsBr systems can be explained by employing Born's phenomenological treatment of ionic solids with a four-parameter repulsive term; we however, find it necessary to employ a higher

van der Waals term in order to obtain satisfactory solutions. The Born treatment could account for the stabilization of the 30% KCl solid solution in the Fm $\bar{3}$ m structure as well as the increase in transition enthalpy with % CsBr.

The Pm $\bar{3}$ m-Fm $\bar{3}$ m transformation temperature of CsCl is slightly lowered by the incorporation of vacancies (through the addition of Sr⁺²). In order to obtain the formation energies of Schottky defects in the Pm $\bar{3}$ m and Fm $\bar{3}$ m structures of CsCl, we have carried out ionic conductivity measurements on Sr⁺² doped CsCl samples; the formation energies thus obtained are 1.4 eV and \sim 2.0 eV respectively. These studies indicate that the Pm $\bar{3}$ m-Fm $\bar{3}$ m transformation may be facilitated to a small extent by cation vacancies even though the basic mechanism may involve dilatation along the body diagonal.

The cation vacancy migration energy in CsCl is considerably lowered by the addition of K⁺ and Rb⁺ (especially at compositions where Fm $\bar{3}$ m phase gets stabilized); Br⁻ slightly increases the cation migration energy. These results can be understood in terms of the differences in the sizes of the additive ions. The association enthalpy for the formation of the complex between the cation vacancies and the Sr⁺² ions has been calculated from conductivity data. The values in the Pm $\bar{3}$ m and Fm $\bar{3}$ m phases are found to be 0.40 and 0.35 eV respectively; after making corrections for the long range

interactions (Debye-Hückel corrections), the value in the $Fm\bar{3}m$ phase is increased by $\sim 20\%$.

Phase transformations in silver iodide, including the interesting transition from B3 (low cubic, sphalerite) \longrightarrow B4 (hexagonal, wurtzite) have not been clearly described in the literature. While we have no doubt regarding the existence of the B3 polytype, we find no evidence from differential thermal analysis (DTA) or x-ray studies for the existence of the B3 \longrightarrow B4 transformation. Both B3 and B4 seem to directly transform to the B23 (high cubic) structure in the range $140-146^\circ\text{C}$. Electrical conductivity studies seem to suggest the possibility of the B4 intermediate in the B3 \longrightarrow B23 transformation, but we failed to see any reflections due to B4 in the high temperature x-ray patterns.

Addition of AgBr to AgI decreases the temperature of the B3/B4 \longrightarrow B23 transition, up to $\sim 10-15\%$ AgBr; the thermal hysteresis and ΔV accompanying the transformation increase slightly with % AgBr (upto $\sim 10\%$ AgBr). It appears that $\sim 10\%$ AgBr goes into solid solution with AgI in B3, B4 and B23 structures and the solid solutions retain the first order characteristics of the B3/B4 \longrightarrow B23 transition of AgI. At higher percentages of AgBr, solid solutions of B1 ($Fm\bar{3}m$, NaCl type) structure are formed; we may note here that the B1 structure of pure AgI is noticed only at high pressures. AgI goes into solid solution (of B1 structure) with AgBr

upto $\sim 25\%$ AgI. All these data along with the melting characteristics of the solid solutions have been employed to construct a partial phase diagram of the AgI-AgBr system (Fig. IV.7) Born model of ionic solids with two repulsive parameters explains the $B3/B4 \rightarrow B23$ transition of AgI as well as the relative stabilities of the B3 and B1 phases of the AgI-AgBr solid solutions. The Born model also explains the ($B3 \rightarrow B1$) pressure transition of AgI as well as the pressure transitions of AgBr and AgCl from B1 to B2 ($Pm\bar{3}m$, CsCl type) structure. We have found it necessary to employ higher van der Waals terms in the lattice energy expressions of these solids as well.

The enthalpy and thermal hysteresis in reversible crystal structure transformations are considerably affected by particle size effects. The thermal hysteresis, ΔT , decreases with increasing particle size and for a given sample ΔT decreases with the rate of heating. We find large thermal hysteresis ($\sim 12^\circ$) even in quartz when the particle size is around 5 microns. The variation of thermal hysteresis with particle size has been explained in terms of Turnbull's theory of heterogeneous nucleation. We have calculated interfacial energies from Turnbull's theory as well as from the DTA curves. From a knowledge of the crystal structures of the initial and final phases, interfacial energies have been estimated following the procedure of Bruce. These different estimates of interfacial energies show fair agreement with one another.

The enthalpy change associated with the phase transformation of a solid increases with decrease in particle size. This effect is likely to be due to the higher surface energy of the smaller particles. We have attempted to treat the effect of particle size on the enthalpy change quantitatively.

Crystallization of amorphous oxides is found to be highly exothermic; the energy of activation for crystallization is quite small. The heat of crystallization of amorphous oxides will undoubtedly depend on the method of preparation, sample history etc.

Thermal and particle size effects in magnesium oxide form an interesting aspect of study in this thesis. The heat of solution of MgO decreases with the temperature of preparation. While the surface area decreases with the temperature of preparation, crystallite size increases enormously. We are unable to explain the higher energy associated with finely divided MgO samples (prepared by the low temperature decomposition of the hydroxide) on the basis of particle size effects alone. Apparently, there is some pseudocrystallization of MgO particles accompanied by a small evolution of heat.

Metal oxides such as VO_2 and V_2O_3 are semiconducting or metallic depending on the temperature. The semiconductor-metal transition of VO_2 at 69°C is accompanied by a transition from the monoclinic (MoO_2 type) to the tetragonal (rutile) structure.

The addition of ions like Ti^{+4} (upto $\sim 40\%$) decreases the monoclinicity of the low temperature form of VO_2 . The temperature and also the enthalpy of the transition decrease with increasing percentage of Ti^{+4} . The magnitude of the change in electrical conductivity at the transition temperature is also lowered appreciably by Ti^{+4} . These results are understandable since the magnitude of crystal distortion in the transition decreases with $\% \text{Ti}^{+4}$.

In the monoclinic structure of VO_2 , addition of Ti^{+4} creates holes in the valence band and decreases the energy gap thereby causing higher σ at $T < T_t$ and lower $\Delta\sigma$ at T_t . In VO_2 , the homopolar $\text{V}^{4+} - \text{V}^{4+}$ bonds can trap conduction electrons in the low temperature phase. Apparently, the heteropolar bonds in the solid solutions are not as effective in the trapping of charge carriers. The c/a ratio of the high temperature rutile phase approaches the value in pure TiO_2 at high Ti^{+4} content. This would cause a decrease in σ above T_t with increase in $\% \text{Ti}^{+4}$ as observed experimentally.

NbO_2 undergoes a transformation from distorted rutile to rutile structure at $\sim 800^\circ\text{C}$. Addition of Nb^{+4} to VO_2 has profound effects on the phase transition of VO_2 . 2 % NbO_2 reduces the T_t ($\sim 42^\circ\text{C}$) and ΔH of the transition. The solid solution containing 5% NbO_2 seems to indicate two phase transitions at $\sim 7^\circ\text{C}$ and 38°C . 10% NbO_2 stabilizes the solid solution in the rutile structure and

we fail to see any transition corresponding to either VO_2 or NbO_2 . The solid solution $\text{V}_{0.98}\text{Mo}_{0.02}\text{O}_2$ shows a transition at $\sim 45^\circ\text{C}$.

All the solid solutions of VO_2 presently studied show semiconducting behaviour above the transformation temperature. It appears that the semiconductor-metal transition of VO_2 becomes a semiconductor-semiconductor transition with the incorporation of even the smallest amounts of ions like Ti^{+4} ($\sim 1\%$) and Nb^{+4} .

Compounds of the general formula CsPbX_3 ($\text{X} = \text{Cl}, \text{Br}$ or I) show interesting phase transformations. CsPbCl_3 transforms from distorted tetragonal to cubic perovskite at 47°C with a low enthalpy of about 20 cal mol^{-1} . The volume change and thermal hysteresis are negligible. A dielectric constant anomaly is also observed at $\sim 47^\circ\text{C}$. CsPbBr_3 transforms from a distorted perovskite to a cubic perovskite at $\sim 130^\circ\text{C}$ with an enthalpy of $\sim 250 \text{ cal mol}^{-1}$. The ΔV and ΔT are small as in CsPbCl_3 . A dielectric anomaly is noticed at $\sim 139^\circ\text{C}$. CsPbI_3 transforms from a monoclinic structure to a monoclinically distorted perovskite structure at $\sim 305^\circ\text{C}$ with a $\Delta H \sim 1000 \text{ cal mol}^{-1}$; a dielectric anomaly is also seen at $\sim 340^\circ\text{C}$. It is possible that the phase transformations of the three CsPbX_3 compounds are associated with a change from an antiferroelectric phase to a paraelectric phase.

RbCdCl_3 undergoes a series of transformations. It changes from orthorhombic to tetragonal at $\sim 137^\circ\text{C}$ ($\Delta H \sim 2300 \text{ cal mol}^{-1}$).

which further changes to a perovskite cubic structure at $\sim 190^\circ\text{C}$ ($\Delta H \sim 200 \text{ cal/mole}^{-1}$). The cubic perovskite is readily reversible to tetragonal whereas the tetragonal reverts to orthorhombic structure over a period of time. X-ray and DTA investigations on quenched RbCdCl_3 reveal that the tetragonal phase is metastable. The phase transformations of RbCdCl_3 are accompanied by dielectric anomalies. There was no evidence for ferroelectricity in RbCdCl_3 .

Preliminary studies on RbCdBr_3 and RbCdI_3 show that RbCdBr_3 is orthorhombic at 25°C (isostructural with RbCdCl_3) and that RbCdI_3 is distorted tetragonal (similar to CsPbCl_3). RbCdBr_3 and RbCdI_3 show phase transitions at 120° and 130°C respectively with enthalpies of 1060 and 2250 cal/mole respectively. These transformations are also accompanied by dielectric anomalies at T_t .

CsCuCl_3 transforms from hexagonal to face-centered cubic structure at $\sim 140^\circ\text{C}$ with an enthalpy of about $450 \text{ cal/mole}^{-1}$. The transformation is accompanied by thermal hysteresis ($\sim 10^\circ$), suggesting that it is possibly of first order.

OTHER PUBLISHED WORK OF THE AUTHOR

Effect of Impurities on the Phase Transformations and Decomposition of CaCO_3

G. V. SUBBA RAO, M. NATARAJAN, and C. N. R. RAO

THE transformation of aragonite to calcite (A-C) is an irreversible reconstructive transformation involving a change from 6 to 9 in the primary coordination. The transformation is therefore expected to be sluggish and associated with high activation energy.¹ Although the thermal transformation of A to C has been examined by several workers, there is limited information in the literature on the effect of impurities on the enthalpy, kinetics, and energetics of the transformation. Such a study is of value because most reported preparations of aragonite were in the presence of impurities. Furthermore, it is well documented that impurities markedly affect the phase transformations of solids.¹ The effect of impurity cations on the A-C transformation was recently studied, the cations being chosen on the basis of their size and their effect

Received November 16, 1967; revised copy received December 21, 1967.

Supported by the Council of Scientific and Industrial Research of India and the United States National Bureau of Standards.

At the time this work was done, the writers were, respectively graduate research assistant, graduate research fellow, and professor, Department of Chemistry, Indian Institute of Technology Kanpur, India. C. N. R. Rao is now visiting professor of chemistry, Purdue University, Lafayette, Indiana 47907.

¹ C. N. R. Rao and K. J. Rao; pp. 131-87 in *Progress in Solid State Chemistry*, Vol. 4. Edited by Howard Reiss. Pergamon Press, New York, 1967.

² Yasushi Kitano, "Behavior of Various Inorganic Ions in the Separation of Calcium Carbonate from a Bicarbonate Solution," *Bull. Chem. Soc. Japan*, 35 [12] 1973-80 (1962).

VITAE

Dharmathanapuram Mahadeva Natarajan was born on 25.5. 1940 at Gauhati in Assam. His School education was in Kumbakonam where he graduated, with a first class from Government Arts College (popularly known as 'Cambridge of South'), Kumbakonam in the year 1960. He served as a Demonstrator in Chemistry for two years in the same college and took his M.Sc., degree with high first class from Pachaiyappa's College, Madras (University of Madras) in 1964. He worked as an Assistant Professor in Govt. Arts College, Cuddalore and later joined the Faculty of Vivekananda College, Madras, where he taught Physical Chemistry to the M.Sc., classes.

By January, 1966 he joined the Solid State Research group of Professor C.N.R. Rao as a graduate student in the Ph.D. Programme, of the Department of Chemistry. Presently he is a Senior Research Fellow in the N.B.S. Scheme, with Professor C.N.R. Rao.